University of Southampton

Faculty of Natural and Environmental Sciences

School of Chemistry

High-throughput electrochemistry (HTP) - A new approach to the rapid development of modified carbon electrodes

by

Aleksandra Pinczewska

A Thesis Submitted for the degree of

Doctor of Philosophy

December 2011

This thesis was submitted for examination in December 2011. It does not necessarily represent the final form of the document deposited in the university after examination

University of Southampton

Faculty of Natural and Environmental Sciences

School of Chemistry

Doctor of Philosophy

High-throughput (HTP) electrochemistry – A new approach to the rapid development of modified carbon electrodes

by Aleksandra Pinczewska

Abstract

The major aim of this project was development of novel covalently modified glassy carbon electrodes for application in NADH-dependent biosensors using combinatorial and high-throughput methods. Studies on transition metal complexes containing redox active 1,1-phenanthroline-5,6-dione (phendione) ligand(s) showed they are effective electrocatalysts for oxidation of NADH. In order to covalently tether the metal complexes at the GC surface, the design of GC electrodes modified with novel metal complexes bearing phendione ligand(s) was proposed based on sequential electrochemical and solid-phase synthesis methods. Initial work involved optimisation of the process for modification of individual GC electrodes. Firstly, following earlier work, the GC electrodes were electrochemically functionalised by primary amines or a diazonium salt bearing Boc-protected amine groups, which allowed introduction of chelating ligands at the GC surface under solid-phase coupling conditions. The final step involved coordination of the bidentate ligand at the GC surface to the metal centre and formation of novel metal complexes under solid-phase coupling conditions. The successfully modified individual electrodes were applied in the design of a library of GC electrodes modified with different linkers, ligands and metal complexes and prepared in a combinatorial and parallel way. The library was electrochemically screened in a high-throughput way using a multichannel potentiostat, which allowed instant comparison of electrochemical and electrocatalytic properties between different members of the library. The experimental data extracted from HTP screening of the library were used for evaluation of a) the surface coverage obtained for different library members; b) the catalytic activity towards NADH oxidation and c) the kinetics parameters k_{cat} and K_M for the electrocatalytic oxidation of NADH for all members of the library.

Table of Contents

DECLARATION OF AUTHORSHIP

I, Aleksandra Pinczewska, declare that the thesis entitled

High-throughput electrochemistry (HTP)-A new approach to the rapid development of modified carbon electrodes and the work presented in the thesis are both my own, and have been generated by me as the result of my own original research. I confirm that:

- this work was done wholly or mainly while in candidature for a research degree at this University;
- where any part of this thesis has previously been submitted for a degree or any other qualification at this University or any other institution, this has been clearly stated;
- where I have consulted the published work of others, this is always clearly attributed;
- where I have quoted from the work of others, the source is always given. With the exception of such quotations, this thesis is entirely my own work;
- I have acknowledged all main sources of help;
- where the thesis is based on work done by myself jointly with others, I have made clear exactly what was done by others and what I have contributed myself;
- initial parts of this work involving electrochemical covalent attachment of different linkers have been published as:

Ghanem, M. A.; Chrétien, J.-M.; Pinczewska, A.; Kilburn, J. D.; Bartlett, P. N. *J. Mater. Chem.* **2008**, *18*, 4917.

Signed: ……………………………………………………………………..

Date:……………………………………………………………………………….

Acknowledgment

Firstly, I am truly indebted and thankful to my supervisors Prof. Phil Bartlett and Prof. Jeremy Kilburn for giving me an opportunity to work on the Phd project where I gained and developed broad range of synthetic and electrochemical skills. Phil, thanks for all your patience and understanding when explaining all the electrochemical problems and your enthusiasm for the three years. Jeremy, many thanks for your patience and understanding when the things did not turn out right in the lab and your advice on organic and synthetic problems and also for giving me an opportunity and trust to carry on the HTP project in QMUL.

I would like to thank my advisor, Dr Martin Grossel, for his advices and overall enthusiasm during my three years of Phd study. Prof. Gill Reid for her valuable advice on synthesis of metal complexes and being so supportive whenever I have asked for help and advice.

I would like to thank past and present members of the research project, Jean-Mathieu Chretien and Mohammed Ghanem for introducing me into the project and their huge patience and support during my learning process. Also Dr Sally Dixon, for her priceless advice on synthesis and guidance during my synthetic work and for setting a great example as a researcher. Thanks to Dr Maciej Sosna for his help, involvement and enthusiasm in latter stage of the work with the HTP library.

I have been extremely lucky to work with both electrochemical and synthetic research groups where I met fantastic people and this is why I thank following friends:

Biniam, Emma, Will and other present and past member of Jeremy's group for being such lovely and understanding friends and for their help with different problems in the synthetic lab.

Thanks to fantastic and enthusiastic people in Phil's group who helped me understand many aspects of practical electrochemistry and were always happy to help with everyday trouble shooting in the lab and answer my endless electrochemical questions.

Finally, I would like to say how much I appreciate the support and help I have received from my family, and most importantly Ross, who supported me during all this time and always believed in me. I bet you would be very happy to read this acknowledgment because it means I have finished writing!!

I have met many fantastic people in Southampton, who were not only my research mates, but also became dear friends. Amongst them was also Angie, Magda and Ala and I do really appreciate all your support and the precious advice I have received from you girls.

List of Symbols

Symbol	Description	Unit
A	geometrical electrode area	cm^2
D	diffusion coefficient	$cm^2\ s^{-1}$
$E^{\circ\prime}$	formal redox potential	V
E_a	potential of anodic peak	V
E_{bind}	binding energy	eV
E_c	potential of cathodic peak	V
dE_p	separation peak potential	V
E_{mp}	middle peak potential	V
F	Faraday constant	$C\ mol^{-1}$
ρ	surface roughness factor	-
Γ_{med}	surface coverage of mediator	$mol\ cm^{-2}$
i	Current	A
i_{cat}	catalytic current	A
i_{norm}	normalised catalytic current	A
j	current density	$A\ cm^{-2}$
n	number of electrons	-
k_{cat}	catalytic reaction rate	s^{-1}
k_D	mass transport rate constant	$cm\ s^{-1}$
K_D	dissociation constant	$mol\ cm^{-3}$
k_E	rate of electrochemical regeneration of mediator at the GC surface	s^{-1}
k_{ME}	effective electrochemical rate constant	$cm\ s^{-1}$
K_{ME}	effective Michaelis-Menten equilibrium constant	$mol\ cm^{-3}$
K_M	Michaelis-Menten equilibrium constant	$mol\ cm^{-3}$
pH	$-\log_{10}[H^+]$	-
R	gas constant	$J\ K\ mol^{-1}$
Q	charge density	$C\ cm^{-2}$

T	Temperature	K
ν	scan rate	V s^{-1}
V	kinematic viscosity	cm^2 s^{-1}
V_o	kinematic initial viscosity	cm^2 s^{-1}
V_{max}	kinematic maximum viscosity	cm^2 s^{-1}

Common Abbreviations

Symbol	Description
Ag/AgCl	silver/silver chloride reference electrode
BA	benzylamine linker
BDA	1,4-butanediamine linker
$CDCl_3$	deuterated chloroform
CME	chemically modified electrode
CV	cyclic voltammetry
DCM	dichloromethylene
DIPEA	diisoproylethylamine
DMF	*N, N*-dimethylformamide
DMSO-d_6	dimethylsulphoxide dueterated
EDA	1,2-ethylenediamine
EDDA	2,2'-(ethylenedioxy)diethylamine linker
ES+	electron spray positive ionisation
EtOH	Ethanol
GC	glassy carbon
HBTU	*O*-(benzotriazol-1-yl)-*N,N,N',N'*-tetramethylammonium hexafluorophosphate
HCl	hydrochloric acid
HDA	1,6-hexanediamine linker
HR-MS	high resolution mass spectroscopy
HTP	high-throughput
IR	infrared spectroscopy
LR-MS	low resolution mass spectroscopy
MeCN	acetonitrile
MS-MALDI	matrix assisted laser/desorption ionisation mass spectroscopy
NMR	nuclear magnetic resonance

NAD^+	nicotine adenine dinucleotide in oxidised form
NAD_∞^+	nicotine adenine dinucleotide in oxidised form in bulk solution
NAD_o^+	nicotine adenine dinucleotide in oxidised form at electrode-solution interface
NADH	nicotine adenine dinucleotide in reduced form
$NADH_\infty$	nicotine adenine dinucleotide in reduced form in bulk solution
$NADH_o$	nicotine adenine dinucleotide in reduced form at electrode-solution interface
[NADH-Q]	NADH and mediator intermediate complex at the electrode surface
phendione	1,10-phenanthroline-5,6-dione
[Q]	oxidised form of mediator at the electrode surface
[OH]	reduced form of mediator at the electrode surface
SCE	standard calomel reference electrode
TBATFB	*tert*butyl ammonium tetrafluoroborate salt
TFA	trifluoroacetic acid
XDA	*p*-xylene diamine linker
XPS	X-ray photoelectron spectroscopy

Index of Figures

Index of Schemes

Index of Tables

1 Literature introduction

1.1 Principles of combinatorial and high-throughput methodology.

1.1.1 General

Combinatorial and high-throughput (HTP) techniques are powerful tools widely used in development and evaluation of biological systems, pharmaceuticals, catalysts and many classes of inorganic compounds.[1-4] The combinatorial and HTP method involve design, synthesis and rapid evaluation of large numbers of structurally and compositionally diverse compounds (libraries or arrays) in order to identify the compounds or family of lead compounds, with the desired properties. Combinatorial methodology was developed by Hanak,[5] where the "multiple sample concept" was applied for discovery of new materials. Since then, this method has been widely used in the pharmaceutical industry, where the long and expensive drug discovery process was accelerated by rapid and cost effective combinatorial and HTP strategies.

In general, the principles of combinatorial and HTP chemistry are as follows:

- Rapid synthesis of a large number of diverse new materials from different combination of specific building blocks or processing conditions to create a library of analogous products at the same time under identical reactions conditions.
- Rapid evaluation of one or more chemical or physical properties of each library member and selection of the lead compounds to be used for further investigation.
- Further optimisation of leads varying the stoichiometries or structures followed by their rapid evaluation, resulting in a more focused library of compounds.
- Preparation of compounds with the best properties in quantities sufficient for their detailed characterisation.

1.1.2 Combinatorial synthesis methods.

The combinatorial synthetic approach is based on the preparation of many compounds at the same time in a systematic manner, which is more effective than the longer, classical, one compound at time method. As a result, the set of products of all possible combinations of building blocks creates a combinatorial library (Scheme 1.1).

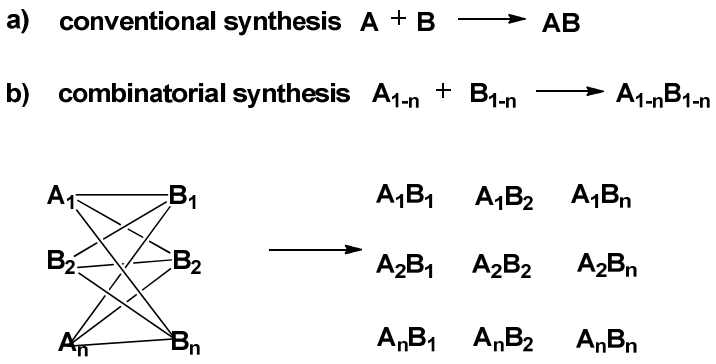

Scheme 1.1 a) Conventional synthesis: one building block A reacts with one reagent B; b) combinatorial synthesis: each of the building blocks of series A_{1-n} reacts with each of the building blocks of series B_{1-n} at the same time to give series of products A_nB_n.

In combinatorial synthesis, the total number of library members is given by $N=b\times x$, where b is the number of building blocks used in each reaction and x is the number of reaction steps where new building blocks were added.

Combinatorial synthesis can be carried out in solution or on solid supports such as resin beads, chips and pins. However, solid-phase conditions are more common due to easier parallel work-up and high yield of the solid-phase reactions as one can use excess of reagents in solution. The solid-phase condition has been widely used in development of new organic compounds, particularly in peptide synthesis.[3,6-8] Depending on the synthetic strategy and the library size, the library can contain of a mixture of different compounds or separate, single substances. Two main combinatorial synthesis methods exist:

- *Parallel synthesis* can be performed in solution or on solid supports, using ordered arrays of separated reaction vessels according to the conventional "one compound-one vessel" rule. The advantages of this method are the control over the purity of the products. In addition, defined location of the

product in the array provides structure of the products prepared and that the structure of the product is known from its defined location in the array. This method can be applied to the synthesis of medium size of libraries (several thousand compounds).

- *The split-pool synthesis* procedure allows for preparation of libraries of many products using a few reaction vessels. In the first step, the resins are split between, for example, three vessels and each resin is coupled with three different building blocks A_1, A_2 and A_3. After this step, all the three products are pooled together in one vessel where common steps such as deprotection or resin washing are carried out. Analogous to the first step, the mix of resins is divided into three vessels and each of them reacts with building blocks B_1, B_2 and B_3. The split and pool processes were repeated until the desired combinatorial library is obtained. Each bead in the library is attached to just one single compound.

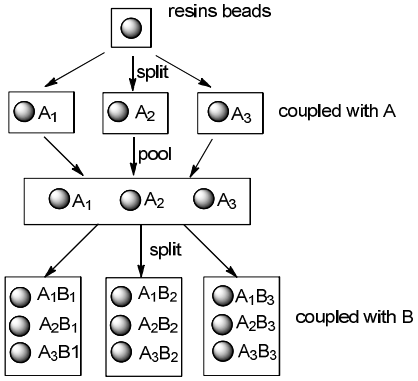

Figure 1.1 Split-pool synthesis to prepare combinatorial libraries of compound mixtures; spheres represent resin beads; A, B and C represents the set of building blocks; border are the reaction vessels. In the case where two building blocks are used, in each coupling step after two stages, a total number of 9 different compounds are formed, one on each resin bead.

1.1.3 HTP screening strategies

Characterisation of combinatorial libraries can be carried out one by one using conventional analytical methods or by using high-throughput parallel screening. Analytical methods such as mass spectroscopy, NMR and IR are applicable for screening of single substances from the library. In the case of larger libraries of

mixtures of compounds, accurate structural determination by analytical methods is difficult due to the similarity of the structures and properties of the evaluated compounds. Therefore, in order to determine the lead compound(s) in the combinatorial library different screening strategies were developed.[9]

For combinatorial libraries which comprise of a mixture of up to several thousand compounds, deconvulation screening methods can be applied for determination of the structure and biological activity of the hit compound(s).[9-13] Probably the most straightforward deconvolution strategy is iterative deconvolution, which has been used successfully in identifying several biologically active compounds.[14] This strategy is based on the synthesis of sub-libraries with compound mixtures (pools) were one of the building blocks are fixed and the rest of the building blocks are set up in a combinatorial way (Figure 1.2). After screening, the pool with the most desired properties is resynthesised with a second building block fixed. This process is repeated until the combination of building blocks with the best properties is obtained.

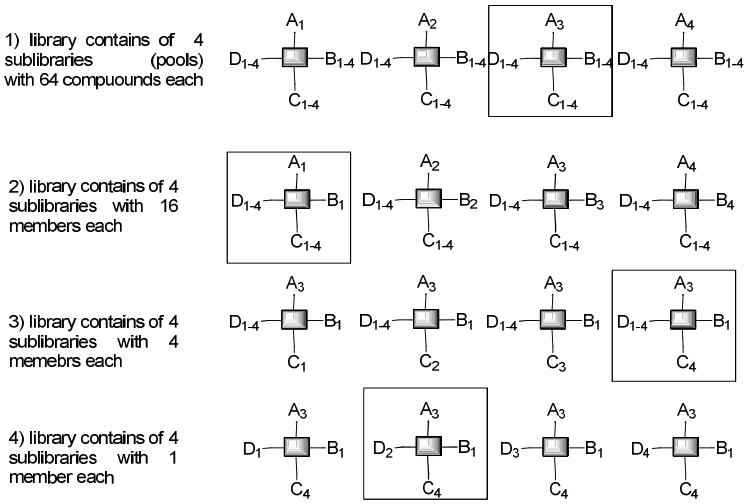

Figure 1.2 Process for the iterative deconvulation screnning of the combinatorial library containing variable building blocks A, B, C and D; compounds placed in brackets are hits obtained after each iterative step.

Although iterative deconvulation approach has found a few practical applications, the rate of hit compound discovery is limited by the requirement for several rounds of the synthesis and testing.[10,11,13] To overcome this, HTP deconvulation screening may be performed by positional screening, where all the possible combinations of the

building blocks are prepared at once (Figure 1.3).[9] Each of the sub-libraries contains one of defined building blocks at one position and a mixture of building blocks at the others. The number of sub-libraries is the same as the number of variable positions in the substitution pattern. This method of HTP screening is faster and allows screening of all of the possible combinations of building blocks in one measurement. However, this also requires preparation of larger libraries. Screening of the library all at once allows for direct deduction of hit compounds.

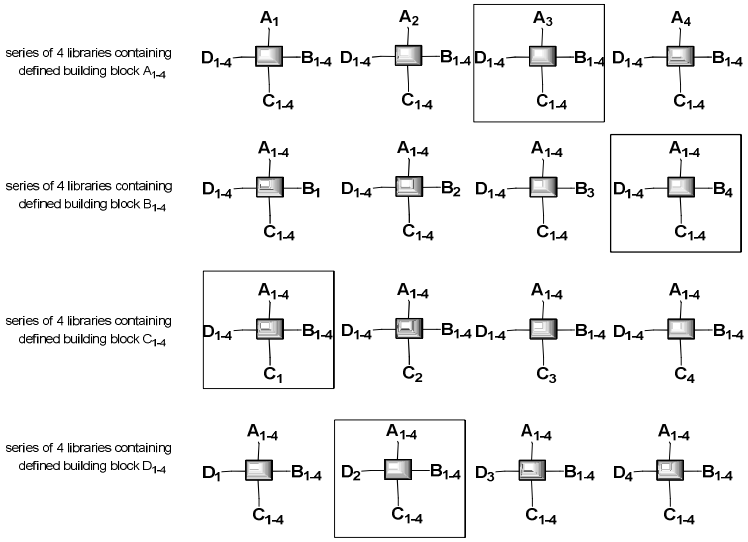

Figure 1.3 HTP positional scanning deconvulation method, where each of 16 sublibraries (pools) is containing one defined building block $A_{1\text{-}4}$ -$D_{1\text{-}4}$ were screened at the same time.

In the case of combinatorial libraries comprising mixtures of solid-bound compounds, the compounds can be screened still attached to the solid support using "on-bead" screening.[9]

This method works particularly well in the case of compounds with biological activity, where the solid-bound library is treated with a labelled soluble biological target. Example of the "on-bead" screening strategy includes employing fluorescent label receptors, which bind to the compounds with the highest affinity for biological receptors.[15,16] The "on-bead" screening is particularly useful for libraries of several thousand to a million compounds and isolation of a few bioactive compounds from many inactive ones.

The HTP screening of combinatorial libraries using the general strategies such as deconvulation and "on-bead" attracted significant interest mostly in development of pharmaceuticals and biologically active compounds.[17] The combinatorial and HTP

methodologies have also been applied for development of new solid-state materials, including superconducting materials, magnetoresistants, zeolites or polymers.[2,18-21] Significant advances in the development of combinatorial and HTP approaches have been also observed in discovery of new catalysts,[22-29] including asymmetric catalysts for organic synthesis,[2,26] metal binding peptidic ligands[22,29] or metal complexes[27] as enzyme mimetics. Common HTP techniques for screening the combinatorial libraries towards development of new catalysts and materials include mass spectrometry, circular dichroism, IR thermography as well as increasing number of electrochemical techniques.[2]

1.1.4 Application of combinatorial and HTP methods in electrochemistry.

Combinatorial and HTP methodology is a rapidly growing field of electrochemistry, including new methods for electrosynthesis of small organic compounds, heterogeneous catalysis and synthesis of conducting solid supports.[2,17]

The first example of combinatorial electrochemistry was reported by Reddington *et al.*[30] describing an automated method for preparation of large libraries of metal alloy catalysts for methanol oxidation. The HTP electrochemical screening of the array way was based on the optical response of a fluorescent dye due to pH changes caused by the local proton release during the electroxidation of methanol. Similar optical methods were reported for HTP electrochemical screening of combinatorial libraries of electrocatalysts for fuel cells[31,32] and Pt-Pb alloy catalysts for enzyme free amperometric sensors.[33] A disadvantage of the HTP optical screening method is limited sensitivity of the optical response, which can not distinguish small differences in electrocatalytic current between different members of the array. In addition, the fluorescent dye can be adsorbed at the electrode surface and affect the activity of studied catalyst.

This problem was overcome in report by Ward *et al.*[34] for electrochemical HTP screening of an array of gold electrodes modified with different organothiols, where fluorescent screen was replaced by more sensitive direct measurement of electrochemical current. This allowed the authors to distinguish slight variations in the current recorded for different modifications. Combinatorial electrochemical screening was accomplished using a computer-automated analysis, in which each electrode of the library was examined serially in the same electrochemical cell under

identical conditions. A disadvantage of this method is that all the electrodes remain in the solution in contact with the reactants, while only one active electrode is screened at a time. This might result in inaccurate results obtained for the array of modified electrodes.

Simultaneous electrochemical screening of all members in the combinatorial array was achieved by introduction of multichannel potentiostat/galvanostat, which was initially applied for redox recycling of p-aminophenol - a product of protein and DNA-enzyme linked sorbent assay with sensitive electrochemical detection.[35] In this method, the same potential was applied to all electrodes followed by automated serial data acquisition with integrated computer software. Literature examples of HTP screening using multichannel potentiostat include combinatorial preparation and screening of lithium batteries[36], arrays of Pt-catalysts loaded on carbon for oxygen reduction, CO electroxidation[37] and methanol oxidation.[38]

In this project, the combinatorial methodology described in Sections 1.1.2 and 1.1.3 using solid-phase synthesis followed by HTP electrochemical screening by a multichannel potentiostat was applied for discovery of novel electrocatalysts for biosensor development.

1.2 Chemically modified electrodes (CMEs)

One of the major aspects of research in electrochemistry within the last 30 years has been the design of electrode materials in order to provide control over their interactions with their environment. This has found particular interest in electroanalytical chemistry, where tailored electrode surfaces with their unique properties have been used in various practical applications, such as biosensors, molecular electronics, corrosion protection and energy conversion.[39,40]

Electrode surfaces functionalised by conducting or semiconducting materials are defined as chemically modified electrodes (CMEs), where design of these materials at the surface allows control over the surface performance and properties, such as selectivity, sensitivity, chemical and electrochemical stability, breadth of potential window and resistance to fouling.

Immobilised redox active species (mediators) work as catalysts for the oxidation/reduction of the analyte in solution and allow molecular control over the kinetics of electron transfer at the electrode/solution interface. The redox reaction of the solution species occurs through chemical reaction with the redox mediator followed by electrochemical regeneration of the mediator at the electrode surface (Scheme 1.2).

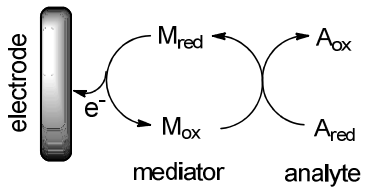

Scheme 1.2 General representation of an electrochemical redox reaction catalysed by a mediator.

An effective redox mediator can significantly catalyse a chemical reaction and electron transfer at low overpotential. The strategy of electrode modification has been successfully applied in bioelectrochemistry to enable electrochemistry of redox proteins and enzymes[41] and for application in biofuel cells[42], biosensors[43-45] and electrosynthesis.[46]

Mediators can be immobilised at electrode surfaces by covalent or non-covalent bond formation divided into three general methods:[47]

- *Chemisorption (adsorption)* is particularly effective if the mediator contains a group strongly and irreversibly adsorbing onto the electrode surface. This

approach is commonly used in attachment of mediators with thiol functionality onto gold electrodes yielding monolayer coverage.[48] Alternatively, the electrode surface may be functionalised by strongly adsorbed species with functional groups, which permit further covalent attachment of the mediator molecules.[49]

- *Immobilisation of polymeric films* at the electrode surface can be obtained using two general methods: coating of a preformed polymer or *in situ* electrochemical polymerisation-deposition at the electrode surface. Using these methods, multilayers of polymer films are created at the electrode surface. These films can act as a catalyst by themself or be used as a matrix to incorporate mediator species.
- *Covalent functionalisation* of the electrode surface with organic molecules enables control over the surface modification using organic synthesis methods. Examples of covalently modified electrodes include organosilanes at metal oxide electrodes such as ruthenium (IV) oxide, Pt/PtO and Si/SiO.[39] Formation of strong Au-C covalent bonds can be obtained by reduction of diazonium salts at the gold surface yielding stable monolayers and multilayers of the aryl derivatives at the electrode surface.[50,51] Due to the scope of this project, we will focus on the covalent functionalisation of the GC electrodes.

The use of carbon as an electrode material has the advantages over metal electrodes in low cost, a wide potential window and electrocatalytic activity for a variety of redox reactions.[52] Different allotropic forms of carbon such as graphite (powdered, pyrolytic and highly ordered pyrolytic graphite (HOPG) and different carbon structures such as (vitreous) carbon (GC) and carbon nanotubes (CNT) have been applied in both analytical and industrial electrochemistry.[52] Well-known applications are examples of commercially available electrochemical blood-glucose strips based on screen-printed carbon paste electrodes.[53]

1.2.1 Covalent modification of carbon electrodes

The covalent functionalisation of easily handled and versatile carbon materials makes them very attractive CMEs with a potentially wide range of practical applications. The carbon materials are in the form of extended networks of fused aromatic rings with the terminal surface region of the networks often rich in reactive

sites. Hybridised sp^2 carbons enable the terminal region to take part in organic addition reactions or can be easily oxidised to active hydroxyl or carboxylic groups.[39] Two main methods of covalent modification of carbon electrodes exist: chemical and electrochemically assisted. The easily oxidised carbon surface creates reactive functional groups, including carboxylic acids, ketones and alcohols.[47] Electrochemically assisted direct covalent bond formation occurs between aromatic carbon atoms at the surface and organic molecules in the solution.

1.2.2 Chemical functionalisation of the carbon electrode

Chemically active terminal regions of the carbon surface are easily oxidised to create a number of functional groups, such as ketones and aldehydes and carboxylic groups. With such an activated carbon surface, it is possible to covalently attach different molecules including redox centres or spacer units to create metal complexes.[39,54-57] Some oxidation of the carbon surface occurs on exposure of the carbon surface to the air or during the polishing process. However, in order to increase the density of the functional groups at the carbon surface, the electrodes are normally pretreated by heating in air, by oxygen plasma treatment or by oxidation in nitric acid.[58,59] The reactivity of the resulting carboxylic groups can be improved by converting them into more active acyl chlorides, which can react more rapidly with amines or alcohols. Thionyl chloride is also used as oxidising reagent, which additionally increases the surface density of carboxylic groups (Figure 1.4).

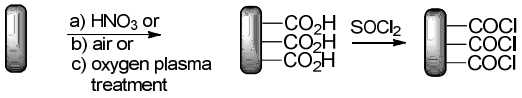

Figure 1.4 Functionalisation of the carbon surface by oxidation followed by conversion of the carboxylic acids into more active acyl chlorides.

Hydroxyl groups at the carbon surface produced by reduction of carboxylic groups using lithium aluminium hydride as reducing reagent work effectively for the introduction of organosilanes at the electrode surface (Figure 1.5).[60] Although silane chemistry is very versatile, it is difficult to obtain layers with a well-defined thickness and they show poor reproducibility and stability. Hydroxyl groups can also be reacted with cyanuric chloride, which has three reactive sites. This leaves one or two reactive sites to react with amines, Grignard reagents, alcohols or hydrazines.[39]

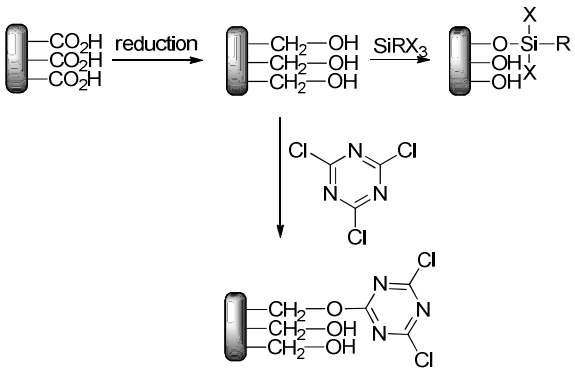

Figure 1.5 Chemical functionalisation of the carbon surface by hydroxyl groups followed by attachment of organosilanes or cyanuric chloride.

1.2.3 Electrochemical functionalisation of carbon electrodes

The formation of a covalent bonds between organic molecules in a solution and sp^2 carbon atoms at the surface can proceed via electrochemical heterogeneous reactions and electrodes prepared by this approach have found a number of analytical applications. In general, activation of a chemical reaction is initialised by electron transfer that creates intermediate unstable radicals, which react with carbon atoms at the electrode surface. However, faradaic efficiency for this type of modification is low due to the fact that intermediate radicals can dimerise or react with other reagents in the solution. Electrochemically assisted covalent attachment at the carbon surface has been successfully accomplished by oxidation of amines[61,62] and arylacetylates,[63] reduction of diazonium salt[64] and anodization (oxidation) in solution with alcohols.[65]

The electrochemical oxidation of carboxylates (Kolbe reaction) is the oldest known electroorganic reaction.[63] The Kolbe reaction is known as decarboxylative dimerisation and proceeds via a radial reaction mechanism (Figure 1.6). However, if the oxidation of carboxylate is performed at a carbon electrode, the R groups are covalently attached at the carbon surface. Firstly, the carboxylate ion transfers an electron to the electrode surface, yielding carbon dioxide and the R radical (Figure 1.6). The radical $R^{\cdot}$ can then be oxidised to the corresponding carbocation, which forms a C-C bond with carbon atoms at the surface.[65]

Figure 1.6 Electrochemical functionalisation of electrodes surface by applying Kolbe reaction at metal and carbon electrodes.

Similarly, amine-functionalised carbon electrodes may be prepared by electrochemical oxidation of primary aliphatic amines.[61,62,65,66] This method is based on electrochemical generation of primary or secondary amine radicals, which react with aromatic carbons at the electrode surface to create a covalent bond (Figure 1.7). X-ray photoelectron studies (XPS) have shown that the extent of the immobilisation strongly depends on the degree of amine substitution. Porter *et al.*[62] found that primary amines are much easier to oxidise than secondary amines, while tertiary amines show no evidence of surface attachment. This might be due to the steric effect of substituents in the tertiary amines, which limit the access of the amine radical to surface binding site.

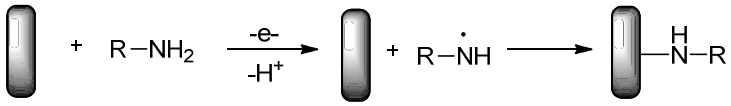

Figure 1.7 Electrochemical functionalisation of carbon electrode by oxidation of primary amines.[65]

Moreover, the surface attachments with primary/secondary amines or carboxylic acid, might also consist of the additional active group in their structures, which enables further introduction of redox centres, linkers and spacers at the electrode surface using organic synthesis methods. In the case of aliphatic α, ω-diamines both of the amine groups may be anchored at the carbon surface and create bridge structures by coupling both of the intermediate radicals of the same diamine molecule.[61] This undesirable effect was overcome by anchoring *mono*-protected diamine linkers, where the free amine group was first oxidised at the carbon surface so that subsequent deprotection of the second amine group leads to an amine modified carbon surface. These surfaces are analogous of the aminomethyl resins widely used in solid-phase synthesis.[55,57]

Examples of this approach include recent work on electrochemical attachment of *mono*-Boc protected primary diamines with different lengths and structures (aliphatic, alkyl and ether) (Scheme 1.3). After electrochemically assisted attachment of the linkers, an anthraquinone as a model redox centres was covalently attached using solid-phase synthesis methodology. XPS and electrochemical studies showed that the length and structure of the linker has an effect on the surface coverage and

kinetics of the redox species at the electrode surface. The anthraquinone surface coverage was found to decrease as the chain length of the diamine linker increased and faster electrode kinetics were observed for lower coverages and more flexible linkers.[55,57]

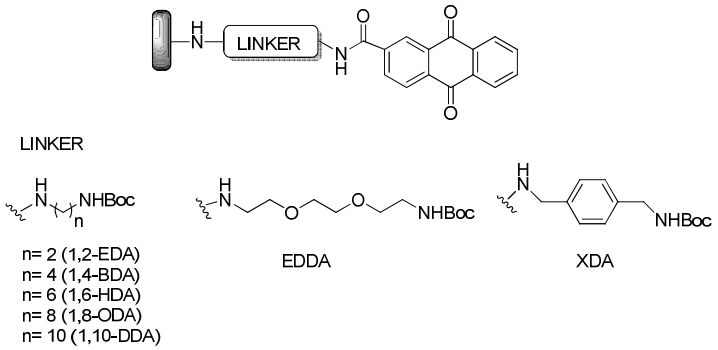

Scheme 1.3 General scheme of the GC electrodes modified by various diamine linkers and the anthraquinone redox centre.[57]

Electrochemical oxidation was also used for the introduction of oxygen functionality at carbon surfaces.[65,67] Formation of ether groups at the carbon surface was possible by applying high anodic potentials in acidic solution of primary alcohols; this creates the hydroxyl radical followed by its coupling at the carbon surface. As a result, the alcohol chain R was covalently bonded at the surface through an ether functional group (Scheme 1.4). The ether functionalised GC electrode was applied for indirect detection of calcium ions based on voltammetric response of ferricyanide.[67,68]

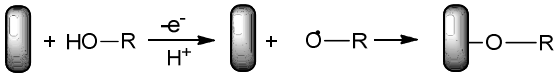

Scheme 1.4 Electrochemical covalent attachment of primary alcohols at the carbon surface.

Derivatisation of carbon electrodes can be achieved by electrochemical reduction of diazonium salts leading to the formation of a very stable covalent bond between the aryl groups and sp^2 carbon atoms at the surface. This covalent attachment was first described by Pinson and Savéant,[64] who observed an irreversible one-electron reduction wave in the presence of a diazonium tertafluoroborate salt. The reaction of wide range of phenyl amines with sodium nitrate at low temperature leads to phenyl diazonium reagents, usually isolated as tetrafluoroborate salt. Since then, functionalisation of the carbon electrodes by reduction of diazonium salts has been

found a number applications.[45,65,69,70-72] The literature on modified electrodes prepared by reduction of diazonium salts bearing a wide variety of functionality has been reviewed.[65,68,73]

Binding of the aryl groups to the carbon surface is likely to be a two-step process. Firstly, electrochemically assisted one-electron reduction of the diazonium salt generates an aryl radical and molecular nitrogen. This is followed by coupling of the radical to sp^2 carbon atoms at the electrode surface (Scheme 1.5).[74] Covalent anchoring of the diazonium salt to the electrode surface is favoured due its ability to adsorb on the surface and the relatively positive potential for diazonium reduction of about – 40 mV vs. SCE, which prevents simultaneous reduction of the aryl radical.[64,65]

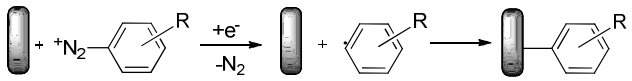

Scheme 1.5 Electrochemical functionalisation of carbon electrodes by reduction of a diazonium salt.

The very active phenyl radicals may react with phenyl groups already attached on the surface yielding multilayers. This occurs under certain conditions, particularly at high diazonium salt concentration and long reduction times and allows deposition of the multilayers of the aryl compounds at desired thickness up to 25 nm.[65,74,75]

Introduction of aryl derivatives bearing active functional groups enables further modification of the electrode surface by attachment of additional redox centres, spacers or linkers using solid-phase organic synthesis methods, as shown in recent work by Bartlett and Kilburn.[55] In this work, the diazonium salt was attached at the GC surface, followed by further functionalisation of the electrode using solid-phase methodology (Scheme 1.6). An electrochemical reduction of 4-(*N*-Boc-aminomethyl)benzene diazonium tetrafluoroborate salt allowed for formation of a monolayer of benzylamine at the GC surface due to the fact that the bulky *Boc* group prevents the formation of multilayers of benzyl groups. After removal of *Boc*-protecting group, an anthraquinone carboxylic acid (AQ) redox centre was attached using solid-phase conditions. The modified electrodes were electrochemically characterised and show good long-term stability. In comparison to the analogous modification by *mono*-Boc protected diamine linkers, GC electrodes modified by the diazonium salt show slower electron transfer and lower surface coverage after

attachment of the AQ redox centre. This strategy, which combines electrochemical and solid-phase synthetic methodologies, constitutes a versatile and flexible approach for functionalisation of different carbon materials.

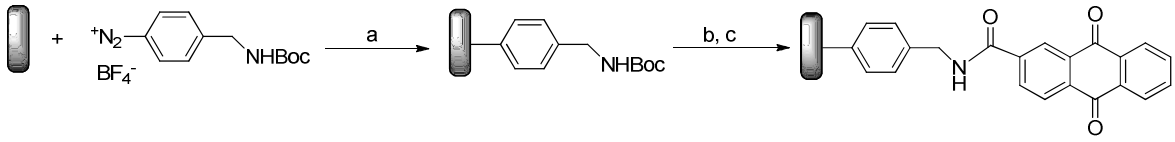

Scheme 1.6 Covalent functioanlisation of the GC electrodes by 4-(*N*-Boc-aminomethyl)benzene diazonium tetrafluoroborate salt linker and AQ redox centre; a) from 0.6 to −1 V vs. Ag/AgCl in 0.1 M TBATFB in MeCN; b) 4.0 M HCl in dioxane; c) Anthraquinone-2-carboxylic acid (AQ), HBTU, DIEA, DMF, R.T., 16 h.[55]

1.3 NADH co-enzyme and its electrochemical oxidation

Redox enzymes (oxidoreductases) exist to catalyse both electron transfer reactions and the transfer of atoms or small groups of atoms, to or from a range of substrates in a large number of biological processes. Some of these require small non-proteinaceous molecules, called co-enzymes in order to be active. The co-enzyme acts as an acceptor or donor of a small group of atoms or electrons and provides the driving force for the redox reaction of the substrate.[43]

An important group of redox enzymes are dehydrogenases, responsible for the transfer of hydrogen atoms and electrons during biological reactions and pathways in living organisms. Over 300 dehydrogenases are known, each of them specific for one substrate or group of substrates.[43] Most of the characterised dehydrogenases are dependent on soluble pyridine nucleotide cofactors, which occur in two biologically active forms of β-NAD (nicotinamide adenine dinucleotide) and its phosphorylated version, bearing a 2'-phosphate at the ribose ring β-NADP (nicotinamide adenine dinucleotide phosphate) (Figure 1.9). These coenzymes work as an acceptor/donor of a hydride ion (H^-) to/from a substrate during oxidoreductase-catalysed redox reactions. The NAD(P) coenzyme reacts with the substrate in 1:1 stoichiometric reactions. Changes of the NAD(P) concentration in solution during enzymatic reaction can be monitored by UV spectroscopy since NADH has strong adsorption at wavelength of 340 nm.[76]

In general, the active site of a redox enzyme contains complexing groups, which binds with the substrate and co-enzyme $NAD(P)^+$/NAD(P)H to bring them into correct relative orientation (Figure 1.8). The $NAD(P)^+$/NAD(P)H co-enzyme binds first at the active site to give a haloenzyme, followed by binding of a substrate. The redox reaction between enzyme and the substrate transfers atoms and electrons to/from the electron acceptor, which in this case is the co-enzyme, followed by dissociation of the product and coenzyme from the active site.

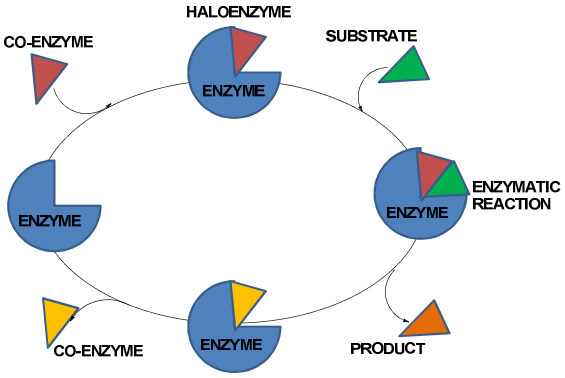

Figure 1.8 The general mechanism of an enzymatic reaction catalysed by NAD(P)+/NAD(P)H co-enzyme.

In the case of the dehydrogenases, the enzymatically active $NAD(P)^+$ works as an acceptor of two electrons and one proton (hydride transfer H^-) during substrate oxidation to obtain NAD(P)H.[76,77] The redox active part of this coenzyme is the nicotinamide ring, which exists as pyridinium salt for oxidised $NAD(P)^+$ and as the 1,4-dihydropyridine form for reduced NAD(P)H (Figure 1.9).

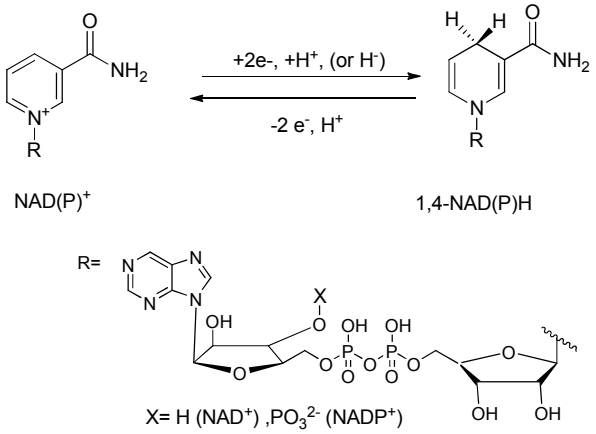

Figure 1.9 Structures of NAD and NADP and their reversible redox reaction by hydride ion transfer between oxidised form of $NAD(P)^+$ and reduced form of NAD(P)H carried out at C-4 of the enzymatically active nicotinamide ring; substituent R represents enzymatically inactive linkage consists of ribose, adenine base and phosphate groups and substituent X at one of the ribose rings is H for NAD and a phosphate group PO_3^{2-} for NADP.

The rest of the molecule including the adenine rings, ribose and phosphate groups are responsible for specificity and affinity of binding with the active site of the enzyme.[78] During the enzymatic redox reaction, hydride transfer occurs with one of the C-4 hydrogen atoms at the nicotinamide ring. Dehydrogenase enzymes are each

specific for one of the enantiotopic C-4 protons of NAD(P)$^+$/NAD(P)H: some of them react with the 4R hydrogen and the others with the 4S hydrogen (Figure 1.10). The stereospecificity of the dehydrogenase enzymes can be determined by well-established deuterium labelled experiments.[76,79,80] Stereospecificity of the dehydrogenase enzymes is due to the orientation of the NAD$^+$/NADH in the enzyme active site.[76]

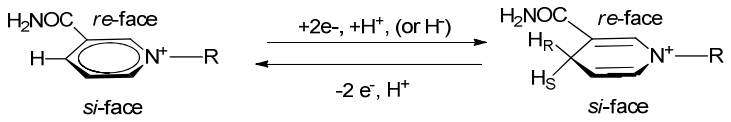

Figure 1.10 Stereospecific hydride transfer during redox reaction between NAD(P)$^+$ and NAD(P)H.

In solution, NAD(P)$^+$ exists in a folded conformation where parallel-ring stacking of the adenine and pyridine molecules creates an intramolecular complex with an average inter-ring distance of 0.52 nm and the nicotinamide ring *si*-side facing the adenine and confirmed by spectroscopic analysis [81] and molecular dynamics simulation.[78,82]

The unfolded, extended structure of the coenzyme is observed in the case of NAD(P)$^+$/NAD(P)H coordinated with proteins in the enzyme active site.[83] For most dehydrogenase enzymes, extended NAD$^+$ binds to a pair of protein structural domains, known as the Rossmann fold. The Rossmann fold typically consists of six parallel amino acid β-strands and four associated α-helices, with the adenine and nicotinamide rings interact with a pair of β-α-β motifs.[84,85] For dehydrogenase enzymes, it is well known that the domain contains two sets of β-α-β-α–β units joined across a two-fold axis such that the first strands of each unit are adjacent. The strand order is thus 6 5 4 1 2 3 (Figure 1.11).[86,87] The only adjacent strands, which have helical connections in opposite directions are 1 and 4. They create cervices, where the phosphate groups of the coenzyme bind to the corresponding carboxy ends of these two strands. The long loop (cross-over) between strands 3 and 4 creates a cavity that participates in the binding of the adenine ring of the coenzyme.

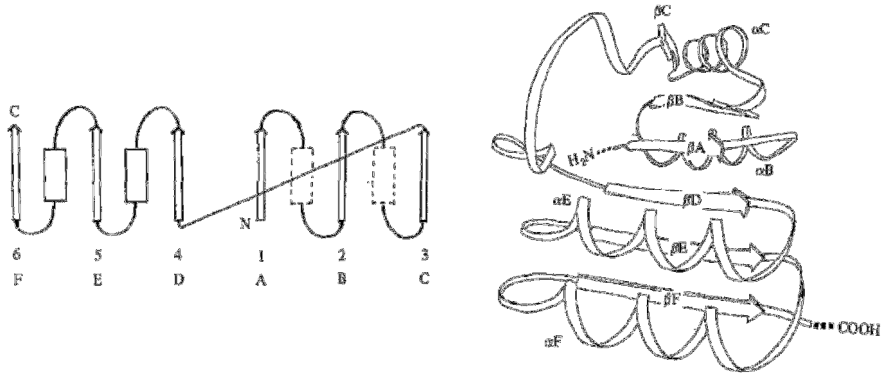

Figure 1.11 Schematic diagrams illustrating the Rossmann folding of β-strands and α-helices in the NAD-binding protein domain of dehydrogenase enzyme.[87]

Despite their very similar structures, identical thermodynamic properties and reaction mechanism, β-NADP and β-NAD coenzymes participate in different biological processes within the living cell.[77] β-NADP works with enzymes that catalyse anabolic reactions supplying electrons needed to synthesise energy-rich biological molecules. β-NAD is found in mitochondria where it is essential for the conversion of ADP to ATP through the oxidation of foodstuffs (catabolic function). ATP molecules are used elsewhere in the cell to provide the energy for thermodynamically unfavourable reactions required to build essential cell components. Most nicotinamide-dependent dehydrogenase enzymes are specific for $NAD(P)^+$/NAD(P)H or the form (NAD^+/NADH) of the co-enzyme.

NAD(P)-dependent dehydrogenase enzymes catalyse oxidation of their substrates according to the general reaction scheme:

$$SH_2 + NAD(P)^+ \underset{k_b}{\overset{k_f}{\rightleftharpoons}} S + NAD(P)H + H^+$$

where S and SH_2 are the oxidised and reduced forms of the substrate and k_f and k_b are the rate constants for the forward and backward reactions. This general enzymatic reaction in the presence of NAD^+ is modified, depending on the structure of the substrate and classification of those enzymatic reactions has been reported in the literature.[77,88] $NAD(P)^+$ coenzymes are most commonly used in enzymatic oxidation of alcohols to carbonyls, including alcohol dehydrogenases, which catalyse oxidation of ethanol to acetaldehyde.

$$\text{ethanol} + NAD^+ \underset{k_b}{\overset{k_f}{\rightleftharpoons}} \text{acetaldehyde} + NADH + H^+$$

The biological importance and the redox properties of $NAD(P)^+$/NAD(P)H coenzyme have attracted significant interest for its application in enzymatic synthesis catalysed by NAD(P)H-dependent enzymes and amperometric biosensors. The enzyme-catalysed synthesis of different compounds has found practical application in pharmacology, biotechnology, food additives, perfumes, pesticides and insecticides.[89] Because of the very high price of NAD(P)H and the fact that it needs to be used in stoichiometric quantities during enzymatic reaction, its use in industry is limited and needs to be justified by the high price of the final product. Hence, there is significant interest in developing *in situ* NADH regeneration methods to re-use the initial amount of the active NAD(P)H. One of the most popular regeneration methods include reduction of NAD^+ to NADH by formate catalysed by formate dehydrogenase (FDH) enzyme. Electrochemical methods of the NAD(P) would remain the best means of regeneration because these do not need an additional donor/acceptor of the electrons and no side products are produced. Similarly, the redox properties of the NAD(P) co-enzyme have found extensive application in design of the amperometric biosensors. However, electrochemical behaviour of the NAD(P) at a bare electrode is complex and results in number of site reactions, therefore bioelectrocatalysis, new electrochemical mediators and modifications to the electrode surface have attracted a lot of attention.

1.3.1 Electrochemistry of NADH/NAD^+

The development of electrochemical biosensors based on NADH-dependent dehydrogenases is an attractive goal for many researches mainly due to the large field of potential substrates to analyse and their diversity in commercial applications.
The electrochemistry of the redox couple NAD^+/NADH has been extensively studied. The experimentally obtained formal redox potential ($E^{\circ\prime}$) of the NAD^+/NADH couple is −0.315 V vs. NHE and −0.560 vs. SCE at pH 7.[90,91] The NAD(P) dependent biosensors found practical application due to the fact that the redox process of NADH(P) is more favoured than most of the substrates catalysed by the NAD(P) coenzyme as value of $E^{\circ\prime}$ for NAD(P) is lower than most of the substrates. In particularly, biosensors based on oxidation of NADH to enzymatically active NAD^+ were considered for more detailed studies and development. Biosensors based on the reduction of NAD^+ would be impractical due to a series of interfering

side reactions occurring at more negative potentials, such as oxygen reduction, which would disturb the reliability of the biosensor.

Initial studies on NAD redox behaviour at bare electrodes indicated that the electrochemistry of the NAD^+/NADH is irreversible with an anodic wave observed at high overpotentials.[92] The choice of electrode material has a significant effect on the anodic potential with values of 0.4, 0.7, 1 V *vs.* SCE for carbon, platinum and gold electrodes, respectively.[93,94] It has been established that the oxidation of the NADH in aqueous solution occurs via a two-electron process[77,92,95]

$$NADH \longrightarrow NAD^+ + H^+ + 2e^-$$

Electrochemical oxidation of the NADH at bare electrodes depends on the electrode material, NADH concentration and electrode pre-treatment. Quantitative recovery of NAD^+ was obtained after electrochemical oxidation at Pt electrodes at low NADH concentrations (NADH < 0.1 mM).[92,94] Control experiments for the pre-adsorbed NADH at Pt and Au surfaces showed that NADH is oxidised at the electrode surface and undergoes further oxidation processes leading to unspecified products, which might result in fouling of the surface.[93]

Studies on the oxidation of NADH at the carbon electrodes showed that the oxidation product NAD^+ adsorbs strongly at the surface and acts as an inhibitor for further NADH oxidation.[93,96] This results in shifts to anodic potential with changing NADH concentration. A stable anodic potential was observed, when NAD^+ was present in excess in the solution or when the electrode was pre-treated with NAD^+ prior to the electrochemical experiment.

1.3.2 Mechanism of direct electrochemical NADH oxidation

Reviews by Bartlett and Gorton provide a summary of the mechanistic studies on the electrochemical oxidation of NADH at bare electrodes.[77,97] In general, investigation on the mechanistic aspects of the NADH oxidation was based on discussion whether the NADH electrochemical reaction occurs as a single two-electron step or involves consecutive one-electron transfer steps. Oxidation of NADH model compounds at Pt electrodes in aprotic solvent and without the presence of base gave strong indication that reaction occurs in two one-electron steps and is highly irreversible.[95] A number of further experimental studies at NAD^+ coated electrodes suggested that electrochemical oxidation of NADH proceeds according to an ECE mechanism

$$NADH \xrightarrow{-e^-} NADH^{\bullet+} \underset{+H^+}{\overset{-H^+}{\rightleftharpoons}} NAD^{\bullet} \xrightarrow{-e^-} NAD^+$$

The first step is an irreversible, potential-determining electron transfer, yielding a cation radical $NADH^{+\cdot}$. The high activation energy required for the first step might be due to the fact that 1,4-NADH must undergo rearrangement before losing the electron (Figure 1.12).[98] The amide group can take part in the oxidation process since only 1,4-NADH is enzymatically active.

The enol resonance form might also participate in the electron transfer as was observed during oxidation of the NADH by orthoquinones.[98,99] The second step involves deprotonation of $NADH^{+\bullet}$ yielding the neutral radical $NAD^{\bullet}$. This step is also considered as irreversible since the presence of the radical at the pyridine aromatic ring is more stable than the cation radical.[98,99] The deprotonation is relatively fast with a calculated rate constant $k_{H+} > 10^6$ s^{-1} measured for NADH oxidation at GC electrodes coated with NAD^+. $NAD^{\bullet}$ radical can be rapidly dimerised as has been identified during reduction of NAD^+, where formation of dimer $(NAD)_2$ from coupling of two radicals $NAD^{\bullet}$ was observed at about −1.1 V *vs.* SCE.[100] The dimer is oxidised at −0.4 V *vs.* SCE and yields NAD^+. Therefore, oxidation of $NAD^{\bullet}$ to NAD^+ in the final step of oxidation of NADH would be sufficiently rapid to outrun the dimerisation and practically no dimers would be produced.[77]

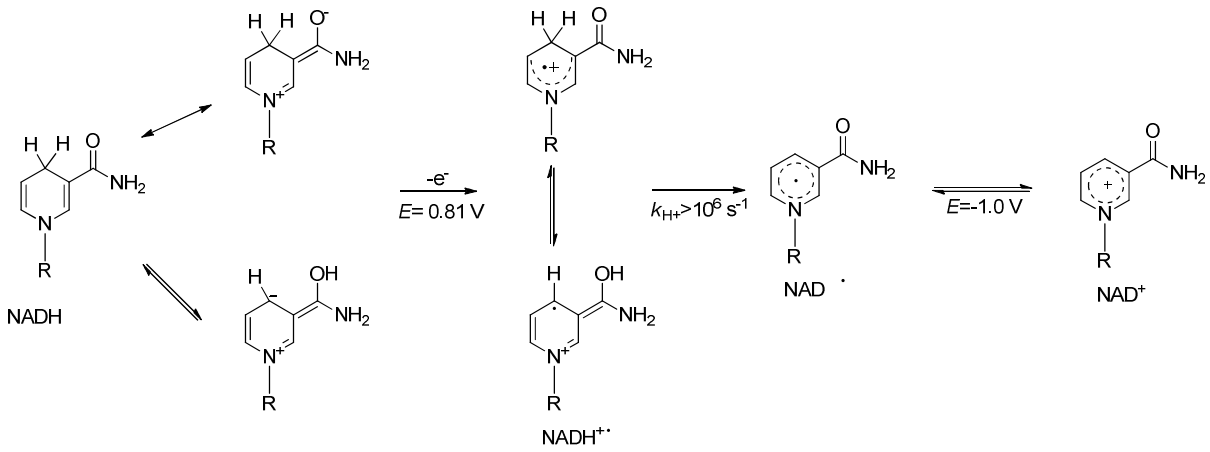

Figure 1.12 Proposed reaction pathway for the electrochemical oxidation of NADH according to the ECE mechanism; k_{H+} is a deprotonation rate constant.

In addition, the neutral radical $NAD^{\bullet}$ might exchange an electron with the more reactive cation radical $NADH^{+}$ during a chemical disproportionation reaction (DISP), leading to NADH and NAD^{+}

$$NADH^{\bullet+} + NAD^{\bullet} \Leftrightarrow NADH + NAD^{+}$$

Studies by Blankespoor and Miller[96] observed that 95% of the oxidation product is formed through the ECE pathway. The predominance of the ECE pathway might be explained by the fact that significantly rapid deprotonation of $NADH^{+\bullet}$ creates $NAD^{\bullet}$ radicals at a short distance from the electrode surface. The $NAD^{\bullet}$ generated close to the surface having relatively high potential, can easily lose an electron before it diffuses away from the electrode surface. Hence, electrochemical electron transfer (ECE) is favourable over the homogenous electron transfer (DISP), when the rate constant k_{H+} is relatively high.

In the case of electrodes, which are not covered with adsorbed NAD^{+}, the NADH oxidation might be mediated to some extent by oxygen adsorbed at the Au and Pt eletrodes (eg. $OH^{\bullet}_{ads}/H_2O$ and $O_{ads}/OH^{\bullet}_{ads}$) or by organic functional groups created during oxidation at carbon surface (e.g. quinone, semiquinone and hydroquionone systems).[77,93,101]

The electron-transfer path involves electron exchange between energy levels located at the surface oxygen atoms and the electrode, coupled with the electron exchange

between energy levels of the surface oxygen atoms and the solution species (Figure 1.13).

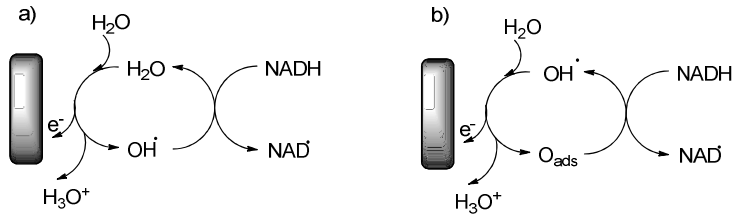

Figure 1.13 General scheme of the possible electron transfer pathway during NADH oxidation mediated by surface oxygen redox systems; a) mediated by hydroxy groups; b) mediated by molecular oxygen.[77,93,101]

The proton transfer pathway includes transfer of the proton from the C-4 of the nicotinamide ring to the proton acceptor, such as a water molecule, and possible intermediate formation of a bond to the surface oxygen atoms (Figure 1.14).

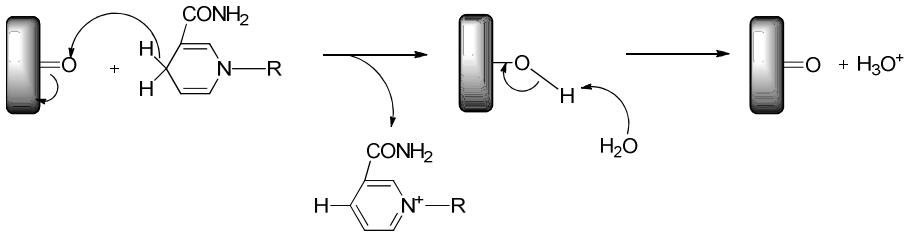

Figure 1.14 Possible proton transfer mechanism during oxidation of NADH involving movement of a proton from C-4 of the nicotinamide ring to a proton acceptor such as water molecule.[77,93,101]

The existence of functional oxides at the carbon surface is well established and is known as one of the methods of carbon surface modification (Section 1.2.2). However the type of the oxygen functional groups and their quantity at the electrode surface varies between different carbon materials and oxidation method.[77] Studies on oxidised carbon electrodes suggested that possible oxygen redox mediators at the surface might decrease the anodic potential for NADH oxidation causing the oxidation reaction to become kinetically more rapid. However, this electrocatalytic effect was found to be of low stability, which might be due to surface blocking by the oxidation product NAD^+.[77,94]

1.3.3 NADH oxidation at modified electrodes

In order to design effective biosensors based on the electrochemical oxidation of NADH, pre-treatment of the electrode surface is required to overcome problems of the high overpotential and ECE mechanism, resulting in fouling of the electrode surface. During initial studies on oxidised Pt and carbon electrodes a decrease of the overpotential for NADH oxidation to approximate 0.2 V vs. SCE was observed. This suggested that presence of quinone and hydroxyl groups at the electrode surface act as mediators for electron transfer between the electrode and NADH molecules.[94,99] Since then, a large number of the redox systems have been investigated as electrocatalysts for NADH oxidation, including homogenous electron-transfer mediators, which are known to successfully catalyse the NADH oxidation.[97] However, the disadvantage of using soluble mediators is the possibility that they can diffuse away from the surface and no longer be available to catalyse the electrode reaction. Hence, most of the mediators applied for NADH oxidation are immobilised at or very close to the electrode surface to create CMEs.

The perfect mediator has to meet a number of criteria:

I. Acceptor of the hydride ion

An essential feature of the effective NADH mediators is their ability to act as two electrons ($2e^-$), one proton (H^+) acceptors during oxidation of NADH to produce enzymatically active NAD^+. The reaction between NADH molecules and the mediator occurs via formation of an intermediate charge transfer complex with the NADH. Efficient electrocatalyst immobilised at the electrode surface reacts rapidly with the NADH at low overpotential. This means that the oxidation of NADH to NAD+ should proceed via single hydride transfer H^- rather than sequential one electron transfers since the radical intermediates for NADH oxidation are unstable and undergo side reactions. After oxidation of the NADH, the reduced form of the mediator must be regenerated at the electrode surface to the reoxidised form. Bartlett *et al.*[102] proposed a general reaction mechanism, where the mediator reoxidation proceeds via sequential one electron and proton steps and may vary depending on the mediator and conditions (Figure 1.15).

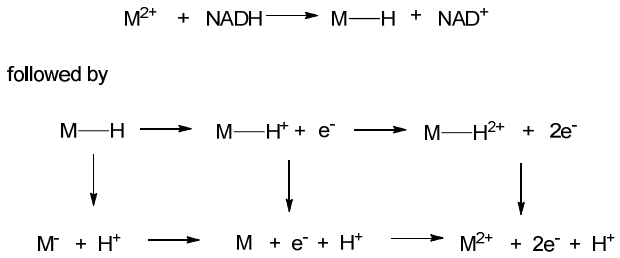

Figure 1.15 The catalytic cycle for the oxidation of NADH by the mediator M immobilised at the electrode surface.[43,102]

II. Low overpotential

The perfect mediating system should be able to reduce the overpotential down to optimal range of −0.1-0.1 V to avoid an oxidation of substrates such as ascorbate, urate and acetaminophen and avoid the potential region for reduction of molecular oxygen and where the potential of zero charge results in low a background current and noise for most of the electrode materials. For design of the amperometric biosensors, low redox potential of the mediator also prevents oxidation of other species in the biological sample.

III. Fast reaction kinetics

The mediator should be able to react rapidly with the NADH coenzyme followed by fast electron transfer during electrochemical regeneration of the mediator at the electrode surface. Ideal second order rate constants for the reaction between the NADH and the mediator should be above 10^6-10^7 M^{-1} s^{-1}, approaching a diffusion controlled reaction. In the case of dehydrogenase enzymes, the high rate constant between NADH and mediator k_{obs} is particularly important due to the fact that reaction between substrate and coenzyme is thermodynamically favourable and reaches its equilibrium rapidly. As a result, the rate k_{obs} needs to be higher than the rate of the back reaction k_b in order to increase the rate of product formation k_f (Figure 1.16). If $k_{obs} < k_f$, the electrochemical response will be mostly dependent on the product concentration.[77]

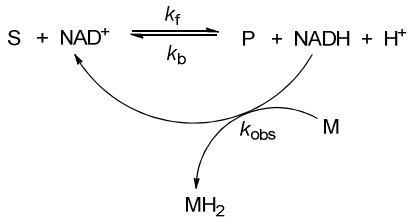

Figure 1.16 Enzymatic reaction of the substrate S catalysed by NAD^+ followed by electrochemical reoxidation of the NADH by the mediator M at the rate constant kobs, which is in kinetic competition with the rate constant k_b of the enzyme catalysed back reaction of NADH with the product P.

IV. Long-term stability (at least weeks or months)

This includes irreversible attachment of the mediator at the electrode surface followed by its electrochemical and chemical stability (hydrolysis, chemical oxidation or photo-decomposition). In addition, the mediating systems should not take part in the radical site reactions with NADH, should be selective towards NADH and show well-defined stoichiometry.[77]

A first attempt at a CME for NADH oxidation was reported by Kuwana and Tse[99] where they covalently immobilised primary amine-containing *o*-quinones at a carbon surface activated with cyanuric-chloride. These redox systems at the surface showed an anodic peak in the presence of NADH at around 0.2 V vs. SCE. However, a substantial decrease in the stability of the CMEs was observed during NADH electroxidation. Further investigation for *o*-quinones incorporated into a larger aromatic derivative 4-(2-(1-pyrenyl)vinyl)catechol), reported by Kuwana *et al.*,[103] indicated long term stability of the mediator in its reduced form. When the strongly adsorbed mediator was kept at a potential close to its formal redox potential, site reactions occurred caused by reaction of the *o*-quinone groups with catechol. Additionally, a deactivation reaction of the mediator in its reduced form was suggested, where they were reacting with the $NADH^{+\bullet}$ radical to give an inactive compound leading to poisoning of the electrode surface (Figure 1.17).

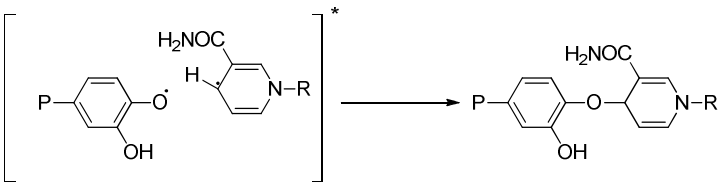

Figure 1.17 Possible deactivation mechanism for the adsorbed o-quinone mediator and $NADH^{+\cdot}$ radical during electrochemical oxidation of the NADH.[77,103]

Since the first attempts at preparation of CMEs for electroxidation of NADH, a significant amount of work has been reported on the development of the CMEs and is summarised in a number of reviews.[77,97,104,105] In general, two main development routes were identified during evolution of the CMEs. The first, involved searching for different methods for the immobilisation of mediators at the electrode, discussed in more detail in Section 1.2. The second route involved the development of new mediator structures, other than *o*-quinones, which could effectively catalyse NADH oxidation at low overpotential and have long-term stability.

In general, redox systems contain the structural features depicted in Figure 1.18 are found as effective $2e^-$, H^+ acceptors and to successfully catalyse NADH oxidation at low overpotential.[43] The essential features of the effective NADH mediator are the presence of the hydride accepting group and the ability to delocalise the charge within the mediator (Figure 1.18).

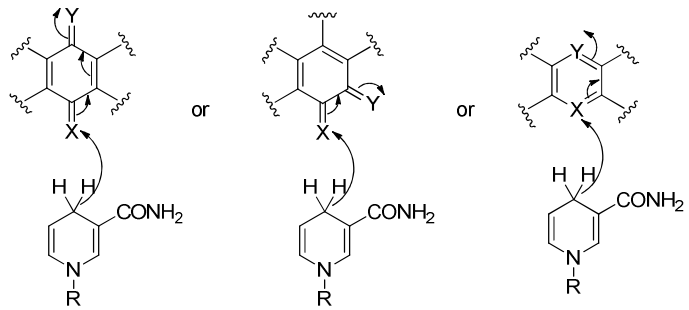

Figure 1.18 Proposed mechanism of the NADH oxidation catalysed by redox mediator, X is a group working as a hydride acceptor; Y is an electron deficient group.[106,107]

The most commonly suggested model for the reaction between the mediator and NADH is a two-step reaction mechanism,[108] analogous to the Michaelis-Menten enzyme kinetic model, described in Section 1.5.

Effective NADH mediators containing the necessary conjugated structures can be differentiated into a few general classes depending on the immobilisation method and the structure of the mediator:

I. Quinones

Since the initial study by Kuwana *et al.*,[99] a number of workers have reported CMEs with quinone and dihydroxy functionalities. Examples includes *ortho*- and *para*-dihydroxybenzaldehyde derivatives electropolymerised or adsorbed at the electrode surface, which were found to effectively catalyse NADH oxidation at low overpotential and exhibit a good stability during electrochemical screening.[109]

Recently, a novel HTP methodology for the functionalisation of GC electrodes was reported with use of the dihydroxy derivatives as mediators. The GC electrodes, covalently modified by two different diamine linkers (Section 1.2.3) were coupled by 3,4-dihydroxybenzaldehyde derivatives in a combinatorial way, followed by their electrochemical screening towards NADH oxidation.[56] This novel approach allowed for rapid evaluation of various dihydroxybenzene mediators towards electrocatalytic NADH oxidation with the highest catalytic activity obtained for electrodes modified with p-benzylamine linker and 3,4,5-trihydroxybenzene. Disadvantage of the dihydroxybenzene mediators is their low electrochemical stability.

II. Redox dyes

Commercially available phenoxazines and phenothiazines redox dyes such as meldola blue, nile blue or methylene blue effectively catalyse NADH oxidation at potential about −0.1 V vs. SCE. In general, this type of mediator shows relatively low chemical and physical stability. In order to overcome this problem, the redox dyes were derivatised in position 3 or 7 with amine functionalities, aromatic aldehydes or acid chlorides to donate beneficial new properties to the original dye, such as resistance to the pH changes or higher adsorption stability.

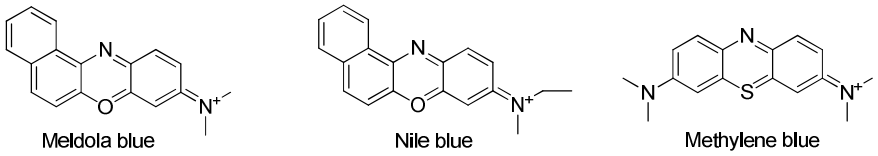

Figure 1.19 Examples of common redox dye mediators applied as effective catalysts for NADH oxidation.

The redox dyes were also incorporated into carbon paste,[43] electropolymerised (poly(nile blue)[110] or poly(methylene blue)[111]) at the electrode or covalently attached to a compound strongly adsorbed at the surface (monolayers of various redox dyes attached at the gold surface through self-assembly cysteamine or 3,3'-dithiobis(succineimidylpropionate) in order to reduce the desorption problem and catalyse NADH oxidation at desired formal potential about −0.1 V.[112,113]

III. Conducting polymers

Conducting polymers such as poly(aniline) doped with poly(anions) such as poly(vinylsulphonate), poly(styrenesulphonate) or poly(acrylate) show catalytic activity for NADH oxidation at potentials around 0.1 V vs. SCE.[102,106,114] The

electrodeposited polymers can act as a host matrix for the mediator, which can be incorporated into the polymer film as a counter ion during the polymerisation process or covalently attached to the monomer and then polymerised at the electrode. Examples of the mediators incorporated into the polymer matrices include pyrrole substituted by mediators with quinone functionalities[115] or the redox dye methylene blue incorporated into poly(pyrrole) film, which oxidises NADH at about 0.1 V vs. SCE.[116]

IV. Metal Complexes

Metal complexes with redox active ligands constitute an interesting group of mediators towards NADH oxidation. They were normally electrodeposited or electropolymerised at the electrode surface. Examples include polyvinylimidazole (PVI) coordinated to an osmium metal ion and deposited at carbon fibre electrodes to catalyse NADH between 0.1 and 0.5 V *vs.* Ag/AgCl.[117] Other examples include various catechol-pendant metal complexes (Co, Cr, Os, Ru, Fe, Ni) with terpyridine electrodeposited onto GC electrodes which were found to effectively reduce the NADH oxidation potential to about 0.3 V vs. SCE.[118] In these cases, the NADH oxidation is governed by the redox process of the metal ion and have found practical application in peroxidases based biosensors.[119] However, this method has a disadvantage of necessity of addition of soluble quinoid compound that in a first step oxidise NADH to NAD^+ and then is reoxidised by molecular oxygen to produce hydrogen peroxide, which can react with peroxidase and osmium complex immobilised at the surface and generate the response current.[105]

An interesting group of the mediators for NADH oxidation are metal complexes with redox active 1,10-phenanthroline-5,6-dione ligands, their more detailed characterisation is presented in the following Section.

V. Other redox systems

CMEs based on conducting organic salts such as N-methylphenazinium tetracyanoquinodimethane (NMP-TCNQ) (Figure 1.20) work effectively as catalysts for NADH oxidation at low overpotentials around 0.2 V *vs.* SCE and with relatively high reaction rates.[120]

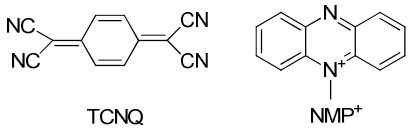

Figure 1.20 Structures of the organic conducting salts N-methylphenazinium tetracyanoquinodimethane (NMP-TCNQ) as effective mediators for NADH oxidation.

Organic compounds containing nitro functional groups such as nitro-fluorenone derivatives[121,122] or dithio-bis(2-nitropyridine)[123] can be electrochemically reduced to nitroso/hydroxylamine, which can then catalyse the NADH oxidation at potential around −0.15 V *vs.* SCE as shown in Figure 1.21.

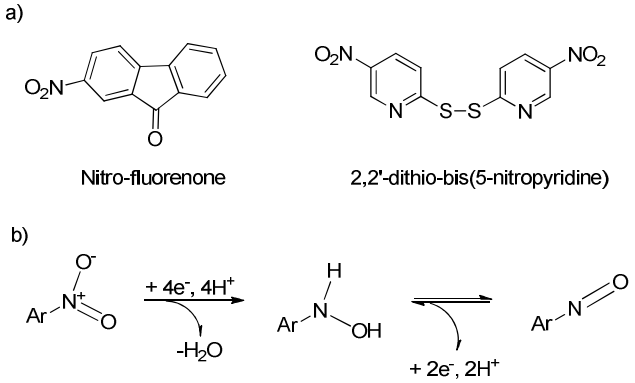

Figure 1.21 a) Examples of the mediators consisting of the nitro functional groups; b) electrochemical formation of the nitrosyl catalytic active form.[122]

1.4 Metal complexes with 1,10-phenanthroline-5,6-dione as electrocatalysts for NADH oxidation.

An interesting group of mediators towards NADH oxidation are metal complexes with the redox active phenathroline-5,6-dione (phendione) bidentate ligand, where the quinone functionalities act as hydride acceptors during the NADH electroxidation.

The structure of the non-coordinated phendione ligand contains of two electrochemically active sites: the *o*-quinone and imine functionalities. Some of electrochemical properties of the phendione and its derivatives have been reported in the literature due to their interest in synthetic and biological applications.[124,125] Study on the electrochemical behaviour of the quinone functionalities suggested that their electrochemistry strongly depends on the reaction conditions, such as pH and solvent.[126]

Cyclic voltammetry of phendione in aprotic solvents shows two reversible-one electron waves at –0.45 and –1.25 V *vs.* SSCE, representing formation of the stable intermediate anion radical (semiquinone) and dianion, respectively (Figure 1.22).

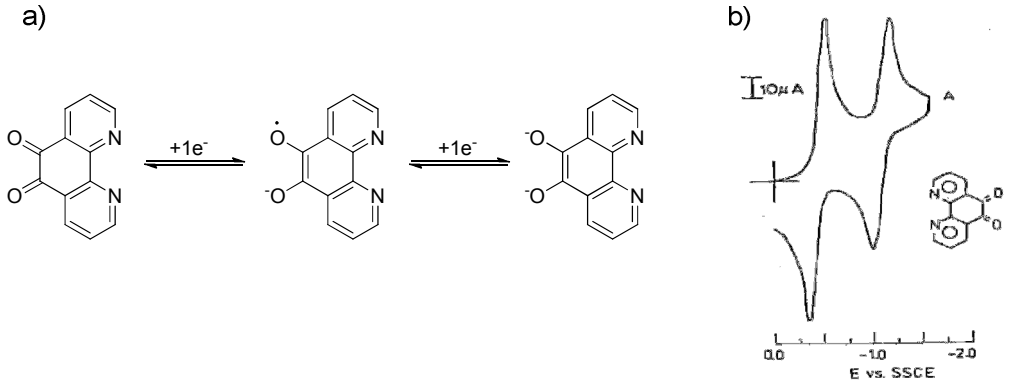

Figure 1.22 a) The reaction pathway of the phendione redox process in aprotic solvent; a) Cyclic voltammogram for 1.2 mM solution of the phen-dione in MeCN containing 0.1 M TBAP at graphite electrode.[127]

In aqueous solvents, the reduction of the quinone to the 5,6-dihydroxy occurs as a two-electron, two-proton process so that only a single, pH-dependent electrochemical wave is observed.

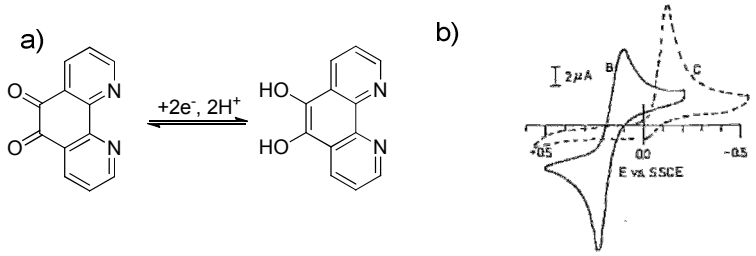

Figure 1.23 a) General scheme of the reversible electrochemical redox reaction of the phendione ligand in aqueous solvent; b) Cyclic voltammograms for 1.1 mM solution of phendione in aqueous solution at pH 2.85 (curve B) and pH 6.8 (curve C) at a Pt electrode and sweep rate 0.2 V s^{-1}.[127]

Abruña *et al.* reported a shift of 63 mV/pH unit in aqueous buffer solution, close to expected value of 59 mV/pH unit for two-electron, two-proton process.[88] At pH > 5, an irreversible reduction peak was observed, which might result from intramolecular complexing of the 5,6-dihydroxy groups and unprotonated imine functionalities through hydrogen bonding (Figure 1.24).[128,129]

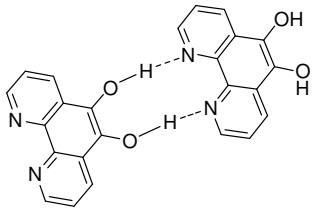

Figure 1.24 Formation of the hydrogen bridge between 5,6-dihydroxy and imine groups of the phendione species as proposed to explain of the irreversible cyclic voltammograms observed at pH>5.[126,129]

The problem of the irreversibility at pH > 5 was overcome by coordinating the imine groups with a transition metal ion to obtain metal complexes. The phendione forms stable metal complexes with a wide range of the transition metal ions, which decreases the electron density within the three ring system of the ligand and shifts redox potential of the quinone groups to more positive values. As a result, such metal complexes potentially allow for the variation of the redox properties of the phendione quinone groups including the tuning of the potential through pH changes.[127]

Examples of the synthesis of metal complexes with phendione ligands and their application for NADH oxidation are reported in the literature. Abruña *et al.*[127] presented the synthesis and electrochemical characterisation of Ru, Co, Fe and Os

complexes with the phendione in the general forms of $[M(phendione)_3]^{2+}$ (Figure 1.25a), $[M(phendione)_2(bpy)]^{2+}$ and $[M(phendione)(bpy)_2]^{2+}$, where bpy is a 2,2'-bipyridine ligand. Cyclic voltammograms of the metal complexes in aprotic solvents showed two waves corresponding to the anion radical and dianion of the quinone group at potentials more positive than for the free phendione ligand. A one electron wave was observed at relatively positive potential from 0.65 V *vs.* SSCE for $[Co(phendione)_3]^{2+}$ to about 1.4 V vs. SSCE for various tris ruthenium complexes bearing from one to three phendione ligands coordinated to the ruthenium metal centre (Figure 1.25b).

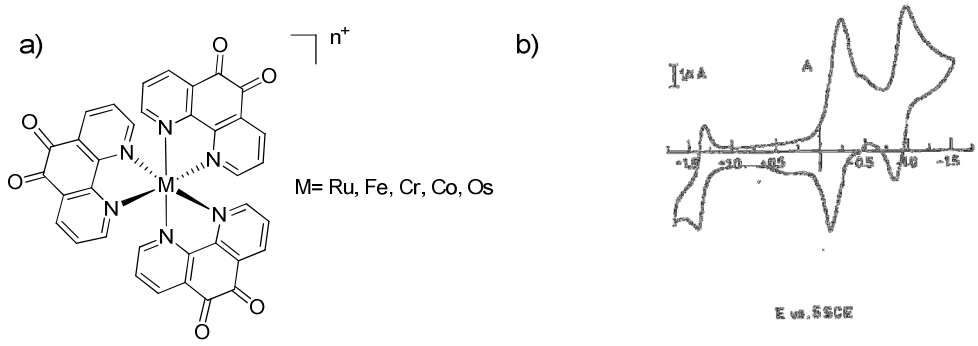

Figure 1.25 a) Structure of the metal complex of general form of $[M(phendione)_3]^{2+}$; b) Typical cyclic voltammogram at a Pt electrode at scan rate of 20 mV s^{-1} for 0.5 M $[Fe(phendione)_3]^{2+}$ in aprotic solvent with 0.1 M TBAP, reported by Abruña et al.[127]

The osmium complexes were adsorbed at the electrode surface and showed significant catalytic activity towards NADH oxidation which decayed with time due to desorption of the complex. The ruthenium complexes in homogenous solution were evaluated as electrocatalysts for NADH oxidation and showed significant catalytic currents at about 0.05 V *vs.* SSCE. In addition, electrocatalytic activity of the $[Ru(phendione)_3]^{2+}$ complex in solution was evaluated in the presence of malate and lactate dehydrogenase enzymes and it was confirmed that this complex works as an effective electrocatalyst for NAD^+ regeneration after an enzyme turnover.[130]

Other examples include osmium and ruthenium complexes with phendione ligand(s) mixed with carbon paste electrodes (CPE), which provide stable and reversible systems for electroxidation of NADH at low overpotential at around 0.1 V and 0.05 *vs.* Ag/AgCl for the osmium and ruthenium complexes, respectively.[131,132] The modified CPEs electrodes were applied for reagentless ethanol biosensors, where Ru and Re complexes with phendione, NADH and alcohol dehydrogenase

were incorporated into the carbon paste and worked effectively as ethanol biosensors.[133]

The metal complexes of general structure $[M(phendione)_3]^{2+}$ (M= Fe, Ru, Co, Cr, Ni) or $[Ru(v\text{-}bpy)_2(phendione)](PF_6)_2$ (v-bpy is 4-vinyl-2,2'-bipyridine ligand) and $[Re(phendione)(CO)_3]^{2+}$ were electrochemically deposited or electropolymerised at the GC surface and worked as effective mediators for NADH oxidation at potentials around 0 V *vs.* SCE.[116] The highest catalytic activities during NADH oxidation were observed for the electrodes with electrodeposited $[Fe(phendione)_3]^{2+}$. This complex also exhibits the fastest kinetics, with a calculated second order rate constant of 5.6×10^3 M^{-1} s^{-1}, probably due to the larger number of the phendione ligands present in comparison to the Re or Ru complexes.

Popescu *et al.*[134] reported a more detailed study on the electrochemical behaviour of osmium complexes with the phendione ligand adsorbed at graphite electrodes and its electrocatalytic activity towards NADH oxidation. As a result, they confirm that the redox process of the phendione is a two electron, two proton reaction with an estimated rate constant for the heterogeneous electron transfer between phendione and the electrode surface of about 20 s^{-1}. In addition, this mediator at the surface exhibits a significant and persistent electrocatalytic activity towards NADH oxidation with calculated values of the second order rate constant about 1.9×10^3 M^{-1} s^{-1}.

1.5 Enzyme kinetics - the Michaelis Menten approximation

In 1905 Henri and Brown reported studies on reactions catalysed by enzymes in which they suggested that the fundamentals accepted at that time for chemical catalysis were not applicable for enzymatic reactions.[76,77,135] Further work by Michaelis and Menten gave an insight into the mechanism of enzymatic reactions. Based on studies of conversion of sucrose catalysed by invertase or saccarase enzymes, they found that the velocity of the enzymatic reaction is dependent on the substrate concentration S, resembling hyperbolic curve (Figure 1.26). They suggested a mechanism, where enzyme E and substrate S first form an intermediate complex ES and this subsequently breaksdown, giving a product P and the free enzyme

$$S+E \underset{k_{-1}}{\overset{k_1}{\rightleftarrows}} SE \xrightarrow{k_2} P+E$$

where k_1, k_{-1} and k_2 represent the rate constants for the individual steps. The theoretical model proposed by Michaelis and Menten was based on the following general assumptions:

- Formation of the ES complex is reversible and reaction between E and S remains in equilibrium. Any effects interfering with this equilibrium are negligible.
- Forward and backward reactions of the intermediate complex ES reaches the equilibrium rapidly and concentration of ES remains constant on the time-scale of the enzymatic reaction (steady-state assumption).
- The substrate S is assumed to be in a great excess over the enzyme E (S >> E), therefore the concentration of free substrate S can be taken as an equal to its initial concentration at every point during the reaction.
- Formation of the product P is a rate determining step ($k_2 << k_1$ and $k_2 << k_{-1}$) and its initial velocity (rate) V_0 equals

$$V_0 = \frac{\mathrm{d}[P]}{\mathrm{d}t} = k_2[ES] \qquad 1.1$$

The total concentration of enzyme [E_0] is a sum of the concentration of free enzyme [E] and the concentration of enzyme bounded to the substrate in [ES] complex

$$[\mathrm{E_0}]=[\mathrm{E}]+[\mathrm{ES}] \quad 1.2$$

The concentration of the intermediate ES is difficult to determine experimentally, therefore a different expression needs to be used in order to calculate values of the initial velocity V_0 of the enzymatic reaction.

When, the reversible formation of ES complex stays in equilibrium, the rate of formation of ES is equal to the rate of consumption of ES:

Velocity of the ES formation:

$$V=\frac{\mathrm{d}[\mathrm{ES}]}{\mathrm{d}t}=k_1\left([\mathrm{E_0}]-[\mathrm{ES}]\right)[\mathrm{S}] \quad 1.3$$

Velocity of the ES breakdown

$$V=\frac{\mathrm{d}[\mathrm{ES}]}{\mathrm{d}t}=k_{-1}[\mathrm{ES}]+k_2[\mathrm{ES}] \quad 1.4$$

Mathematically, this assumption means:

$$k_1\left([\mathrm{E_0}]-[\mathrm{ES}]\right)[\mathrm{S}]=k_{-1}[\mathrm{ES}]+k_2[\mathrm{ES}] \quad 1.5$$

And leads to an expression for the concentration of the intermediate complex [ES]

$$[\mathrm{ES}]=\frac{k_1[\mathrm{E_0}][\mathrm{S}]}{k_1[\mathrm{S}]+k_2+k_{-1}} \quad 1.6$$

Combining this relationship with the expression for velocity of product formation:

$$V_0=\frac{\mathrm{d}[\mathrm{P}]}{\mathrm{d}t}=k_2[\mathrm{ES}]=\frac{k_2[\mathrm{E_0}][\mathrm{S}]}{\frac{k_{-1}+k_2}{k_1}+[\mathrm{S}]} \quad 1.7$$

The equation for the initial velocity of product formation is obtained, known as Michaelis-Menten equation:

$$V_0=V_{\max}\frac{[\mathrm{S}]}{K_\mathrm{M}+[\mathrm{S}]} \quad 1.8$$

where $V_{\max}=k_2[\mathrm{E_0}]$ and it is the maximum velocity of the enzymatic reaction at maximum (saturated) concentration of the substrate. $K_\mathrm{M}=\frac{k_{-1}+k_2}{k_1}$ is a Michaelis-Menten constant (units of mol l^{-1}) and defines a concentration of substrate at half-

maximal rate ($V_0 = \frac{V_{max}}{2}$) (Figure 1.26). In case of slow product formation, the K_M constant reduces to the form of the dissociation constant K_D and can be used as a rough indication of stability of the intermediate complex [ES] (Equation 1.9). When the substrate binds weakly with the enzyme, K_M will have large values and when the substrate binds tightly, the K_M values will decrease.

$$K_D = K_M = \frac{k_{-1}}{k_1}, \text{ if } k_2 << k_{-1} \qquad 1.9$$

Figure 1.26 shows a typical plot of the reaction velocity V as a function of the substrate concentration [S], resembling a hyperbolic curve. In the case when [S] << K_M, the reaction velocity increases linearly with the substrate concentration and the Michaelis-Menten equation is reduced to the form

$$V_0 = \frac{k_2}{K_M}[ES] \qquad 1.10$$

where $\frac{k_2}{K_M}$ is known as a specific rate constant and used in biochemistry to compare the efficiency of different enzymes. Under these conditions, the majority of the enzyme and substrate are free and reaction is considered as bimolecular and the rate of the reaction depends on how efficiently the enzyme can bind to substrate at that concentration. When [S]=K_M, the initial reaction velocity is exactly half the maximum velocity obtained for the enzyme, $V_0 = \frac{V_{max}}{2}$. At high substrate concentrations, [S] >> K_M, all molecules of enzyme are saturated with substrate, therefore the rate has its maximum value and is independent on the substrate concentration, $V = V_{max}$.

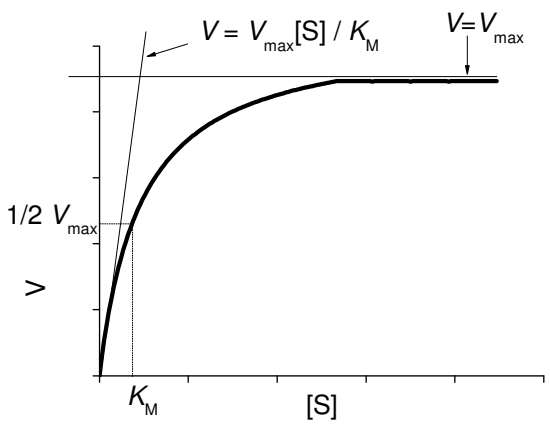

Figure 1.26 Relation between reaction velocity V and the concentration of substrate defined by Equation 1.8.

Values of K_M and k_2 can be determined from graphical representation of the reciprocal forms of the Equation 1.8, yielding straight-line plots and these are often used to obtain K_M and k_2. One of them is the Lineweaver-Burke equation

$$\frac{1}{V_0} = \frac{1}{[S]}\frac{K_M}{V_{max}} + \frac{1}{V_{max}} \qquad 1.11$$

where plotting $1/V$ as a function of $1/[S]$ gives a straight line with intercept equals $\frac{1}{V_{max}}$ and slope $\frac{K_M}{V_{max}}$.

A more common and statistically accurate method to calculate kinetic values of K_M and k_2 for enzymatic reactions obeying the Michaelis-Menten model is to use a non-linear least square fitting routine to directly fit the experimental data to Equation 1.8.

2 Functionalisation of individual GC electrodes

2.1 General

In this project, we are interested in development of new covalently modified carbon electrodes for application in NADH-dependent biosensors. Methodology proposed by Kilburn and Bartlett for covalent functionalisation of glassy carbon (GC) electrodes allows the molecular architecture at the carbon surface to be built up using electrochemical and solid-state synthesis methods (Scheme 2.1).[56,57,136] According to their approach, the initial step of the electrode functionalisation involves electrochemical oxidation of amines or electrochemical reduction of diazonium salts at the electrode surface, leading to formation of a monolayer of the linker at the GC surface. The *mono*-Boc protected amine group of the linker allows for subsequent functionalisation of the GC electrodes using solid-phase synthetic methods. This novel approach towards modification of GC electrodes was successfully applied for introduction of a number of redox active species, including well-known NADH mediators, such as dihydroxybenzene derivatives.[56]

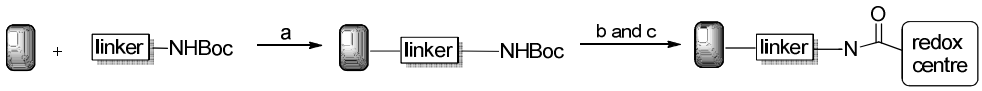

Scheme 2.1 General approach for sequential covalent modification of the GC electrodes developed by Kilburn and Bartlett;[57] a) electrochemical reduction of Boc protected amine diazonium salts or oxidation of *mono*-Boc protected primary diamine; b) removal of the Boc protecting group; c) solid-phase coupling reaction of a redox center at the GC surface.

In this project, we were interested in applying the modification method presented in Scheme 2.1 for covalent attachment of quinone containing structures, reported in the literature as effective mediators for NADH oxidation.[56,99,109] An interesting group of such mediators contain 1,10-phenanthroline-5,6-dione (phendione), a bidentate ligand, coordinated to transition metal ions, which is known to catalyse NADH oxidation at low overpotential when the metal complexes are physically adsorbed at the carbon electrode.[127,130-134] Despite strong adsorption of the phendione at a carbon surface, there was no molecular control over the modified

carbon surface and consequently a risk of decrease in the catalytic activity of the adsorbed metal complex due to desorption from the electrode surface. In order to provide molecular control over the metal complexes with phendione ligand(s) and increase their stability at the electrode surface, the strategy of covalent attachment of the phendione containing metal complexes was proposed (Scheme 2.2). According to this strategy, the *mono*-Boc-protected amine linker was electrochemically attached at the surface followed by coupling of a carboxylic acid-functionalised bidentate ligand using the method optimised previously by Kilburn and Bartlett.[56,57,136] The presence of the bidentate ligand at the GC surface allowed for formation of different metal complexes with the phendione redox active ligand(s). In this way the metal complex containing phendione redox active ligand(s) was covalently immobilised at the electrode surface.

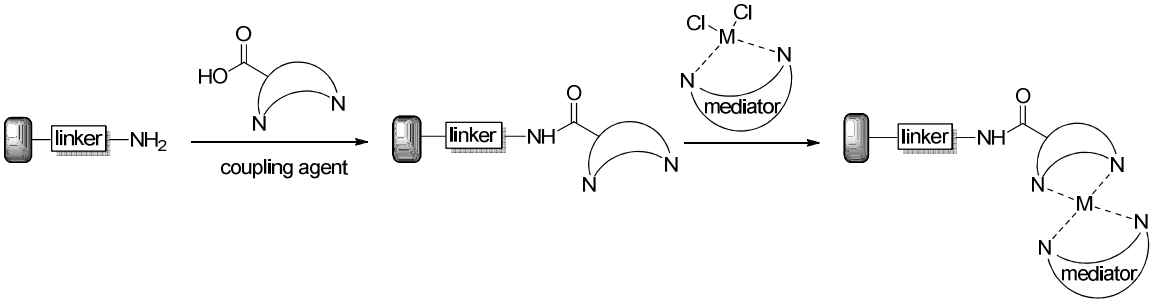

Scheme 2.2 Proposed strategy of covalent immobilisation of metal complexes at the GC electrode using electrochemical and solid-phase coupling conditions.

In this Section, the synthesis of three different octahedral ruthenium complexes containing phendione ligand(s) will be described followed by their electrochemical characterisation in homogenous solution and their covalent attachment to GC electrodes according to the proposed strategy (Scheme 2.2). In order to study the effect of geometry and size of the metal complex, immobilisation of tetrahedral (1,10-phenanthroline-5,6-dione)zinc (II) chloride at the GC electrode was also proposed according to the strategy depicted in Scheme 2.2.

The proposed general strategy of functionalisation of GC electrodes by metal complexes allowed for variation between different linkers, bidentate ligands and metal complexes. Thus, this method was used in further work to design the combinatorial library of modified electrodes followed by HTP screening of the library towards NADH oxidation (Section 3).

2.2 Synthesis of ruthenium complexes with 1,10-phenanthroline-5,6-dione chelating ligand.

Octahedral ruthenium metal complexes with different chelating ligands were synthesised using the well know dichloro*tetrakis*(dimethyl sulphoxide) ruthenium (II) precursor **1**, prepared according to the literature procedure.[137] Reduction of the hydrated ruthenium (III) chloride in neat DMSO gave octahedral complex **1** with chloride ligands in *cis* positions (Scheme 2.3). The structure and geometry of precursor **1** was difficult to determine by NMR due to the fact that the very labile DMSO ligands exchange rapidly with deuterated solvent. A geometrical configuration of the precursor **1** was confirmed by X-ray and clearly shows that the chloride ligands are in *cis* configuration and three molecules of DMSO are coordinated *via* sulfur and one is coordinated through oxygen. This is in good agreement with the literature data, where the distortion in the structure of complex **1** was explained by the steric effect of the methyl groups in DMSO, which prevents all of the DMSO ligands being bonded through sulfur to the ruthenium metal centre.

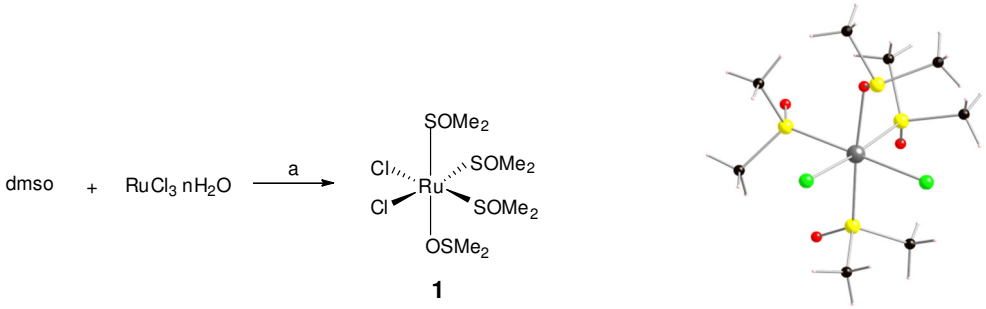

Scheme 2.3 Preparation of the precursor 1 and its X-ray crystallographic structure (right); a) 5 min reflux in neat DMSO under nitrogen, acetone, 52 %.

The precursor **1** was used for synthesis of different octahedral ruthenium complexes with the phendione chelating ligand **2**, which was prepared according to the literature procedure in 60 % yield (*lit.*[138] 86 %). Firstly, two labile DMSO ligands in precursor **1** were replaced with one ligand **2** by mixing one equivalent of the precursor **1** with one equivalent of the ligand **2** in inert solvent. Literature reported reactions between precursor **1** and different nitrogen and phosphorous ligands were performed in nonpolar inert solvents, such as chloroform and toluene.[139] In this case, ethanol was

chosen as the reaction solvent due to low solubility of the ligand **2** in non-polar solvents. The reaction progress was monitored by ^{1}H NMR at intervals of one hour. After 14 h the reaction was completed and characteristic protons of the starting materials **2** were not present in the ^{1}H NMR spectrum. The product was precipitated as a brown microcrystalline solid. Literature examples of the precursor **1** with various nitrogen and phosphorus chelating ligands indicated that displacement of weaker *O*-bonded DMSO ligand in precursor **1** presumably occurs first, followed by displacement of a *S*-bonded DMSO ligand in the *trans* position.[137,140] The precursor **1** obtained as the *cis* isomer in respect to two chloride ligands led to formation of the complex **3** also in the *cis* geometrical configuration, which was confirmed by NMR analysis. The ^{1}H NMR spectrum showed the presence of six resonance peaks in the aromatic region, which correspond to six non-equivalent protons of the phendione ligands in the *cis* position to chlorine and DMSO ligand and the other site being in the *trans* position to the other monodentate ligands. In addition, three singlets between 3.43 and 2.33 ppm, corresponding to twelve protons of methyl groups, confirm the presence of DMSO ligands in the complex **3**.

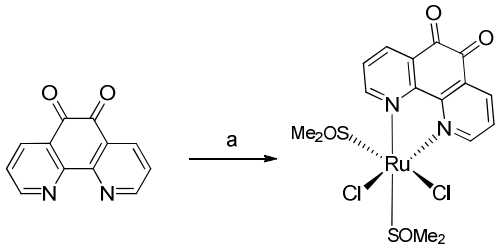

2 **3**

Scheme 2.4 Preparation of complex **3**; a) precursor **1**, ethanol, reflux, 14 h, 60 %.

Literature examples of the metal complexes containing redox-active phendione ligands were studied for their electrocatalytic activity towards NADH oxidation. Abruña *et al.*[127] reported preparation and evaluation of the electrochemical and catalytic properties of complexes of general form $[M(phendione)_3]^{2+}$. Cyclic voltammetry of these complexes in aqueous solution showed reversible electrochemical behaviour corresponding to quinone functional groups at middle peak potential E_{mp} of 0.15 V *vs.* SSCE.[127] A similar result was observed by cycling a 1 mM aqueous solution of the complex **3** (Figure 2.1) in the potential range from −0.5 to 0.3 V *vs.* SCE, which shows the reversible redox process of the quinone functionality at a middle peak potential E_{mp} of −0.18 V *vs.* SCE. The presence of the

peak corresponding to the Ru^{II}/Ru^{III} redox couple was not observed in the chosen potential range. According to studies by Lever[141] coordination of monodentate ligands such as DMSO shifts the potential of the ruthenium Ru^{II}/Ru^{III} redox couple to more positive values of about 1.2 V *vs.* SHE in aqueous solution. In the case of carbon electrodes this peak might overlap with the region corresponding to oxidation of the carbon surface.

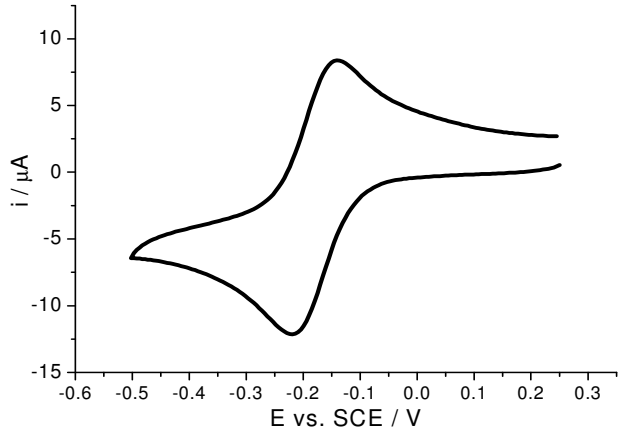

Figure 2.1 Cyclic voltammogram of 1 mM solution of complex **3** in 0.1 M phosphate buffer solution pH 7 at scan rate of 50 mV s^{-1} and GC electrode geometrical surface area of 0.071 cm^2.

The *cis* configuration of chlorine atoms in complex **3** allowed for isomerically controlled substitution of the remaining two DMSO ligands in **3** by one molecule of 2,2'-bipyridyl chelating ligand, using reaction conditions proposed by Grätzel *et al.*.[142] Complex **3** was mixed with one equivalent of the 2,2'-bipyridine ligand in DMF and the reaction mixture was heated under reflux (Scheme 2.5). DMF was chosen as a reaction solvent in order to increase solubility of the complex **3** and the reaction temperature in order to apply higher energy required to displace two DMSO ligands by one more stable 2,2'-bipyridyl chelating ligand.[140] Undesired *cis-trans* isomerisation during complex formation was prevented by performing the reaction under reduced light. Pure *cis*-(2,2'-bipyridyl)(1,10-phenanthroline-5,6-dione)ruthenium (II) chloride complex **4** was obtained after precipitation from methanol. The *cis* geometry of complex **4** was confirmed by NMR analysis. No resonance peaks corresponding to methyl groups of the DMSO ligands were observed, which would suggest that two remaining DMSO ligands in the complex **3**

were completely replaced by one 2,2'-bipyridyl ligand. The ^{1}H NMR spectrum indicated that the two chelating ligands are *trans*, which was indicated as fourteen different resonance peaks in the aromatic region.

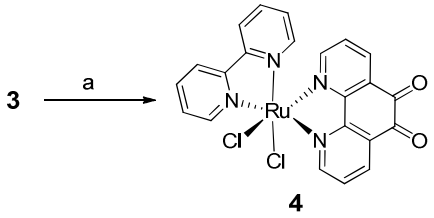

Scheme 2.5 Synthesis of the complex **4**; a) 2,2'-bipyridine, DMF, reflux 4 h, reduced light, 60 %.

Complex **4** was electrochemically characterised in aqueous and non-aqueous solutions (Figure 2.2). The cyclic voltammogram of complex **4** in phosphate buffer solution indicates the presence of a reversible redox couple at a value of E_{mp} of −0.06 V *vs.* SCE, which corresponds to the 2e^{-} redox process of quinone in the phendione ligand.[127] A broad, reversible redox peak at potential of 0.35 V *vs.* SCE suggests the presence of Ru^{II}/Ru^{III} redox couple, which is in good agreement with the theoretical potential values of 0.3 V vs. SHE calculated for the Ru^{II}/Ru^{III} redox center in similar metal complexes according to Lever.[141] Figure 2.2b shows the cyclic voltammogram of the complex **4** in acetonitrile solution, which clearly indicates the presence of two reversible redox peaks at −0.05 and −0.7 V *vs.* Ag/AgCl and corresponds to the one electron, two step redox process of the phendione ligand. At a relatively positive potential of 0.6 V *vs.* Ag/AgCl, one electron redox process of Ru^{II}/Ru^{III} was observed. In addition, at a potential of −1.5 V *vs.* Ag/AgCl, a redox couple was also observed, which might correspond to the 2,2'-bipyridyl ligand. Results of the electrochemical screening of complex **4** in non-aqueous solution are in good agreement with those reported by Abruña *et al.* for similar *bis* and *tris* ruthenium complexes.[127]

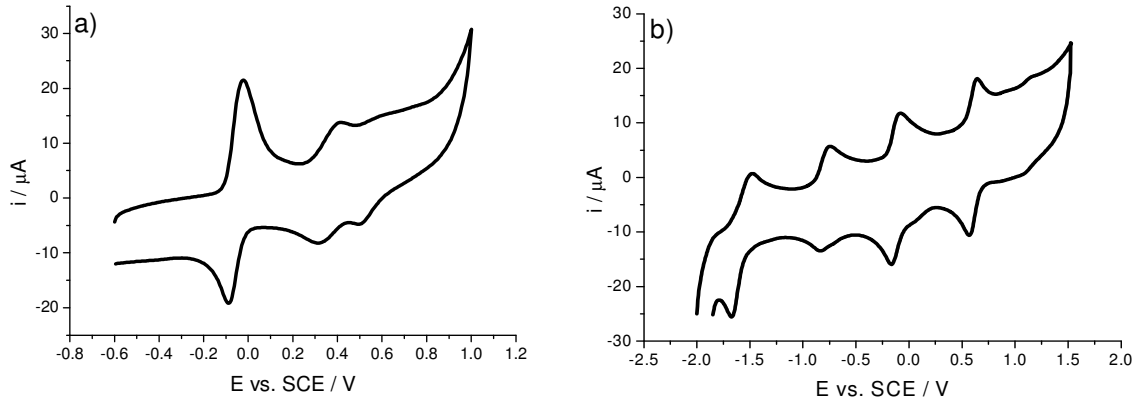

Figure 2.2 Cyclic voltammograms of 1 mM solution of complex **4** at GC electrode (geometrical electrode area of 0.071 cm^2); a) in 0.1 M phosphate buffer solution pH 7 at scan rate of 50 mV s^{-1}; b) in acetonitrile with 0.1 M TBATFB at scan rate of 50 mV s^{-1}.

Finally, precursor **1** was used for synthesis of the octahedral complex *bis*(1,10-phenanthroline-5,6-dione)ruthenium (II) chloride **5**. In this case, addition of two equivalents of the ligand **2** to one equivalent of the precursor **1** in DMF was found to be an effective method for displacement of four DMSO ligands in **1** with two phendione chelating ligands in a single reaction step (Scheme 2.6). Complex **5** was successfully prepared using the same reaction conditions as for formation of the *bis* complex **4** and obtained in 33 % yield as the *cis* isomer with respect to the chlorine ligands. The geometry of complex **5** was confirmed by NMR analysis. The ^{1}H NMR spectrum of **5** shows six resonance peaks in the aromatic region, which correspond to six non-equivalent proton of two mutually adjacent sites of the *trans* phendione ligands.

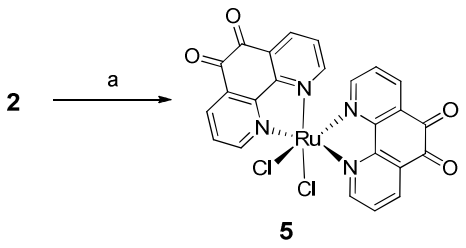

5

Scheme 2.6 Preparation of complex **5**; a) precursor **1**, DMF, reflux 4 h, 33 %.

The precipitated complex **5** shows very low solubility in aqueous and non-aqueous solvents at room temperature, therefore electrochemical characterisation of complex **5** in either aqueous or non-aqueous solution was unsuccessful.

2.3 Attachment of bis-(dimethyl sulphoxide)(1,10-phenanthroline-5,6-dione) ruthenium (II) chloride complex at the GC surface.

Ruthenium complexes **3**, **4** and **5** were applied in the following work for functionalisation of GC electrodes according to the strategy proposed in Scheme 2.2 and evaluated towards NADH catalytic oxidation. The first part of this work involved optimisation of solid-phase reaction conditions for attachment of the complexes **3**, **4** and **5** at the GC electrodes. Each GC electrode was polished on dry silicone-carbide paper (grade 1200) directly prior to modifications, and the polishing process was carried out in the same manner for all GC electrodes discussed below.

According to the proposed strategy for multistep sequential functionalisation of the GC electrodes by various metal complexes (Scheme 2.2), the first step of the modification involved electrochemical attachment of linkers at the blank GC electrodes by electroxidation of primary amines to create a stable N-C bond between the electrode surface and the linker.[56,57,136] Initially, *mono*-Boc protected ethylenediamine (EDA) **6** was chosen as a linker due to relatively high surface coverage obtained for modifications with the linker **6** reported in the literature.[57] The linker **6** was covalently tethered at the blank GC electrode according to the literature procedure, resulting in formation of a monolayer of the mono-*Boc*-EDA at the electrode surface (Figure 2.3). Linker **6** was oxidised at the GC surface by cycling the potential in the range 0 to 2.25 *vs.* SCE. During the initial cycle, a significant oxidation peak at a potential of 1.8 V *vs.* Ag/AgCl was observed, corresponding to formation of an intermediate amine radical in solution and its reaction with carbon atoms at the GC electrode surface. Decrease of the current with following cycles indicates that the electrode surface was blocked by the linker **6**, resulting in formation of the full monolayer of **6** at the GC surface.

It is well known that oxidation of the *mono*-Boc protected diamines at the GC surface prevents formation of bridge structures, where both amine groups are attached at the surface.[57] In addition, presence of the Boc-protected amine at the GC surface allows for control over subsequent chemical steps carried out under solid-phase conditions.

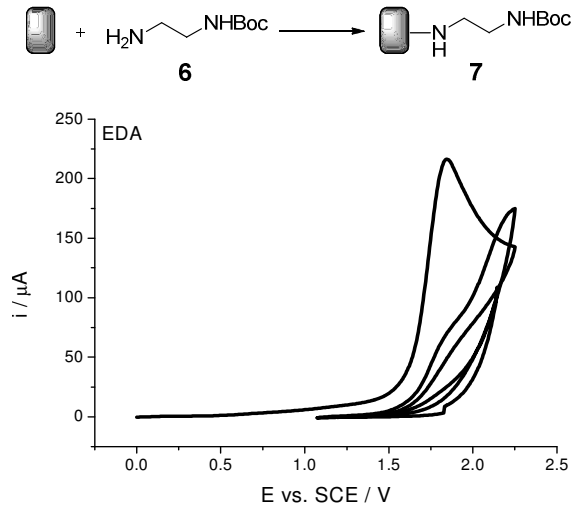

Figure 2.3 Oxidation of linker **6** at the polished GC electrode with geometrical area of 0.071 cm^2; general reaction scheme and cyclic voltammogram for attachment of mono-*Boc*-EDA linker **6** (below) recorded in 10 mL of 15 mM solution of **6** in acetonitrile with 0.1 M TBATFB, from 0 to 2.25 V vs. Ag/AgCl at scan rate of 50 mV s^{-1}.

The Boc protecting group was cleanly removed from the modified electrode **7** using the literature procedure,[57] resulting in free primary amine groups at the electrode surface. According to the proposed strategy (Scheme 2.2) the free amine groups allowed for subsequent introduction of a chelating ligand at the GC surface under solid-phase conditions for amide formation. Initial work involved functionalisation of the GC electrodes with 2,2'-bipyridyl ligand, known to create stable metal complexes with a large number of transition metals. In this work, the 2,2'-bipyirdine chelating ligand was functionalised with a carboxylic acid group **9** in order to covalently immobilise the ligand at the modified electrode **7**. Toy *et a.l*[143] reported preparation of the 2,2'-bipyridine chelating ligand **9** using Kröhnke synthesis of unsymmetrically functionalised 2,2'-bipyridines (Scheme 2.7).[144]

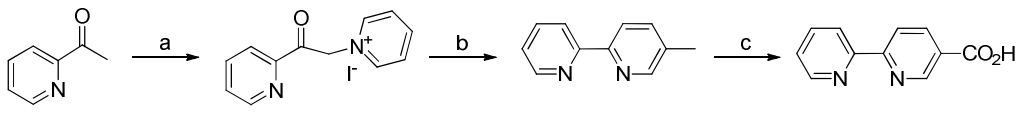

Scheme 2.7 Synthesis of 2,2-bipyridine-5-carboxylic acid **9** according to the literature procedure reported by Toy *et al.*[143;] a) pyridine, iodine, 90 °C, 6 h, 55 %; b) methacrolein, NH_4OAc, formamide, 80 °C, overnight, 90 %; c) potassium permanganate, H_2O, HCl, 70 – 90 °C, 7 h, 55 %.

Ligand **9** was successfully obtained in three steps using this literature procedure in 60 % yield (lit.[143] 80 %) and covalently immobilised at the modified electrode **8**

under solid-phase peptide coupling conditions using HBTU as a coupling reagent. The modified electrode **10** was prepared under solid-phase reaction conditions optimised for covalent attachment of anthraquinone-2-carboxylic acid (AQ) as reported by Kilburn and Bartlett.[56,57,136]

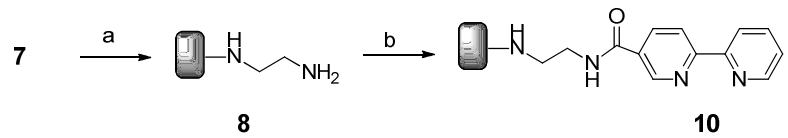

Scheme 2.8 Removal of Boc protecting group from electrode **7** followed by solid-phase coupling of the ligand **9**; a) 4.0 M hydrochloric acid in 1,4-dioxane, 1 h, b) HBTU, DIPEA, DMF, 16 h, room temperature.

The yield of solid-phase coupling of the ligand **9** to the electrode **8** was difficult to determine directly by electrochemical methods. Cyclic voltammograms of the electrode **10** performed in aqueous and nonaqueous solvents did not show redox peaks which could correspond to the 2,2'-bipyridine ligand at the GC surface. Efficiency of this coupling reaction was determined by performing an experiment, where the modified electrodes **7** and **10** were both dipped in the same solution of complex **3** and heated overnight. The resulting modified electrodes were screened by cyclic voltammetry and showed significant presence of the quinone groups at a potential of 0 V *vs*. SCE. In case of the electrode **10**, a relatively high number of the quinone groups were observed in comparison with the electrode with *mono*-Boc protected EDA linker **7** (Figure 2.4). This would suggest that 2,2'-bipyridine at the electrode **10** coordinates to the ruthenium metal ion in complex **3**, resulting in formation of a new ruthenium complex at the electrode surface. For electrode **7**, negligible amount of the complex was present at the electrode surface, which might be rationalised by physical adsorption of this complex at the carbon surface. This control experiment confirmed that the 2,2'-bipyridine was successfully attached at the electrode surface and coordinated to the ruthenium metal ion.

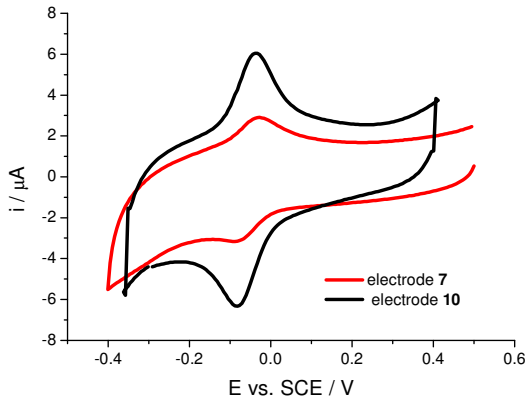

Figure 2.4 Cyclic voltammograms obtained after heating of electrodes **7** (red) and 10 (black) in a solution of the complex **3** in 0.1 M phosphate buffer pH 7 at a scan rate of 50 mV s^{-1} for electrodes with geometrical surface area of 0.071 cm^2.

The final step of functionalisation of the GC electrodes involved coordination of the ruthenium complexes **3**, **4** and **5** to the bipyridyl ligand present at the electrode **10**. Initial experiments involved coordination of complex **3** at modified electrode **10**. Solid-phase coordination of the bipyridyl ligand to ruthenium was carried out by dipping electrode **10** in a solution of complex **3** in DMF. In this case, DMF was chosen as the reaction solvent due to high solubility of the complex **3** and was reported in the literature for formation of different *tris* and *bis* ruthenium complexes.[139,140] The solid-phase reaction conditions, including temperature, concentration of **3** solution and reaction time were optimised as shown in Scheme 2.9.

The effect of different reaction conditions on the yield of attachment of complex **3** at the GC electrode was determined by calculating the surface coverage Γ_{med} of the redox active quinone groups present at the surface. Values of Γ_{med} were estimated from the charge (Q) obtained by the integration of the area under the oxidation and reduction peak in cyclic voltammograms according to Faraday's law

$$\Gamma_{med} = Q/nFA\rho \qquad 2.1$$

where n equals 2 is the number of electrons transferred, F is the Faraday's constant, A is the electrode area and ρ is the roughness of the electrode. A roughness factor of 4 was used in all calculations as this was reported previously for GC electrodes polished in the same manner.[55,57]

Firstly, attachment of complex **3** at the GC surface was performed at three different concentrations of **3** (0.5, 0.1, 0.01 M). Calculated values of Γ_{med} increased with lower concentration of complex **3** (Scheme 2.9). The effect of the reaction temperature on values of Γ_{med} was evaluated by performing the solid-phase coordination reaction at three different temperatures. It was observed that coordination of the 2,2'-bipyridyl present at electrode **10** to the ruthenium metal ion in complex **3** at room temperature was not effective, the cyclic voltammogram of modified electrode **11** prepared at room temperature did not show peaks corresponding to the quinone groups in **3**. Increasing the temperature of the solid-phase coordination process to 80 or 100 °C for modified electrodes **12** and **13** induced the coordination of the 2,2'-bipyridine to the ruthenium metal centre in **3**. Reversible redox processes at 0 V *vs.* SCE were observed for both and values of Γ_{med} of 0.08 and 0.09 nmol cm^{-2} were estimated for **12** and **13**, respectively. For modified electrodes **14** and **15**, where solid-phase reactions were carried out under reflux in DMF for 4 and 16 h, cyclic voltammograms did not show the redox peaks expected for the quinone redox process. The high temperature of the reaction mixture might cause decomposition of the EDA linker at the surface and prevents coordination of **3** to the surface.

From data on octahedral osmium complexes, coverage of 1×10^{-10} mol cm^{-2} represents a monolayer of the osmium complex at the electrode surface.[145] The value of Γ_{med} obtained for modified electrode **13** is closest to the theoretical literature value of a full monolayer of the octahedral complex. For this reason, the reaction conditions applied during modification of electrode **13** were used in further work involving formation of the complex A.

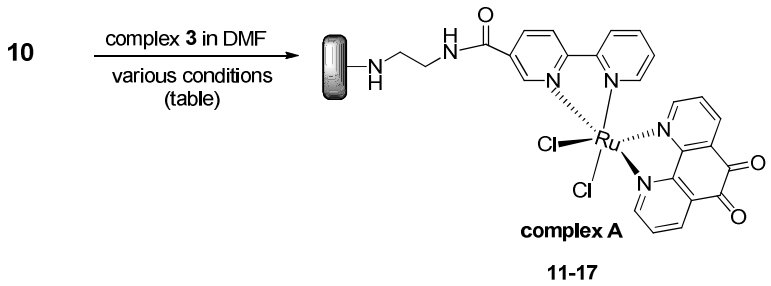

Electrode number	Concentration of complex 3 / mol L^{-1}	Temperature / °C	Time / h	Surface coverage Γ_{med} / nmol cm^{-2}
11	0.1	R.T.	16	No quinones present
12	0.1	80	16	0.081
13	0.1	100	16	0.087
14	0.1	reflux	4	No quinones present
15	0.1	reflux	16	No quinones present
16	0.5	80	16	0.055
17	0.01	100	16	0.11

Scheme 2.9 Optimisation process of the attachment of the complex **3** at the modified electrode **10** under solid-phase reaction conditions.

Modified electrode **17**, which gave the highest calculated values of Γ_{med}, was evaluated towards catalytic oxidation of NADH. The cyclic voltammogram (Figure 2.5) of electrode **17**, recorded in presence of 1 mM NADH, showed a catalytic anodic peak at 0 V *vs.* SCE. This suggests that the phendione at the surface reduced the overpotential by approximate 0.4 V relative to oxidation of NADH at the bare carbon electrode occurring at a potential of 0.4 V *vs.* SCE.[93,146] Presence of NADH peak was shifted by about 40 mV to more positive potential in comparison to the potential of the mediator. This might be caused by slow reaction rate between quinones at the surface and NADH in solution.[97,110]

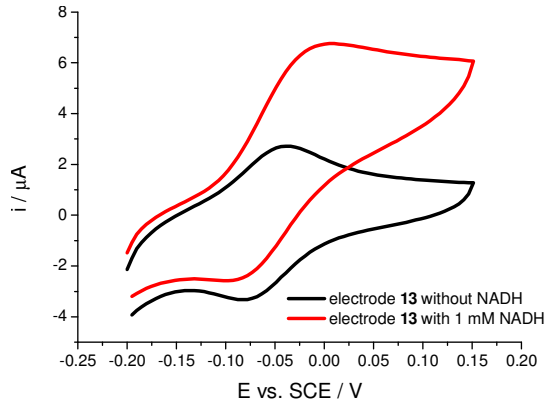

Figure 2.5 Cyclic voltammograms of modified electrode **17** in the presence (red) and absence (black) of 1 mM NADH in 0.1 M phosphate buffer solution pH 7 at a scan rate of 50 mV s^{-1} (geometrical electrode area of 0.071 cm^2).

Based on the successful preparation of the initial modified electrode **17**, the same reaction conditions were applied for covalent attachment of the complex **3** at the GC surface through six different linkers in order to investigate the effect of the structure and length of the linker on the catalytic activity of complex A towards NADH oxidation.

The choice of linker was based on work reported by Bartlett *et al.*[57] describing functionalisation of GC electrodes by AQ redox probe covalently attached at the surface through linkers with various aliphatic chain lengths and structures. Electrochemical characterisation of AQ modified electrodes clearly showed that length and structure of the linker have an impact on surface coverage of the AQ at GC surface and electron transfer kinetics between the AQ redox center and electrode surface.[57] To our best knowledge, the effect of different linkers on NADH electrocatalytic activity for the electrodes modified according to the methodology developed by Bartlett and Kilburn was not reported.

Therefore, covalent attachment of complex A through linkers with different length and structures was proposed in order to evaluate effect of linker on electrochemical and catalytic properties of complex A at the surface.

Based on the successful preparation of the electrode **17** modified with EDA linker, aliphatic diamine linkers with increased chain lengths were chosen, including *mono*-N-Boc-butanediamine (BDA) **18** and *mono*-Boc-1,6-hexanediamine (HDA) **19**. Different lengths of the linker might affect accessibility of complex A during electrocatalytic oxidation of the bulky molecule of NADH in solution. In order to

investigate the structure of diamine linkers, hydrophilic *mono*-Boc-2,2'-(ethylenedioxy)diethylamine chain (EDDA) **20** and aromatic *mono*-Boc-*p*-xylenediamine (XDA) **21** were selected and applied for covalent attachment of the complex **3** according to the strategy proposed in Scheme 2.2.

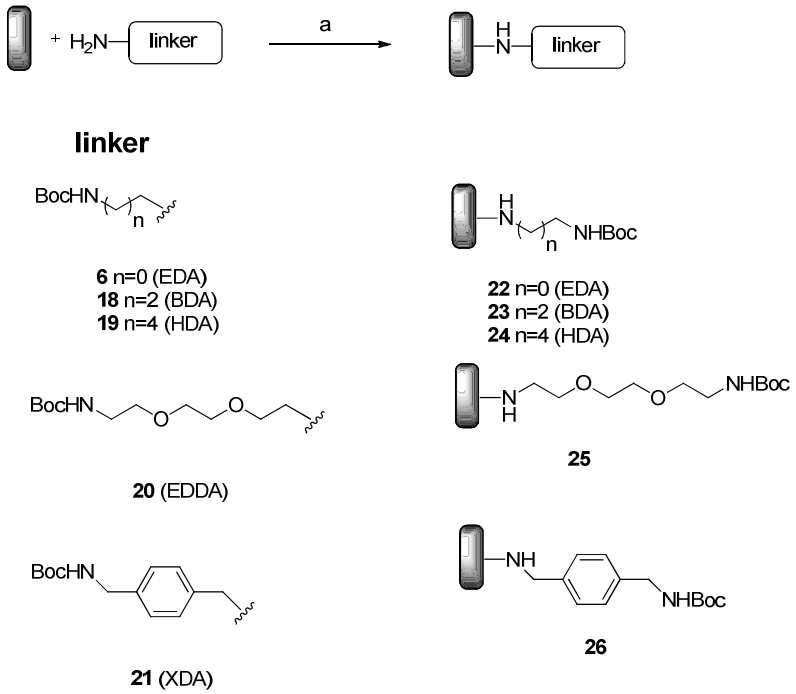

Scheme 2.10 Covalent attachment of linkers **6** and **18-21** at the GC electrodes; a) applied potential from 0 to 2.25 V vs. Ag/AgCl in 15 mM solution of the linker in acetonitrile with 0.1 M TBATFB at scan rate of 50 mV s^{-1}.

Mono-N-Boc protected diamines were electrochemically oxidised at the GC electrode by applying potential range from 0 to 2.25 V *vs.* Ag/AgCl. Figure 2.6 shows an example of a cyclic voltammogram recorded for oxidation of linker **20** at blank GC electrode. Similarly as for attachment of the linker **6**, an oxidation peak at 1.8 V *vs.* Ag/AgCl was observed, corresponding to formation of the amine radical, which reacts with sp^2 carbon atoms at GC and leads to a stable carbon-nitrogen bond at the surface. Decrease of the oxidation current observed in the subsequent scans suggests blocking of the surface with the linker **20**, which is consistent with the result obtained for modification of the electrode with **6** (Figure 2.3), where a full monolayer of the EDA was obtained after three scans. The same cyclic

voltammograms were obtained during oxidation of diamine linkers **18-21** and full monolayer of the linker attached at GC surface was obtained after 3-5 cycles.

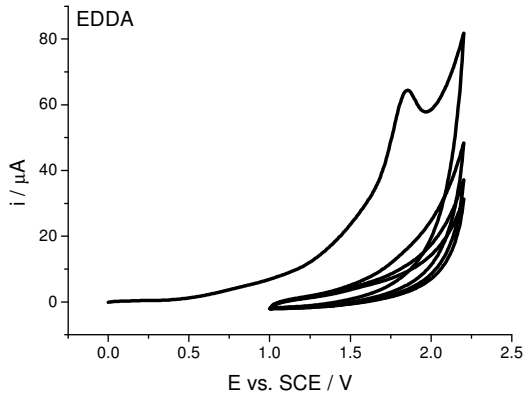

Figure 2.6 Cyclic voltammogram recorded in 15 mM solution of linker **20** in acetonitrile with 0.1 M TBATFB at scan rate of 50 mV s^{-1} at GC surface with geometrical area of 0.071 cm^2.

The versatile methodology for functionalisation of the GC electrodes developed by Bartlett and Kilburn also included covalent attachment of linker using electrochemical reduction of a diazonium salt, which is well known in the literature as an effective method for formation of stable C-C bond between organic molecules and the carbon surface.[64,65,73,74] Electrochemical reduction of 4-(*N*-Boc-aminomethyl)benzene diazonium tetrabluoroborate salt allowed for covalent immobilisation of the AQ according to the methodology developed by Bartlett and Kilburn (Scheme 2.1).[55] In this project, diazonium salt linker **27** was prepared according to literature procedures[147,148] in two steps synthesis (Scheme 2.11).

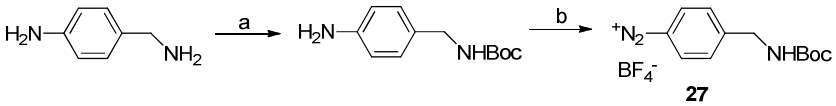

Scheme 2.11 Two steps synthesis of diazonium salt linker **27** perpared according to the literature procedures[147,148]; a) $(Boc)_2O$, DCM, overnight, room temperature, 46 %; b) $NaNO_2$, 40% solution of HBF_4, 1 h, 45 %.

Linker **27** was electrochemically reduced at the GC electrode by applying the potential from 0.6 to −1 V *vs.* Ag/AgCl in non-aqueous solvent. Scheme 2.12 shows example of the cyclic voltammogram recorded for electrochemical reduction of the linker **27** where the broad, irreversible reduction peak occurring at a potential of −0.5 V corresponds to formation of the aromatic radical and formation of stable carbon-

carbon bond with sp^2 atoms at the GC. Subsequent cycling in the same solution showed disappearance of the cathodic wave and this corresponds to fully blocked surface by the organic layer. It is believed that presence of the bulky Boc-protecting group in the C-4 position of the linker **21** prevents formation of multilayers of the aromatic rings at the electrode surface.[65,74,75]

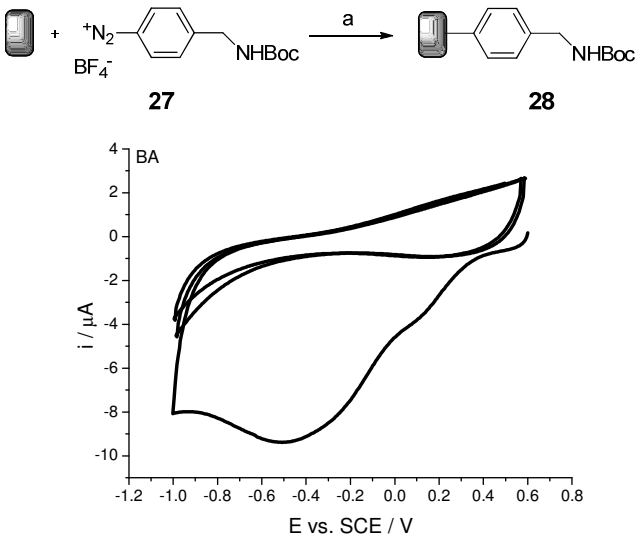

Scheme 2.12 Attachment of linker **27** at the GC electrode; general scheme and cyclic voltammogram of the electrochemical reduction of 15 mM solution of **27** in acetonitrile with 0.1 M TBATFB at scan rate of 50 mV s^{-1} at GC electrode with geometrical electrode area of 0.071 cm^2.

The presence of the protected amine functional groups at the modified electrodes **21-26** allowed for following functionalisation of these electrodes under solid-phase conditions according to the strategy proposed in Scheme 2.2 in order to covalently immobilise complex **3** at the GC electrodes. Three subsequent solid-phase synthetic steps, involving removal of the Boc protecting group, coupling of ligand **9** and formation of complex A at the electrode surface, were carried out under the same reaction conditions as for preparation of electrode **17** (Scheme 2.13). Each of the electrodes **22-26** and **28** were functionalised individually in separate reaction vessels to give electrodes **17** and **35-39,** modified with six different linkers, ligand **9** and complex A.

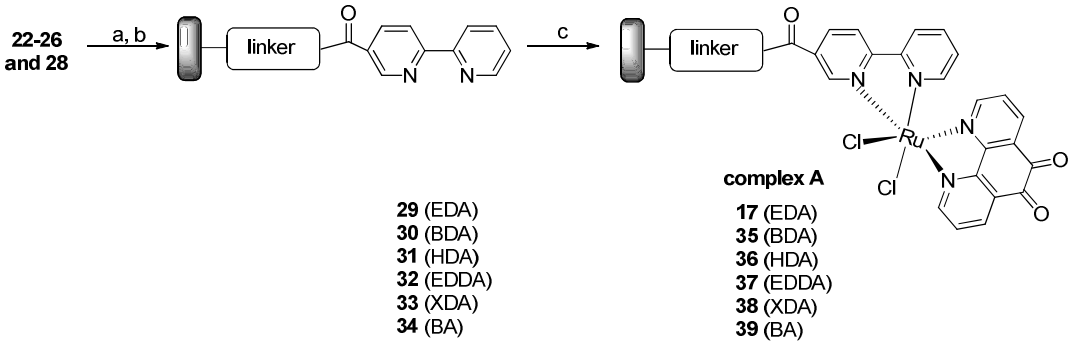

Scheme 2.13 Solid-phase modifications of the electrodes **22-26** and **28**; a) 4.0 M hydrochloric acid in 1,4-dioxane, b) ligand **9**, DMF, HBTU, DIEA, room temperature, 16 h, c) complex **3**, DMF, 100 °C, 16 h.

The modified electrodes **17** and **35-39** were individually characterised using cyclic voltammetry in phosphate buffer solution pH 7. Firstly, each modified electrode was cycled over potential range −0.2 to 0.15 V *vs.* SCE (Figure 2.7). A two electron, reversible redox process was observed for all electrodes modified with the different linkers. Minor changes were observed for the redox midpeak potentials (E_{mp}) between electrodes **17** and **35-39** with an average values of −50 mV *vs.* SCE. Thus, the type of linker does not have a significant effect on thermodynamics for the redox process of complex A at the electrode surface. Similarly, only minor changes were observed in peak potential separation (ΔE_p) between modifications **17** and **35-39** with an average value of 40 mV *vs.* SCE between different linkers at scan rate of 50 mV s^{-1}. This would suggest that the type of linker does not affect the kinetics of electron transfer between the GC surface and complex A.

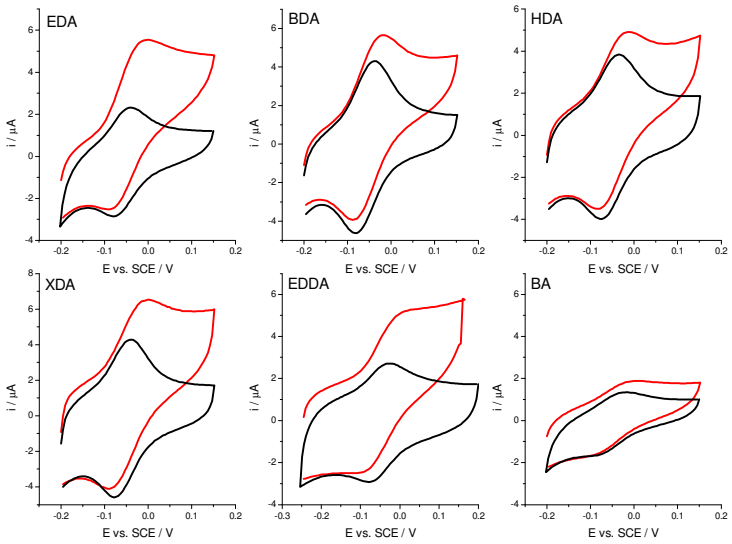

Figure 2.7 Examples of cyclic voltammograms of the modified electrodes **17** and **35-39** in the presence (red) and absence (black) of 1 mM NADH in 0.1 M phosphate buffer solution pH 7 at scan rate of 50 mV s^{-1} (geometrical electrode area of 0.071 cm^2).

The efficiency of formation of complex A attached through different types of linkers was compared by calculations of surface coverages, Γ_{med}, of the phendione using Equation 2.1. Figure 2.8 shows a summary of the values of Γ_{med} calculated for electrodes **17** and **35-39**. For aliphatic diamine linkers, values of Γ_{med} tend to decrease with increasing length of the aliphatic chain, with the highest coverage obtained for EDA and BDA linkers. Relatively low values of Γ_{med} were found for electrodes modified with long HDA and EDDA linkers. This might be rationalised by the fact that the long aliphatic chain in the diamine linker might cause a conformational disorder within the chains and hinder the access of the free amine group to the carbon surface and prevent the amine from being covalently attached to the GC surface.[149] This might result in lower coverage in the subsequent steps of solid-phase coupling of **9** and coordination of complex **3**. In addition, relatively low values of Γ_{med} were obtained for the aromatic diamine linkers XDA and BA. The lowest value of coverage was observed for the complex A attached at the surface through the benzylamine linker (BA). The rigid structure of the aromatic ring directly attached at the GC might limit access of the 2,2-bipyridine to bulky complex A, resulting in low coverage of complex A.

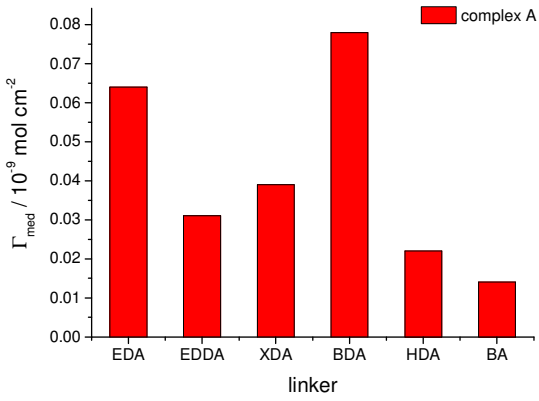

Figure 2.8 Values of Γ_{med} calculated for modified electrodes **17** and **35**-**39**; Each bar represents mean values of Γ_{med} calculated according to Equation 2.1. Each bar represents mean value of Γ_{med} and standard error of the mean of three replicate modified electrodes.

Modified electrodes **17** and **35-39** were evaluated one by one towards NADH catalytic activity by cycling the electrodes in 1 mM NADH solution at pH 7. In the presence of NADH, all of electrodes **17** and **35-39** show a catalytic anodic peak at 0 V vs. SCE, which is consistent with result obtained for initial experiments at electrode **17**. Values of i_{cat} were measured as a difference between the current with NADH and the current without NADH at potential of 0.15 V *vs.* SCE, where all of the mediator is in its oxidised form and allowed for measurement of the catalytic current generated only by NADH.

In general, significant values of i_{cat} were recorded for modifications with diamine linkers and they are comparable with values of i_{cat} found for modification with XDA and EDDA. The lowest value of i_{cat} was recorded for the modification with BA, which might limit access of the phendione mediators at the electrode surface to the bulky NADH molecule in the solution. The values of i_{cat} recorded for the electrode **17** and **35-39** strongly depends on surface coverage of the phendione. In order to calculate efficiency between the modifications **17** and **35-39**, normalised catalytic currents i_{norm} were calculated according to equation

$$i_{norm} = \frac{i_{cat}}{[\text{NADH}]\,\Gamma_{med}} \qquad 2.2$$

where [NADH] is the concentration of the NADH in solution, Γ_{med} is the surface coverage and i_{cat} is the catalytic current. As significant value of i_{norm} was obtained for the electrodes **36** and **37** with long HDA and EDDA linkers, which might enhance

access of the phendione to the folded, bulky molecule of the NADH in solution. In addition, the hydrophilic character of the EDDA linker might enable better interactions of the anionic NADH molecule and surface of the modified electrode **37**. Significant catalytic efficiency was also observed for the electrode with XDA linker, which would indicate that the aromatic structure of this linker increases catalytic efficiency of electrode **38** during NADH oxidation.

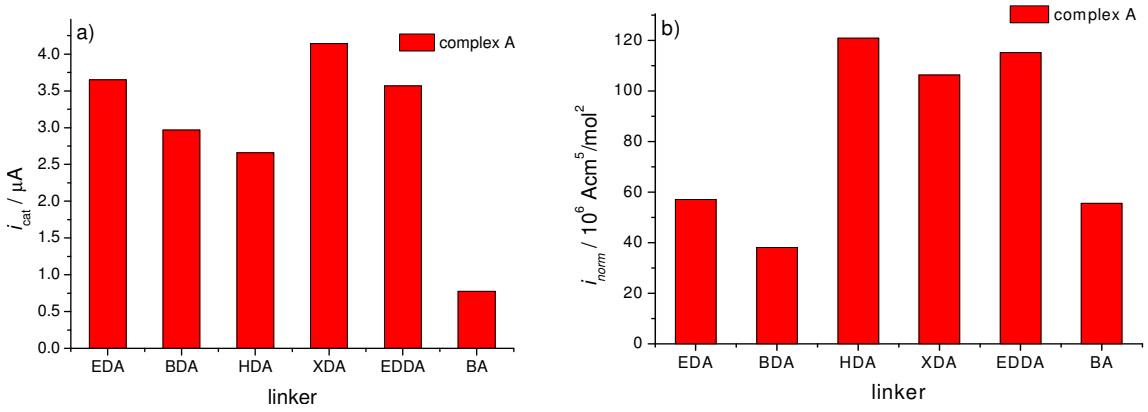

Figure 2.9 a) Catalytic current i_{cat} for modified electrodes **17** and **35-39** recorded in 1 mM NADH solution in 0.1 M phosphate buffer pH 7 at scan rate of 50 mV s^{-1}; b) Normalised catalytic currents i_{norm} for the modified electrodes **17** and **35-39** calculated according to Equation 2.2; Each bar represents mean values of i_{cat} (a) or i_{norm} (b) calculated for a single modified electrode.

In summary, complex **3** was successfully attached at GC through six different linkers according to the proposed strategy, involving electrochemical and solid-phase methodology. All of the modified electrodes showed the presence of the quinone groups, which confirmed formation of the complex A at the electrode surface. A series of the electrodes modified with the complex A attached at the surface through six different linkers showed that length and structure of the linker have an effect on the surface coverage of the complex A and its catalytic activity towards NADH oxidation.

2.4 Attachment of (2,2'-bipyridine)(1,10-phenanthroline-5,6-dione) ruthenium (II) chloride complex at the GC surface.

In order to investigate the effect of different ligands coordinated to the ruthenium metal centre on the NADH catalytic activity of the phendione ligand, complex **4** was covalently attached at the electrode surface according to the strategy proposed in Scheme 2.2. This strategy involved three steps electrochemical and solid-phase synthesis and was successfully applied for modification of the GC electrodes with complex **3** (Section 2.1). Firstly, electrode **10** bearing the EDA linker and ligand **9** was prepared under reaction conditions reported in Section 2.3. The presence of 2,2'-bipyridine ligand at the electrode surface enabled formation of the stable, *tris* ruthenium complex B at the GC by coordination of the 2,2'-bipyridine to the ruthenium metal centre in complex **4** (Scheme 2.14).

Reaction conditions for the final step involving solid-phase formation of complex B on the surface were optimised. Literature reported formation of *tris* ruthenium complexes, where two chloride ligands are displaced by one chelating ligand, were performed under reflux in order to force exchange of the chloride ligands by one molecule of 2,2'-bipyridine.[142] Solid-phase coordination at electrode **10** was carried out in 0.01 M solution of **4**, based on results obtained for optimisation of reaction conditions for attachment of **3** (Section 2.3). The formation of complex B at electrode **10** was initially performed by dissolving complex **4** in a mixture of methanol and water (1 : 1) and heating under reflux overnight.[142] Electrochemical characterisation of electrode **39** indicated that complex B was formed at the GC surface with relatively low coverage of 0.5×10^{-10} mol cm^{-2} in comparison with the theoretical coverage of 1×10^{-10} mol cm^{-2} reported for related octahedral osmium complexes.[145] Formation of complex B in dry DMF solvent for the same reaction time and maintaining reaction temperature at 100 °C gave a coverage of 0.072 mol cm^{-2} for modified electrode **40**. This might suggests that presence of water in the reaction decreases the yield for the attachment of complex B at electrode **10**.

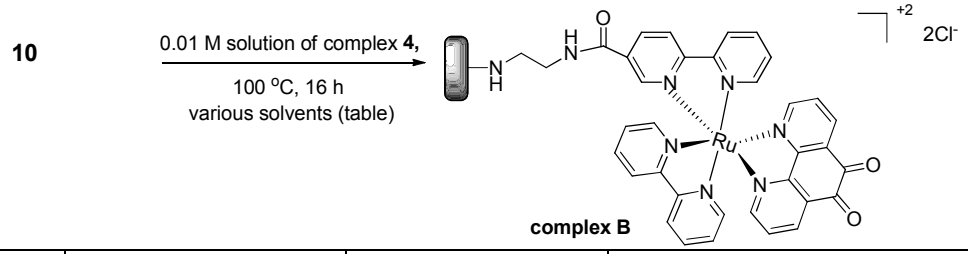

Electrode number	Solvent	Temperature/ °C	Surface coverage Γ_{med} / nmol cm^{-2}
40	methanol/water (1 :1)	Reflux	0.055
41	dry DMF	100	0.072

Scheme 2.14 Optimisation process of the synthesis of complex B at modified electrode **10**.

Modified electrode **41** was evaluated for electrocatalytic activity by screening in 1 mM aqueous solution of NADH. The cyclic voltammetry of electrode **41** in the presence of NADH clearly shows a catalytic anodic process at 0 V *vs.* SCE, which is in good agreement with the potential obtained for complex A and suggests electrocatalysis occurring during NADH oxidation (Figure 2.10).

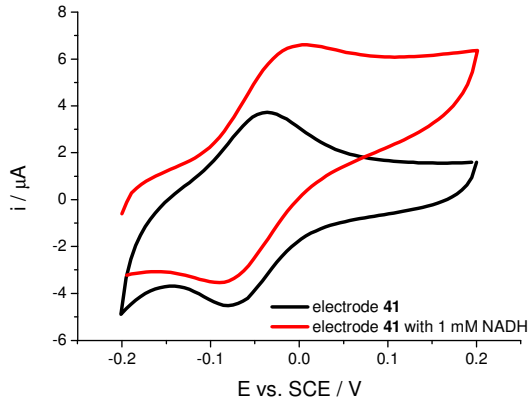

Figure 2.10 Example of cyclic voltammograms of modified electrode **41** recorded in the presence (red) and absence (black) of 1 mM NADH solution in 0.1 M phosphate buffer pH 7 at a scan rate of 50 mV s^{-1} and geometrical electrode area of 0.071 cm^2.

In order to investigate the effect of different linkers at the surface coverage and NADH catalytic activity of complex B, complex **4** was coordinated at modified electrodes **29-34** under solid-phase conditions as optimised for modified electrode **41**. Choice of the linker and functionalisation of the GC electrodes with these linkers was described in detail in Section 2.3. The final step of coordination of complex **4** at electrodes **29-34** was carried out under reaction conditions as optimised for electrode

40 (Scheme 2.15). Each electrode was prepared in individual reaction vessels and characterised one by one using cyclic voltammetry.

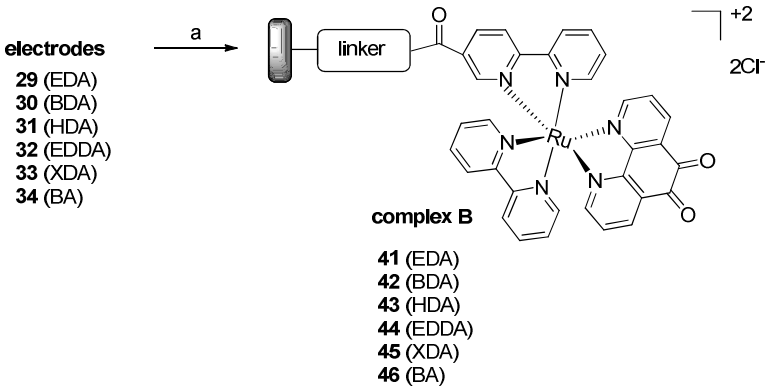

Scheme 2.15 Attachment of complex **4** at electrodes **29-34** functionalised by six different linkers; Each modified electrode **41-46** was prepared individually under the same solid-phase reaction conditions a) 0.01 M of complex **4** in dry DMF, 100 °C, 16 h.

Firstly, electrodes **41-46** were electrochemically screened in phosphate buffer over potential range −0.2 to 0.2 V vs. SCE and reversible, two electrons redox process was observed for all of the modified electrodes (Figure 2.11), which confirms presence of immobilised phendione containing complex B at the electrode surface. Minor changes in values of E_{mp} were observed for modifications with complex B attached at the surface through six different linkers with calculated average value of E_{mp} −65 mV *vs.* SCE. This result is consistent with E_{mp} calculated for series of modified electrodes with complex A, where minor differences in the middle peak potential between modifications **41-46** would suggest that changes in structure and length of the linker does not affect thermodynamics of electron transfer between complex B containing phendione and electrode surface. In addition, similar values of E_{mp} obtained between series of modified electrodes A and B would indicate that presence of different ligands, chloride in complex A and 2,2'-bipyridyl in complex B, does not appear to have a significant effect on the thermodynamics of redox process of the phendione redox centre.

In order to compare effect of different linkers on kinetics of electron transfer between electrode surface and complex B, potential peaks separation ΔE_p were calculated for electrodes **41-46**. Similarly as for series of electrodes with complex A, minor differences in ΔE_p were observed between **41-46**. This clearly suggests, that length and structure of linker does not affect the kinetics of electron transfer for complex B

attached at the surface through six different linkers. In comparison with series of modified electrodes with complex A, the presence of 2,2'-bipyridine in complex B decreases the kinetics of electron transfer with an average value of ΔE_p of 50 mV for electrodes **41-46**.

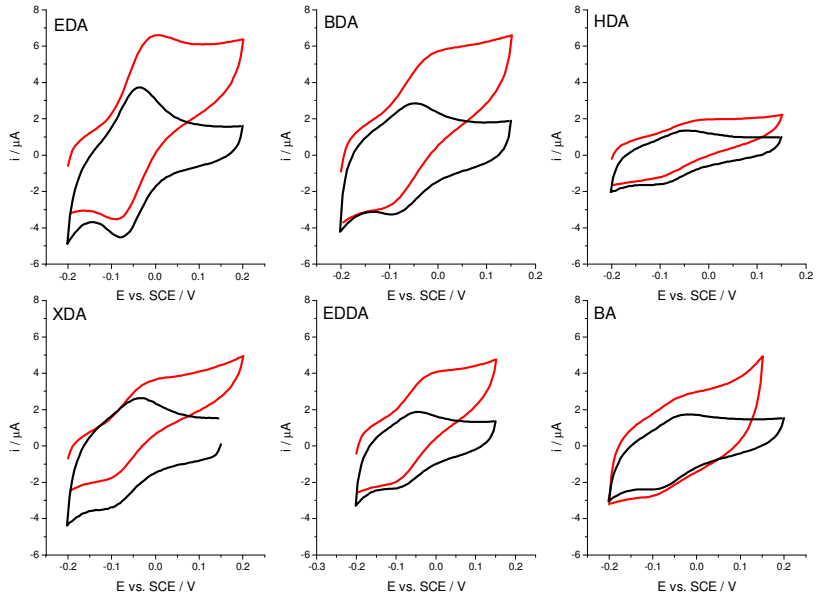

Figure 2.11 Examples of cyclic voltammograms recorded for the electrodes **40-45** modified with complex B attached at the GC surface through six different linkers in presence (red) and absence (black) of 1 mM NADH solution in 0.1 M phosphate buffer pH 7 at a scan rate of 50 mV s^{-1} and geometrical electrode area of 0.071 cm^2.

The efficiency of the formation of complex B attached at the surface through different linkers was compared by calculation of the surface coverage Γ_{med} according to Equation 2.1. In general, values of Γ_{med} calculated for electrodes **41-46** are relatively low in comparison with the coverage obtained for modifications with complex A. This might be rationalised by the displacement of two chloride ligands by bulky 2,2'-bipyridine ligand in complex B, causing steric hindrace and decreasing the amount of complex **4** coordinated to 2,2'-bipyridine at electrode **10**. The effect of the type of linkage on values of Γ_{med} for electrodes modified with complex B was in good agreement with coverages calculated for the series of modified electrodes A (Section 2.3). For short aliphatic linkers EDA and BDA, values of Γ_{med} are relatively high in comparison with the coverages obtained for longer HDA and EDDA linkers

(Figure 2.12). Relatively low values of Γ_{med} were observed for modifications with the aromatic linkers XDA and BA.

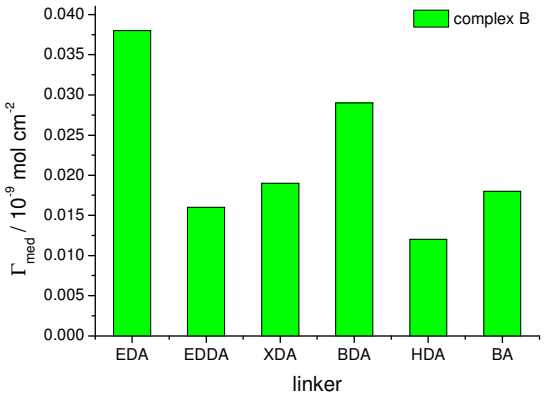

Figure 2.12 Values of surface coverage Γ_{med} of complex B calculated for modified electrodes **41-46** based on experimental data obtained from the cyclic voltammograms depicted in Figure 2.11. Each bar represents mean values of Γ_{med} calculated according to Equation 2.1. Each bar represents value of Γ_{med} obtained for a single modified electrode.

Each of the modified electrodes **41-46** was evaluated towards electrocatalytic activity for NADH oxidation by cycling the electrodes one by one in 1 mM NADH solution. For all electrodes **41-46** a catalytic anodic peak was observed at 0 V *vs.* SCE. Values of catalytic currents i_{cat} measured at 0.15 V *vs.* SCE were compared between electrodes **41-46** (Figure 2.13a). Significant values of i_{cat} were observed for the short aliphatic EDA and BDA linkers and decrease with increasing length of the linkers as was observed for modifications **43** and **44**. There was minor difference in catalytic currents recorded for the two aromatic linkers XDA and BA.

The catalytic efficiency of electrodes **41-46** was evaluated by calculation of the normalised catalytic currents i_{norm} as shown for the series of modified electrodes A, which was calculated according to Equation 2.2. Significant catalytic efficiency was obtained for the electrode with complex B attached at the surface through the long EDDA linker, which would suggest that the long polyethoxy linker provides better accessibility of the phendione ligands at the surface to bulky molecules of the NADH in solution (Figure 2.13b). In contrast, relatively low values of i_{norm} were calculated for electrode **46**, modified with the BA linker, where the rigid structure of the linker might limit access of the quinone redox group to active site of the folded, bulky molecule of NADH in solution. Despite relatively low coverages obtained for

modified electrodes **41-46**, values of i_{norm} obtained for complex B are significantly higher in comparison to values of i_{norm} calculated for the series of modified electrodes with complex A. This suggests that the presence of the chelating ligand in the complex B increases the catalytic activity of the modified electrodes towards NADH oxidation.

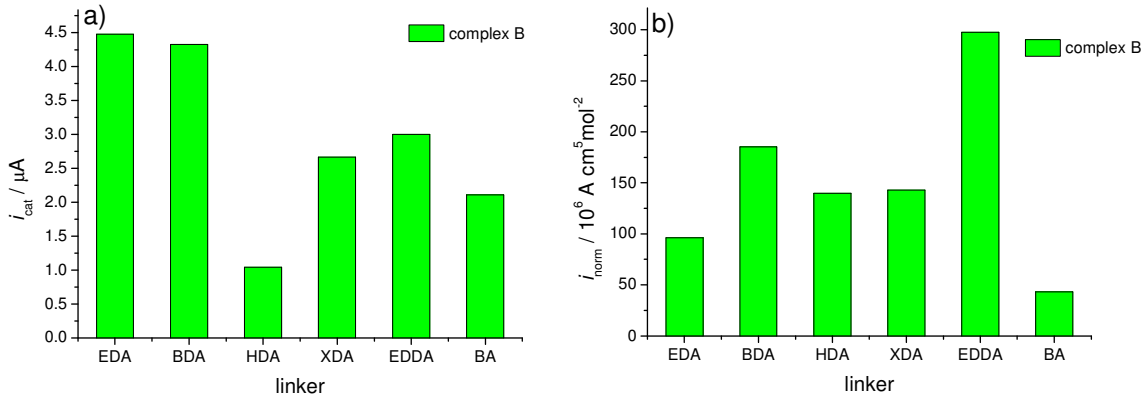

Figure 2.13 a) Catalytic currents i_{cat} recorded for modified electrodes **41-46** in the presence of 1 mM NADH in 0.1 M phosphate buffer solution pH 7 at a scan rate of 50 mV s^{-1}; b) Normalised catalytic currents inorm calculated for electrodes **41-46** according to Equation 2.2. Each bar represents values of i_{cat} (a) or i_{norm} (b) obtained for single modified electrode.

2.5 Attachment of *bis*-(1,10-phenanthroline-5,6-dione)$_2$ ruthenium (II) chloride complex at GC surface.

Based on the successful preparation of the series of electrodes modified with complexes A and B, complex **5** bearing two phendione redox active ligands was also immobilised at the GC surface according to the strategy proposed in Scheme 2.2. Firstly, modified electrode **10** was prepared by electrochemical attachment of EDA linker following by coupling of ligand **9** under solid-phase peptide coupling conditions (Scheme 2.8).

During the final step, the two chloride ligands in complex **5** were replaced by the 2,2'-bipyridine at electrode **10** and the novel *tris* ruthenium complex C was formed at the GC. Reaction conditions optimised for preparation of the similar *tris* complex B were also applied for formation of complex C (Scheme 2.15), bearing two phendione redox active ligands. The cyclic voltammogram in Figure 2.14 clearly shows the presence of a reversible redox process at E_{mp} of 57 mV *vs.* SCE, corresponding to oxidation/reduction of the phendione redox centre. The coverage, Γ_{med}, of complex C at electrode **47** was calculated using Equation 2.1. The calculated value of Γ_{med} of 0.059 nmol cm^{-2} (for n = 4) for electrode **46** is in good agreement with the coverage obtained for electrode **41**, modified with EDA linker and *tris* complex B. The cyclic voltammetry of electrode **47** in 1 mM NADH solution shows significant catalytic current at 0 V *vs.* SCE. This suggests that the phendione in complex C acts as an effective mediator towards NADH oxidation and decreases the overpotential of the oxidation of NADH by about 0.4 V, which is in good agreement with results obtained for complexes A and B. The catalytic current, i_{cat}, recorded at 0.15 V *vs.* SCE is significantly higher than the current obtained for electrode **40** modified with complex B. This would suggest that the increased number of redox active phendione ligands enhances the catalytic activity towards NADH oxidation.

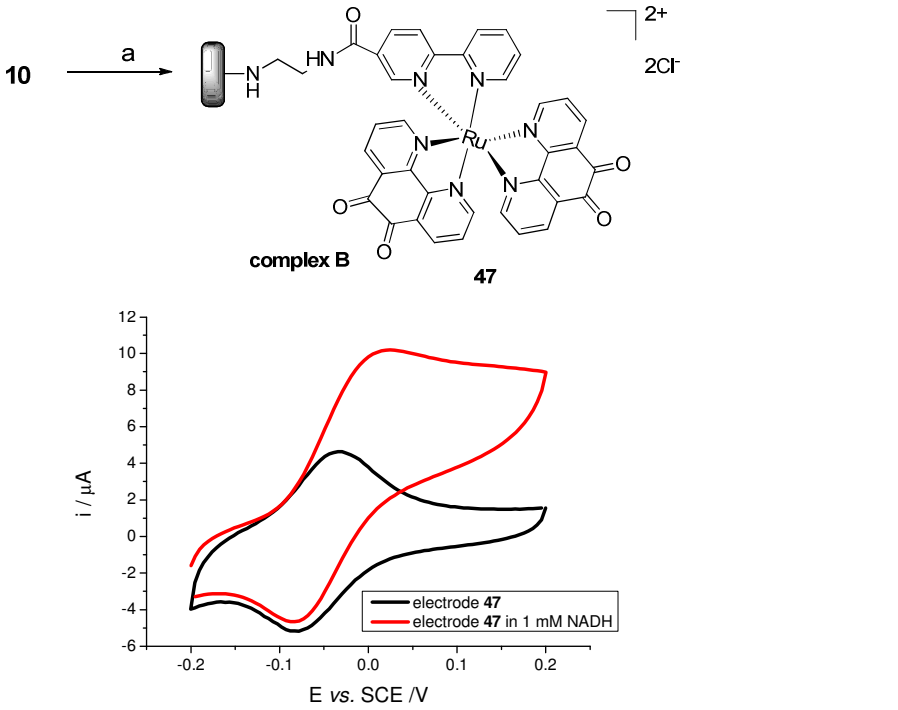

Figure 2.14 Attachment of complex **5** at electrode 10; a) 0.01 M of complex **5** in dry DMF, 100 °C, 16 h; Cyclic voltammograms of electrode **47** recorded in the presence (red) and absence (black) of 1 mM NADH solution in 0.1 M phosphate buffer pH 7 at a scan rate of 50 mV s^{-1} and geometrical electrode area of 0.071 cm^2.

Successful formation of complex C at GC was followed by preparation of a series of electrodes modified with six different linkers as described for the series of electrodes with complexes A and B (Scheme 2.16). Each of modified electrodes **47-52** was prepared in an individual reaction vessel under the same solid-phase reaction conditions and characterised, one by one, using cyclic voltammetry.

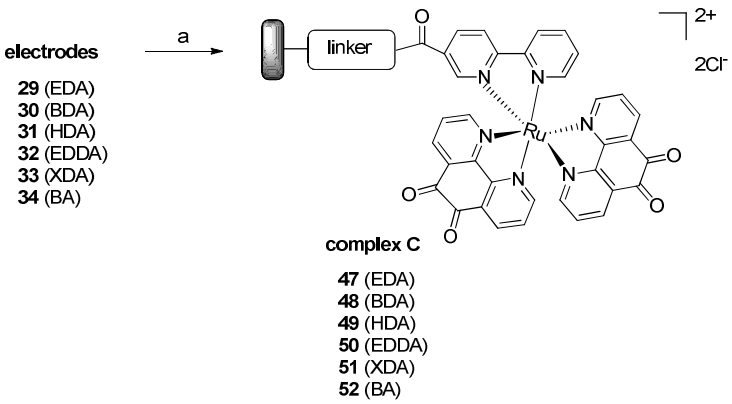

Scheme 2.16 Attachment of complex **5** at electrodes **29-34**; Each modified electrode **47-52** was prepared individually under the same solid-phase conditions a) 0.01 M of complex **5** in dry DMF, 100 °C, 16 h.

Figure 2.15 shows cyclic voltammograms for electrodes **47**-**52** cycled over the potential range −0.2 to 0.2 V *vs.* SCE. The quinone redox peak was observed at an average value of E_{mp} of 50 mV vs. SCE for all of the electrodes. Similarly as for complexes A and B, the type of linkage does not affect the values of E_{mp} for the phendione coordinated to the ruthenium metal centre. An average value of peak separation ΔE_p of 50 mV measured at a scan rate of 50 mV s^{-1} was obtained for electrodes modified with the different linkers. This result is in good agreement with the peak separations obtained for the series of complexes A and B, which would suggest that the additional phendione ligand in complex C does not have an impact on the kinetics of electron transfer between the electrode surface and complex C.

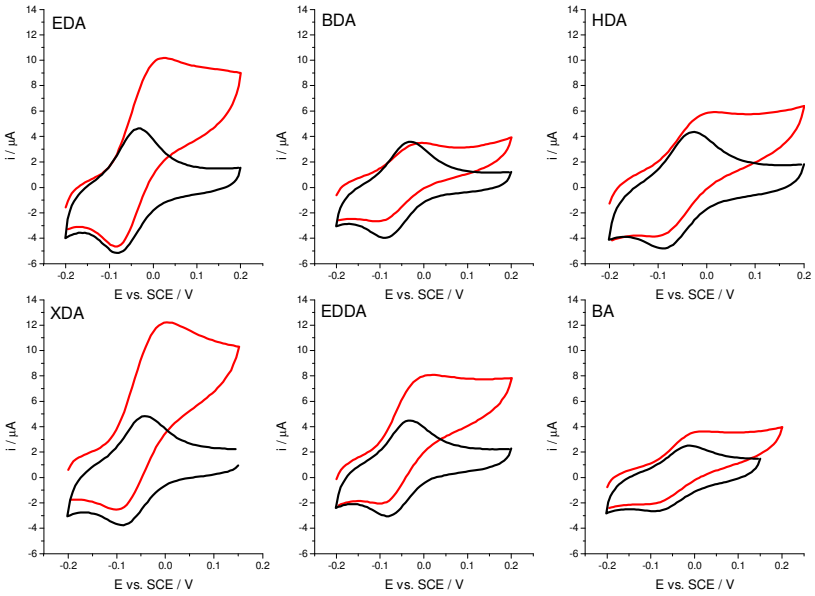

Figure 2.15 Cyclic voltammograms recorded for electrodes **47-52** modified with complex C attached at GC surface through six different linkers in the presence (red) and absence (black) of 1 mM NADH solution in 0.1 M phosphate buffer pH 7 at a scan rate of 50 mV s^{-1} and geometrical electrode area of 0.071 cm^2.

The cyclic voltammograms obtained for electrodes **47**-**52** in phosphate buffer solution allowed for evaluation of the coverage of complex C and evaluation of the effect of the type of linkage on values of Γ_{med}. Figure 2.16 presents values of Γ_{med} for complex C attached at GC through different linkers and clearly shows that significant coverage was obtained for the short aliphatic linkers EDA and BDA. Decrease of Γ_{med} was observed for linkers with longer chains EDDA and HDA, which is consistent with values of Γ_{med} obtained for electrodes modified with complexes A and B. Relatively low coverage was obtained for modification **52**, where the rigid structure of the BA linker might decrease number of 2,2'-bipyridine ligands accessible to coordinate to the rather bulky complex **5**.

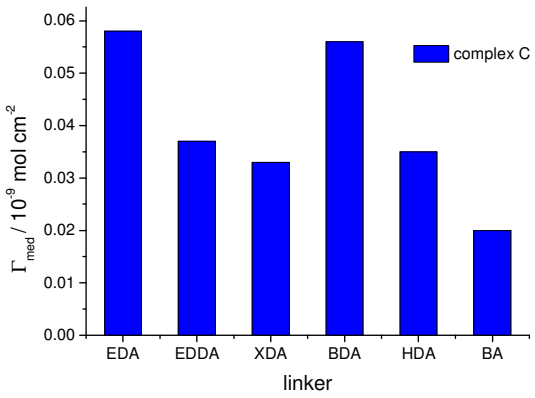

Figure 2.16 Values of surface coverage Γ_{med} of complex C calculated for modified electrodes **47-52** based on experimental data obtained from cyclic voltammograms presented in Figure 2.15. Each bar represents mean values of Γ_{med} calculated according to Equation 2.1. Each bar represents value of Γ_{med} obtained for a single modified electrode.

Electrodes **47-52** were evaluated towards NADH catalytic activity by cycling each of the modified electrodes in 1 mM NADH solution (Figure 2.15). Figure 2.17a presents a summary of the catalytic currents, i_{cat}, recorded at 0.15 V *vs.* SCE for modifications with six different linkers. Significant values of i_{cat} were observed for electrodes bearing the aliphatic EDA linker and the aromatic linker XDA. However, relatively low value of i_{cat} was found for modification with the BDA linker, which was not observed for complexes A and B modified with this linker. Low value of i_{cat} was observed for modification **52**, where the rigid BA linker might decrease access of the two phendione ligands in complex C to folded, bulky molecule of NADH in solution.

In order to compare the catalytic efficiency between electrodes **47**-**52**, normalised catalytic currents, i_{norm}, were calculated using Equation 2.2. High values of i_{norm} were obtained for linkers with aliphatic chains such as EDA or EDDA, which suggests that more flexible linkers would increase access of complex C to the bulky NADH molecules in solution (Figure 2.17a). However, calculated i_{norm} for modification with the BDA linker gave relatively low values of i_{norm} in comparison to other linkers. Similarly as shown for complexes A and B, the rigid BA linker decreases the electrocatalytic efficiency of complex C at the surface due to steric hindrance of the bulky complex C, resulting in limited access of the phendione ligands to NADH molecules in a solution.

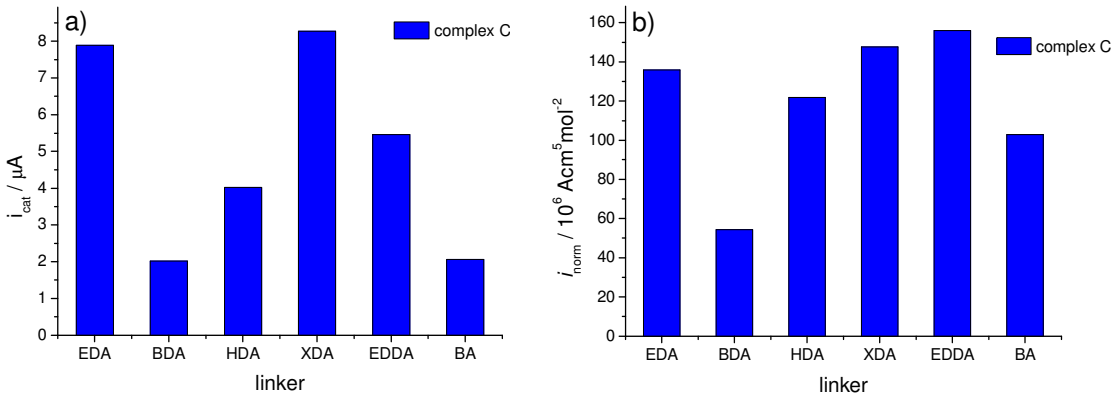

Figure 2.17 a) Catalytic currents icat recorded for modified electrodes **47-52** in the presence of 1 mM NADH in 0.1 M phosphate buffer solution pH 7 at a scan rate of 50 mV s^{-1}; b) Normalised catalytic currents inorm calculated for electrodes **47-52** according to Equation 2.2. Each bar represents values of i_{cat} (a) or i_{norm} (b) obtained for single modified electrode.

2.6 Covalent modification of GC electrodes by (1,10-phenanthroline-5,6-dione)zinc (II) chloride complex.

Successful attachment of ruthenium complexes **3**, **4** and **5** and their catalytic activity towards NADH oxidation at the functionalised GC electrode showed that the design of carbon electrodes proposed in Scheme 2.2 can be applied for introduction of different ruthenium metal complexes containing the phendione redox ligand. The presence of three different ruthenium complexes A, B and C attached at the surface through six different linkers allowed for studies of different octahedral metal complexes and different linkers on the catalytic activity of the phendione ligand(s) towards NADH oxidation.

In order to study the effect of the geometry of complex and different transition metal on surface coverage and NADH catalytic activity, synthesis of tetrahedral zinc complex with the phendione ligand at the electrode was proposed using the strategy shown in Scheme 2.2. Firstly, the tetrahedral (1,10-phenanthroline-5,6-dione)zinc (II) chloride complex **53** was prepared according to literature procedure reported by Boghaei *et al.* and obtained in 60 % yield (lit.[150] 85 %). The structure of **53** was confirmed by NMR analysis and compared with literature data. ^{1}H NMR spectrum showed three resonance peaks in the aromatic region, which corresponds to three equivalent protons in the phendione. NMR data obtained for **53** are in good agreement with experimental data reported in the literature.

Complex **53** was covalently tethered at electrode **10** by replacing two chlorine ligands by one bipyridyl at electrode **10** to form the new, tetrahedral zinc comp00lex D (Figure 2.18). Initially, the literature procedure for synthesis of (2,2'-bipyridine)(1,10-phenanthroline-5,6-dione)zinc (II) hexafluorophosphate complex was applied for formation of complex D at the surface.[150] According to this procedure, silver nitrate salt was added to solution of complex **53** in order to exchange two chlorine ligands for nitrate groups to increase solubility of **53** in non-aqueous solvents. Electrode **10** was dipped in a solution of complex **54**, where the labile nitrate ligands were exchanged by more stable 2,2'-bipyridine to give electrode **55**. Cyclic voltammetry of the modified electrode **53** shows quinone reversible peaks at E_{mp} of −70 mV *vs.* SCE and highly irreversible peaks at a potential of 0.4 V *vs.* SCE, which decreased after subsequent cycling in the same solution. The irreversible

peak might correspond to trace amounts of insoluble silver chloride in solution of **54**, formed as a byproduct of the ion exchange. Despite filtration of the reaction mixture before dipping electrode **10**, a trace amount of silver chloride might be present in solution of **54** and adsorbed at electrode **10** and might affect catalytic activity of the phendione towards NADH oxidation.

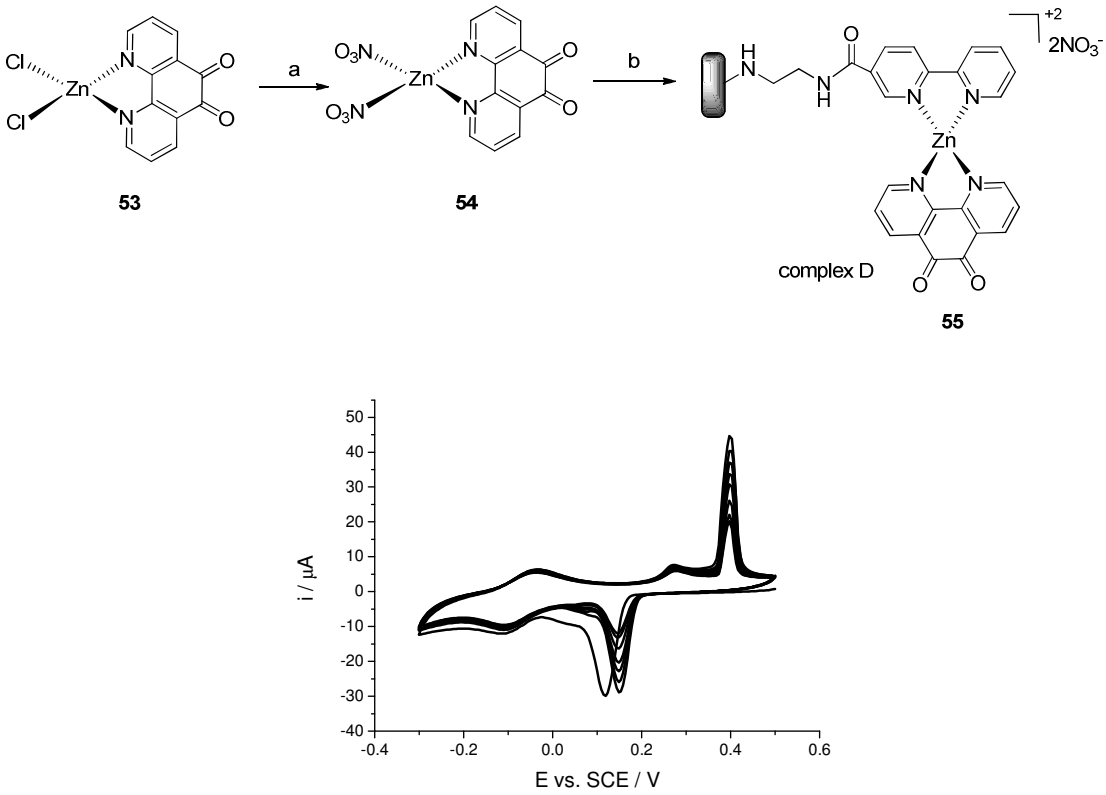

Figure 2.18 Preparation of electrode **55** under solid-phase reaction conditions based on the literature procedure; a) silver nitrate, acetonitrile, complex 53, 16 h, 50 °C b) 0.01M complex **54** in acetonitrile, 50 °C, 16 h; Cyclic voltammogram of electrode **55** in phosphate buffer solution pH 7 at a scan rate of 50 mV s^{-1} and geometrical electrode area of 0.071 cm^2.

In order to eliminate the irreversible peak, possibly caused by adsorption of silver chloride, conditions for solid-phase formation of complex D were optimised by performing a series of individual solid-phase reactions at electrode **10** with complex **5** at various temperature and reaction times (Figure 2.19). Due to the low solubility of complex **5** in acetonitrile, dry DMF was chosen as the reaction solvent. Formation of complex D at the electrode was carried out in 0.01 M solution of **5**, which is the optimum solution concentration as reported for attachment of ruthenium complexes at GC surface (Section 2.3).

In order to optimise the reaction time, individual reaction vessels were prepared containing two electrodes **10** dipped in solution of **5** and heated at 50 °C varying reaction times between 30 minutes to 16 hours. Each of the modified electrodes was characterised by cyclic voltammetry and the surface coverage, Γ_{med}, was calculated using Equation 2.1. It was observed that values of Γ_{med} increased with reaction time and significant coverage of 0.18 nmol cm^{-2} was observed for two electrodes with reaction time of 16 h. An approximate theoretical value for monolayer coverage of 0.2 nmol cm^{-2} for complex D was calculated based upon the geometrical area of the electrode and the size of the zinc complex D.

In order to optimise the reaction temperature for formation of complex D at the electrode surface, reactions for attachment of complex **52** at electrode **10** were carried out at three different temperatures. Electrodes modified at various temperatures were also characterised by cyclic voltammetry and values of Γ_{med} for each electrode were calculated. It was observed that relatively high coverage close to the theoretical value for a monolayer of complex D was obtained for electrodes modified at 50 and 80 °C in comparison to modification carried out at room temperature (Figure 2.19b). A temperature of 50 °C was chosen for following experiments due to the fact that the stability of the GC modified electrodes decreases with temperature as was observed during optimisation of reaction conditions for attachment of ruthenium complexes (Section 2.3).

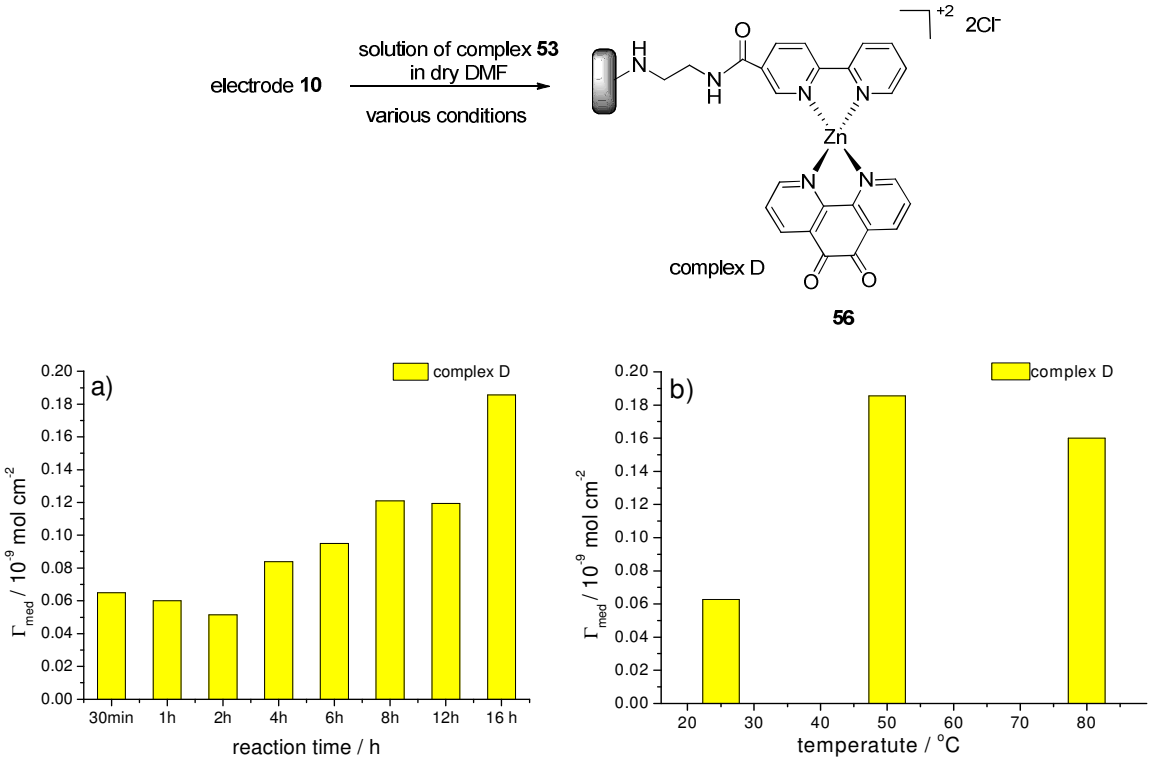

Figure 2.19 Optimisation process of formation of complex D at electrode 10 in 0.01 M solution of **53** in DMF a various reaction time and reaction temperatures; a) Values of Γ_{med} for complex D created at reaction times varying from 30 minutes to 16 h; b) Values of Γ_{med} for complex D created at different reaction temperatures for 16 h.

Optimised reaction conditions were applied for attachment of complex **52** at electrodes modified with six different linkers (Scheme 2.17) as described for ruthenium complexes A, B and C. Each of electrodes **56-61** was prepared individually and characterised one by one using cyclic voltammetry.

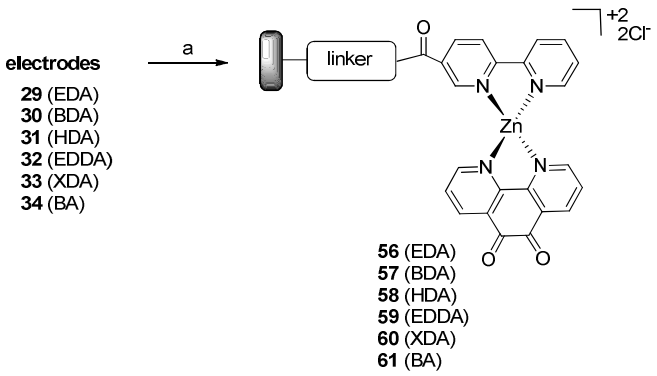

Scheme 2.17 Attachment of complex **53** at electrodes **29-34**, functionalised by six different linkers; Each modified electrode **56-61** was prepared individually under the same solid-phase reaction conditions a) 0.01 M of complex **51** in dry DMF, 50 °C, 16 h.

Cyclic voltammograms of electrodes **56-61** show the presence of reversible peaks in aqueous solution at an average value of E_{mp} of 90 mV *vs.* SCE (Figure 2.20). It was observed that value of E_{mp} for the zinc complex was lower than for the ruthenium complexes A-C by approximate 30 mV, which clearly indicates that the metal centre ion has an effect on the thermodynamics for the phendione ligand(s) redox process. Similarly as for modifications with ruthenium complexes attached at the surface through different linkers, minor differences were observed in the values of E_{mp} between electrodes **55-60**. This result suggests that the length and structure of linker does not affect the thermodynamics of redox reaction between complex D and the electrode. Based on potential peak separation ΔE_p, the kinetics of electron transfer are slower for zinc complex D than for ruthenium complexes an average value of ΔE_p of 85 mV at a scan rate of 50 mV s^{-1} was calculated for electrodes **56-61** and minor differences were observed between complex D attached at the surface through the six different linkers.

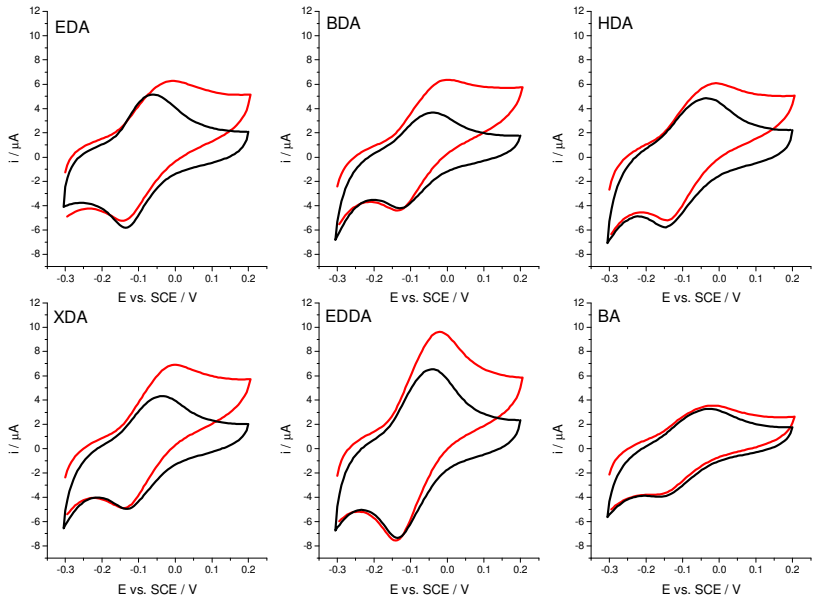

Figure 2.20 Cyclic voltammograms recorded for electrodes **56-61** modified with complex D attached at the GC surface through six different linkers in presence (red) and absence (black) of 1 mM NADH solution in 0.1 M phosphate buffer pH 7 at a scan rate of 50 mV s^{-1} and geometrical electrode area of 0.071 cm^2.

In order to compare the efficiency of attachment of complex D through different linkers, surface coverages for electrodes **56-61** were calculated using Equation 2.1. In general, the surface coverage obtained for the series of modified electrodes with the tetrahedral zinc complex D is higher than for electrodes modified with the more bulky octahedral ruthenium complexes (Figure 2.21). Relatively high values of Γ_{med} were obtained for electrodes modified with the short aliphatic linkers EDA and BDA, which is in good agreement with the coverages obtained for ruthenium complexes for these linkers. The lowest values of Γ_{med} were obtained for the modification with the rigid benzylamine linker BA. Similar effects of the linkers on the values of Γ_{med} were observed for electrodes modified by the different ruthenium complexes.

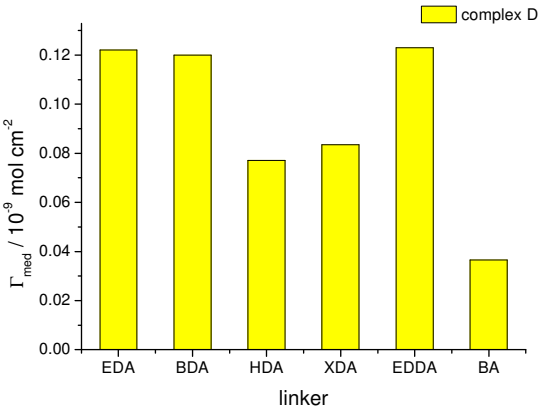

Figure 2.21 Values of surface coverage Γ_{med} of complex D calculated for modified electrodes **56-61** based on experimental data obtained from the cyclic voltammograms in Figure 2.15. Each bar represents value of Γ_{med} calculated according to Equation 2.2 for a single modified electrode.

Electrodes **56-61** were also individually evaluated towards NADH catalytic activity in 1 mM NADH aqueous solution. It was found that phendione coordinated to zinc metal ion catalyses oxidation of NADH at 0 V *vs.* SCE, which is in good agreement with the results obtained for the ruthenium complexes. This result indicates that the different metal centre and different geometry of complex does not have an effect on the potential for catalysis of NADH oxidation. Catalytic currents, i_{cat}, recorded at 0.15 V for electrodes **56-61** show minor differences in values of i_{cat} between electrodes modified with diamine linkers. Relatively low values of i_{cat} were recorded for electrode **61** attached through the benzylamine linker BA, which is consistent with the low values of i_{cat} obtained for ruthenium complexes attached at the surface through the rigid BA linker.

Further analysis involved calculations of normalised catalytic currents, i_{norm}, using Equation 2.2 to investigate the catalytic efficiency of electrodes **56-61** (Figure 2.22b). A significant value of i_{norm} was obtained for modification with *p*-xylene diamine linker XDA and a relatively low value of i_{norm} was obtained for the rigid benzylamine linker BA. In general, the calculated values of i_{norm} for modifications with zinc complex D are relatively low in comparison with values of i_{norm} obtained for modifications with the three ruthenium complexes A, B and C (Sections 2.3, 2.4 and 2.5).

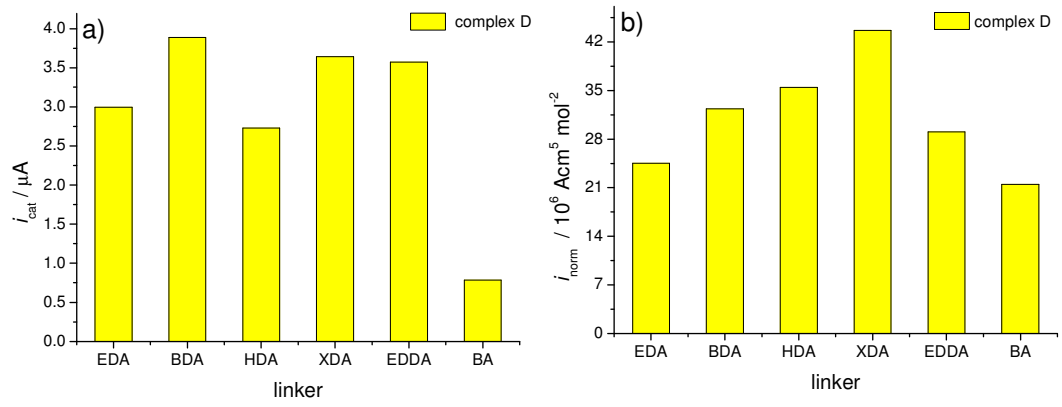

Figure 2.22 a) Catalytic currents i_{cat} recorded for modified electrodes **56-61** in the presence of 1 mM NADH in 0.1 M phosphate buffer solution pH 7 at a scan rate of 50 mV s^{-1}; b) Normalised catalytic currents i_{norm} calculated for electrodes 56-61 according to Equation 2.2. Each bar represents values of i_{cat} (a) or i_{norm} (b) obtained for single modified electrode.

2.7 XPS analysis of the GC electrodes modified with ruthenium and zinc complexes.

The presence of complexes A, B C and D at the modified GC electrodes was confirmed by X-ray photoelectron spectroscopy (XPS), which allowed for qualitative and approximate quantitative determination of elements present at the GC surface functionalised with ruthenium and zinc metal complexes. XPS method is based on irradiation of atoms present in a solid sample with source of monochromatic soft X-rays, with a photon energy range of 200-2000 eV, leading to ionisation and emission of core shell electrons. These photons have limited penetrating power in a solid on the order of 1-10 μm.[151] The emitted electrons have measured kinetic energy E_{kinet}, calculated using the photo-effect equation:

$$E_{kinet} = h\nu - E_{bind} \qquad 2.3$$

where E_{bind} is the binding energy of the atomic orbital, from which the electron originates and hν is the quantum energy of the photon emitted to the surface. In practice, the instrument measures values of E_{kinet} at known hν and this allows calculation of values of E_{bind}, which is sensitive characteristic of chemical bonds present in the sample and is related to the energy of ionisation. Each element has a range of electronic states which are open to excitation by x-rays, resulting in each element having characteristic values of E_{bind} associated with electrons being ejected from various orbital levels. The photoelectron spectrum is presented as a plot of binding energy versus number of detected electrons per energy interval. Relative intensities of the peaks correspond to energy released during ejection of electrons from core orbital levels, which are characteristic for different atoms and type of a bonding. This allows for quantitative evaluation of the sample composition and character of bonding in compounds present at the solid surface.

In this work, XPS analysis was applied for determination of GC electrodes covalently modified with ruthenium and zinc metal complexes according to the strategy proposed in Scheme 2.2. Modifications of GC electrodes with ruthenium and zinc complexes attached at the surface were reproduced at GC sheets using the same electrochemical and solid-phase synthesis methods. Figure 2.23 shows three XPS

photoelectron spectra recorded for a blank GC surface and GC sheets modified with ruthenium and zinc complexes and EDA linker. In all cases, broad peak at about 280 eV was observed, corresponding to electrons ejected from C 1s orbital level. High intensity of this peak represents a large number of electrons ejected from sp^2 carbon atoms of the aromatic structures on the underlying GC sheets. In case of the modified GC sheets (Figure 2.23b and c), the presence of carbon peaks corresponding to electrons emitted from organic molecules occurred after functionalisation of GC was not possible to distinguish due to high intensity of the background carbon atoms.[151]

In comparison with the blank GC (Figure 2.23a), increased intensity of electrons ejection from the O 1s orbital level at 531 eV and the N 1s orbital level at 398 eV were observed for functionalised GC surfaces suggesting successful attachment of linker and complex (Figure 2.23b and c). However, relatively high intensity of the oxygen peak might be caused by the presence of additional oxygen species directly attached at GC surface as a result of electrochemical oxidation of the surface. For the nitrogen peak, it was not possible to distinguish between single nitrogen-carbon bond and the nitrogen-carbon double bond in the structure of bidentate ligands coordinated to a ruthenium metal centre. The presence of the nitrogen with the same binding energy was also observed at the blank GC, which might be rationalised by the presence of residual nitrogen containing polymers used for production of GC materials.[52]

Figure 2.23b shows characteristic peaks corresponding to emission of electrons from ruthenium 3p1/2 and 3p3/2 orbital levels at values of E_{bind} of 484 and 462 eV, respectively.[151] According to the literature, ejection of electrons from ruthenium 3d3/4 and 3d5/2 orbital levels should occur at 284 and 280 eV. However, these peaks overlap with the broad peak of C 1s and were not observed in this case. For GC sheet modified with the zinc complex D, the XPS spectrum showed the presence of additional two peaks at 1022 eV and 1020 eV corresponding to ejection of electrons from Zn 2p3/2 and Zn 2p1/2 orbital levels, respectively.

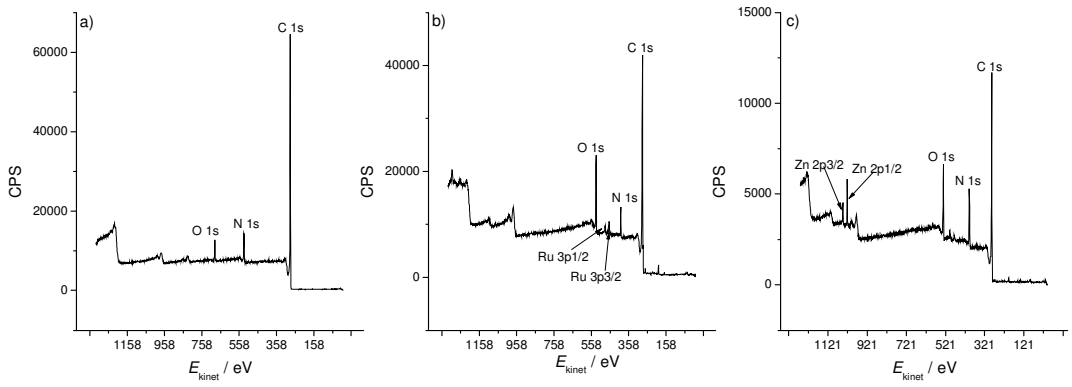

Figure 2.23 Examples of XPS photoelectron spectra recorded for GC sheets; a) polished, blank GC sheet; b) with ruthenium complex A attached at the surface through EDA linker; c) zinc complex D attached at the surface through EDA linker.

XPS analysis allowed also for approximate quantitative analysis of the elements present at the modified GC sheets and comparison of the elemental composition between different modifications. Firstly, each of the modifications with ruthenium complexes A, B and C and zinc complex D attached through different linkers was reproduced at GC sheets using optimised reaction conditions. In order to compare elemental composition of the GC samples with different modifications, only two elements were considered: nitrogen and metal ion. Carbon and oxygen elements were omitted in the quantitative analysis due to presence of carbon background peak with high intensity and possible additional oxygen species caused by oxidation of carbon surface. Table 2.1 presents the theoretical atomic ratios of ruthenium and nitrogen calculated for different modifications and experimental ratios of Ru : N obtained from percentage atomic concentrations between different elements in samples calculated using Casa XPS 2.3 software. The theoretical atomic ratios were based on the assumption that each of the linker at the surface is attached to a metal complex. Thus, we assumed that the theoretical atomic ratio for complexes A and D attached through diamine linkers should be 1 : 6 and increased number of nitrogen per ruthenium should be observed 1 : 8 for *tris* complexes B and C.

An approximate Ru/N ratio of 1 : 10 for the ruthenium complex A and the zinc complex D was calculated from experimental data, which suggests that not all of the linkers are coupled to the metal complex and a number of uncoordinated 2,2'-bipyridine ligands is present at the GC surface. It might be rationalised by the bulky size of the complex, which prevents coordination of each 2,2'-bipyridine ligand at

the surface to the large molecule of zinc or ruthenium complexes. For the *tris* ruthenium complexes B and C, calculated approximate Ru/N ratios based on experimental data were about 1 : 5 and 1 : 1 for complexes B and C, respectively. The experimental results showed the decreased number of the nitrogen per one ruthenium, which might be caused by the bulky size of complexes B and C and prevents the photoelectron effect on nitrogen atoms on underlying linker structures.

Linker	**Approximate atomic ratio**							
	Complex A		Complex B		Complex C		Complex D	
	Ru : N	Ru : N*	*Ru : N*	Ru : N*	*Ru : N*	Ru : N*	*Zn : N*	Zn : N*
EDA	*1 : 10*	1 : 6	*1 : 10*	1 : 8	*1 : 1*	1 : 8	*1 : 10*	1 : 6
BDA	*1 : 10*	1 : 6	*1 : 2*	1 : 8	*1 : 1*	1 : 8	*1 : 10*	1 : 6
HDA	*1 : 8*	1 : 6	*1 : 8*	1 : 8	*1 : 1*	1 : 8	*1 : 9*	1 : 6
XDA	*1 : 10*	1 : 6	*1 : 5*	1 : 8	*1 : 3*	1 : 8	*1 : 8*	1 : 6
EDDA	*1 : 7*	1 : 6	*1 : 4*	1 : 8	*1 : 1*	1 : 8	*1 : 7*	1 : 6
BA	*1 : 10*	1 : 5	*1 : 4*	1 : 7	*2 : 1*	1 : 7	*1 : 5*	1 : 5

Table 2.1 The values of approximate atomic ratios Ru/N for the GC sheets modified with six different linkers and four different metal complexes calculated from XPS experimental data (*italics*). Values of Ru/N* represents theoretical atomic ratios Ru/N based on assumption that each linker at the surface is coupled with a metal complex.

In conclusion, XPS analysis confirmed successful attachment of different ruthenium and zinc complexes using the proposed strategy as shown in Scheme 2.2. The XPS method allowed qualitative analysis of the modified GC sheets and the XPS spectra clearly show peaks corresponding to the presence of ruthenium and zinc at the modified GC sheets. XPS experimental data obtained for the modified GC sheets were also applied for approximate quantification of elements Ru/N ratios in the samples for *bis* ruthenium and zinc complexes and indicated the presence of uncoordinated 2,2'-bipyridine ligands at the GC surface. However, presence of more bulky complexes B and C at the GC sheets resulted in inaccurate ratios Ru/N, which might be caused by limited photoelectron effect on the nitrogen atoms of the underlying linkers.

2.8 Modification of GC electrode by novel zinc complex containing pyridine imidazole ligands.

Modification of GC by octahedral ruthenium complexes A, B and C clearly showed that presence of different ligands affects surface coverage of the attached complex as well as catalytic activity towards NADH oxidation. Successful formation of tetrahedral zinc complex D at the GC surface was achieved by solid-phase coordination of complex **52** by 2,2'-bipyridine ligand covalently immobilised at GC through different linkers (Section 2.3). In order to study the effect of different ligands on the zinc complex, chelating ligands containing the imidazole heterocyclic ring were considered. Zinc complexes with coordinated bidentate and tridentate imidazole ligands are reported in the literature and their interesting chemical and structural properties have been applied in materials science.[152-154] Chelating ligands with imidazole structures were also reported by Schuhmann *et al.* [155] for solid-phase functionalisation of GC electrodes by osmium complexes. In this case, the pyridine-imidazole ligand was functionalised at one of the imidazole nitrogen atoms by a hydroxyethylene group and covalently tethered at the polymer supported GC using solid-phase reaction conditions. In the presence of *bis* osmium complexes, the pyridine-imidazole coordinated to the osmium metal centre and created a new, stable osmium complex at the GC surface, which was applied for bioelectrocatalytic oxygen reduction.

In this project, the design of a functionalised pyridine-imidazole with a carboxylic functional group was proposed, which would allow for covalent tethering of this ligand at GC and enable formation of the zinc complex. Based on the synthetic approach reported by Schuhmann *et al.*,[155] the pyridine-imidazole was functionalised at imidazole N-1 in a three steps synthesis and 2-(2-(pyridine-2-yl)-1*H*-imidazol-1-yl)acetic acid **64** was successfully obtained as the TFA salt form (Scheme 2.18). Firstly, 2-(1H-imidazol-2-yl)pyridine **61** was obtained using a literature procedure[156,157] in 31 % yield (*lit.*[157] 33 %). Addition of 2-bromo-*tert*-butyl acetate to a solution of **62** in the presence of *n*-butylithium allowed nucleophilic substitution of the bromide by nitrogen in the imidazole ring at N-1 position to give compound **63** in 76 % yield. Structure of **63** was confirmed by NMR analysis. ^{1}H NMR shows the

presence of resonance peaks in the aromatic region corresponding to pyridine and imidazole heterocyclic rings. In addition, a singlet at 5.2 for two α-protons of acetate group and a singlet at 1.39 ppm for *tert*-butyl ester were observed. Finally, hydrolysis of the *ter-t*butyl ester **63** in 20 % solution of TFA gave ligand **63** in 98 % yields.

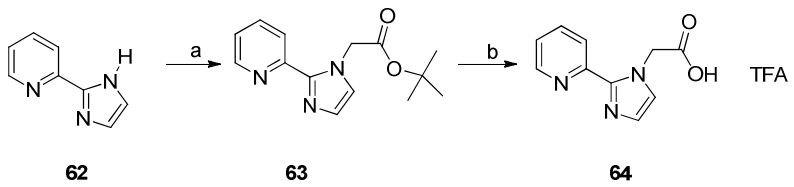

Scheme 2.18 Synthesis of ligand **64**; a) 2.5 M n-buthylithium in hexane, 2-bromo-*tert*butyl acetate THF, 78 °C, overnight, 76 %; b) 20 % trifluoroacetic acid (TFA) in DCM, overnight, R. T., 98 %.

The following work involved covalent immobilisation of ligand **64** under solid-phase peptide coupling conditions as reported for attachment of 2,2'-bipyridine ligand **9** (Scheme 2.19). In this case, diisopropylethylamine (DIPEA) base was used in excess of 10 equivalents in order to neutralise the TFA salt. The presence of the attached pyridine-imidazole ligand at electrode **65** was difficult to evaluate directly using cyclic voltammetry due to the relatively low potential of the imine redox couple as discussed for electrode **10** (Section 2.3). Therefore, electrode **65** was directly used in the following step of coordination of the zinc complex **53** under solid-phase reaction conditions as optimised for coordination of the 2,2'-bipyridine to **53**.

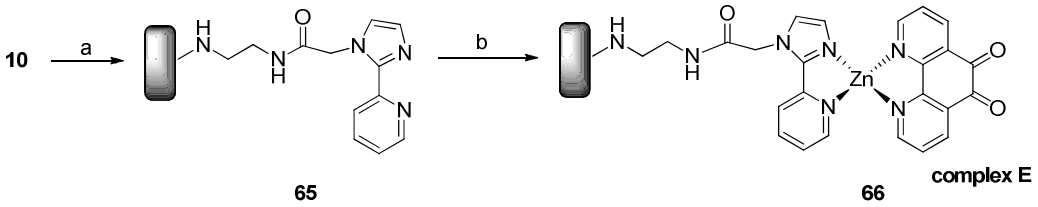

Scheme 2.19 Preparation of modified electrode **66**; a) 1 M solution of **60** in DMF, 10 equiv. of DIPEA, HBTU, R.T., 16 h; b) 0.01 M solution of **53** in DMF, 50 °C, 16 h.

In order to confirm the successful coupling of the novel ligand **64** to the amine groups at the GC, a control experiment was performed. Attachment of **53** was carried out at the same time by dipping electrode **10** containing *mono*-Boc-EDA linker and electrode **65** modified with pyridine-imidazole ligand. Results of the control experiment were evaluated by cyclic voltammetry. For both modified electrodes, a

reversible redox peak corresponding to a redox process of the phendione was observed at E_{mp} of –0.1 V *vs.* SCE (Figure 2.24). However, electrode **66** gave significant coverage Γ_{med} of 1.4×10^{-10} mol cm^{-2} in comparison to the control electrode with a value of Γ_{med} 1.23×10^{-12} mol cm^{-2}.

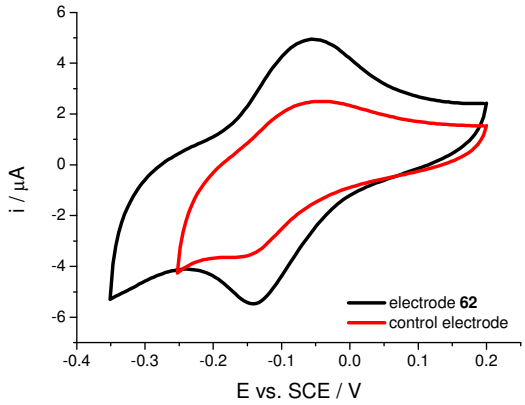

Figure 2.24 Cyclic voltammograms of electrode **66** (black) and control electrode (red) in 0.1 M solution of phosphate buffer pH 7 at a scan rate 50 mV s^{-1} and geometrical electrode area of 0.071 cm^2.

In order to evaluate the effect of the pyridine-imidazole on the catalytic activity for NADH oxidation, electrode **66** was characterised in 0.1 M solution of NADH and shows increased, irreversible anodic process at 0 V *vs.* SCE (Figure 2.25). The catalytic current, i_{cat}, was measured at 0.15 V vs. SCE and is comparable with i_{cat} obtained for complex D. Functionalisation of the GC surface by complex E attached at the surface through different linkers followed by their detailed electrochemical and kinetic characterisation is included in the library of 63 modified electrodes described in Section 3.

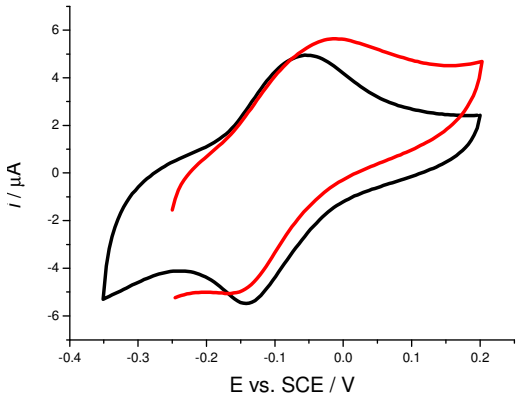

Figure 2.25 Cyclic voltammograms of electrode **66** in the presence (red) and absence (black) of 1 mM NADH solution in 0.1 M phosphate buffer pH 7 at scan rate of 50 mV s^{-1} and geometrical electrode area of 0.071 cm^2.

2.9 Conclusion

A strategy for functionalisation of GC electrodes was designed in order to covalently immobilise metal complexes containing phendione redox active ligands for NADH-dependent biosensors. The strategy, based on sequential electrochemical and solid-phase synthesis steps, allows for control over choice of metal centre, ligand and linker.

According to the proposed strategy, the initial step involved electrochemical oxidation of diamine or reduction of diazonium salt bearing amine functional groups. The presence of amine groups at the GC surface allowed for successful covalent attachment of the 2,2'-bipyridine-5-carboxylic acid bidentate ligand under solid-phase peptide coupling conditions. The final step involved coordination of 2,2'-bipyridine to a metal centre and formation of a novel complex at the surface. Initially, octahedral *bis*-(dimethyl sulphoxide)(1,10-phenanthroline-5,6-dione) ruthenium (II) chloride was successfully attached at the surface through ethylenediamine linker under optimised solid-phase reaction conditions to create the novel *bis* ruthenium complex A. Electrochemical characterisation of the modified electrode showed that complex A exhibits reversible redox behaviour for the phendione and acts as an effective mediator towards NADH oxidation.

Based on the initial result, the same strategy was applied for attachment of octahedral ruthenium complexes, containing various chelating ligands. For this reason, the additional ruthenium complexes were synthesised: (2,2'-bipyridine)(1,10-phenanthroline-5,6-dione) ruthenium (II) chloride and *bis*-(1,10-phenanthroline-5,6-dione)ruthenium (II) chloride and coordinated to 2,2'-bipyridine at the GC surface under optimised solid-phase reaction conditions, resulting in formation of novel ruthenium complexes B and C, respectively. In order to study effect of the geometry of the metal complex, the tetrahedral (1,10-phenanthroline-5,6-dione)zinc (II) chloride complex was attached at the GC surface according to the proposed strategy to give the novel tetrahedral complex D. Results of electrochemical characterisation showed that all of the electrodes were successfully modified with complexes B-D showing semi-reversible redox behaviour for the phendione. Surface coverages were calculated for the different ruthenium complexes, indicating that the value of coverage strongly depends on the size of the metal complex at the surface, where

relatively low coverage was obtained for attachment of the bulky ruthenium complexes B and C and significant coverage was obtained for modification with the tetrahedral zinc complex D.

Different metal complexes were evaluated towards NADH oxidation and preliminary studies showed electrocatalytic activity at low overpotential in all cases. Significant catalytic efficiency was obtained for ruthenium complexes B and C in comparison to the zinc complex D, which would suggest that octahedral complexes with additional bidentate ligands increase the catalytic activity of the modified electrodes for NADH oxidation. This might be explained by the fact that delocalised *Π*-electrons in the 2,2'-bipyridine ligand, which increases the electron transfer between phendione and the electrode surface.

Further work involved preparation of electrodes modified with complexes A, B and C attached at the surface through various linkers in order to study the effect of length and structure of the linker on the electrochemical and catalytic properties of the complexes. In general, values of surface coverages calculated for ruthenium complexes A-D decrease with long aliphatic linkers. Relatively low coverages were observed for the benzylamine linker, where the direct bond between the benzyl ring and the carbon surface forms a rigid structure at the surface, resulting in limited accessibility of the 2,2'-bipyridine to coordinate to the bulky ruthenium complex. These results are with good agreement with the results reported for immobilisation of the anthraquinone using the same methodology.

Attachment of complexes A-D through linkers with different flexibility and length also affected catalytic activity of the modified electrodes for NADH oxidation. In general, significant catalytic efficiency was obtained for flexible EDDA and XDA linkers for all complexes. Relatively low catalytic efficiency was calculated for the short aliphatic linkers EDA and BDA and the rigid benzylamine linker BA, which can be rationalised by low accessibility of these linkers to the bulky, folded molecule of NADH in solution.

The presence of complexes A-D attached at the surface through different linkers was confirmed by X-ray photoelectron spectroscopy, which allowed for qualitative and quantitative determination of elemental composition of the modified electrode surface. Comparison of XPS spectra for the blank GC surface and GC functionalised

by complexes A-D according to the proposed strategy, showed the presence of peaks characteristic for ruthenium or zinc elements.

In order to investigate the effect of different ligands on the coverage and catalytic activity of the tetrahedral zinc complex, the novel 2-(2-(pyridine-2-yl)-1*H*-imidazol-1-yl)acetic acid chelating ligand was synthesised and attached to the surface through an ethylenediamine linker according to the proposed strategy. The (1,10-phenanthroline-5,6-dione)zinc (II) chloride complex was successfully coordinated by the pyridine-imidazole at the GC surface and the novel, tetrahedral zinc complex E was successfully formed under solid-phase reaction conditions. Electrochemical characterisation of complex D at the GC surface indicates that this complex acts as an effective mediating system for NADH oxidation. Attachment of complex E through different linkers and detailed electrochemical characterisation are included in Section 3 describing preparation and HTP evaluation of a library of different modified electrodes.

In conclusion, molecular design of GC electrodes for electrocatalysis of NADH oxidation was successfully achieved by applying electrochemical and solid-phase methods. The proposed strategy involved sequential functionalisation of GC electrodes in a controlled manner, designed for covalent tethering of different metal complexes bearing the phendione redox active ligand. As a result, metal complexes with different geometry and ligand(s) were attached at the surface through linkers with various lengths and flexibility and successfully applied as an effective mediating system for oxidation of NADH. Initial studies of the individual modified electrodes clearly showed that the proposed design of the electrode surface allowed for control over electrocatalytic performance of the modified electrodes. Synthesis and electrochemical results presented in this chapter was applied for more detailed investigation of modifications A-E and comparison with the literature examples in Chapter 3.

3 Library of modified electrodes - preparation and HTP screening

3.1 Objectives

In the previous chapters, methodology and optimisation for the covalent modification of GC surfaces by various metal complexes were described using the strategy outlined in Scheme 3.1.

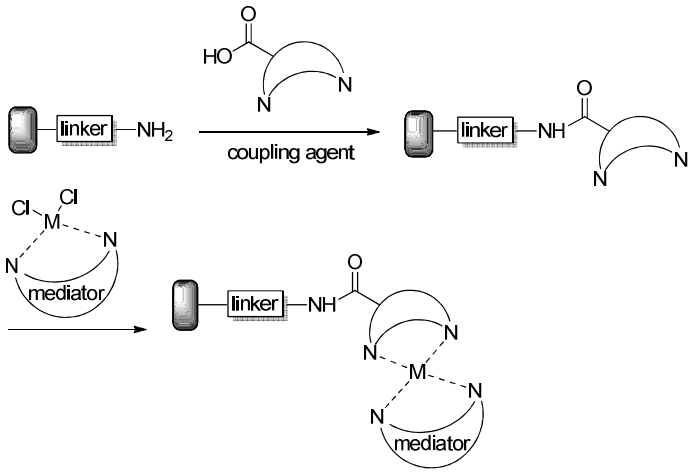

Scheme 3.1 General approach to covalent modification of GC electrodes by metal complexes.

As described in Section 2, ruthenium (II) and zinc (II) metal complexes with phendione bidentate ligand(s) were successfully attached to a GC surface through different linkers. The single electrode results show that the nature of the linker and structure of the complex have an impact on the amount of attached metal complex at the surface and its catalytic activity of towards NADH oxidation.

Applying the same methodology, we therefore set out to prepare a library of modified electrodes, which could be electrochemically characterised in HTP mode using parallel cyclic voltammetry. It was anticipated that HTP would allow the direct and rapid comparison of many different modifications during a single set of measurements and rapid identification of the best modification with respect to the surface coverage and catalytic activity towards NADH oxidation.

Twenty different modifications were planned with each repeated three times to assess the variability of different modifications towards NADH catalytic oxidation. The final three members of the library were control electrodes. The design of the library is presented in Table 3.1. The four selected linkers offer a variety of functional

groups and lengths in order to investigate their affect on the surface coverage of the attached metal complex and catalytic activity towards NADH oxidation. Two of the linkers have aliphatic chains with different lengths (EDA and HDA). The third was a flexible 2,2'-(ethylenedioxy)diethylamine chain (EDDA), in which hydrophobic aliphatic chains are replaced by more hydrophilic ethoxy units. Benzylamine BA was also selected as a linker, in which the aromatic ring was directly bonded to the GC surface to create a short and rigid linkage between mediator and electrode surface (Table 3.1).

Single electrode experiments had shown that bulky octahedral ruthenium complexes A, B, C and tetrahedral zinc complex D when attached through different linkers at the surface gave different catalytic activities towards NADH oxidation. The same metal complexes were selected for the library in order to investigate effect of size and geometry of the metal complex on catalytic activity towards NADH catalytic oxidation (Table 3.1). In addition, three octahedral ruthenium complexes A, B and C, which were different in the size and structure of the chelating ligands attached to ruthenium metal ion. These included chloride ions (complex A), 2,2'-bipyridine (complex B) and phendione ligand (complex C). This allowed us to observe possible effect of these ligands on the electrochemical and catalytic properties of the complexes A, B and C attached at the surface.

Successful modification of electrodes by complex E attached at the surface through the EDA linker has been described previously in Section 2.8. The library allowed us to explore this modification by including complex E attached through the four different linkers.

Electrodes **70a-c** (Table 3.1) were modified with the EDA linker, the 2,2'-bipyridine ligand at the surface and the electrochemically inactive (2,2'-bipyridine)zinc (II) chloride are included as a control modification to observe the electrochemical changes due to covalent functionalisation by a metal complex in the absence of the redox active phendione ligand.

	EDA	HDA	EDDA	BA
A	13a, 13b, 13c	36a, 36b, 36c	37a, 37b, 37c	39a, 39b, 39c
B	41a, 41b, 41c	43a, 43b, 43c	44a, 44b, 44c	46a, 46b, 46c
C	47a, 47b, 47c	49a, 49b, 49c	50a, 50b, 50c	52a, 52b, 52c
D	56a, 56b, 56c,	58a, 58b, 58c	59a, 59b, 59c	61a, 61b, 61c
E	66a, 66b, 66c	67a, 67b, 67c	68a, 68b, 68c	69a, 69b, 69c
control electrodes	70a, 70b, 70c			

Table 3.1 Design of the library of 63 modified electrodes; the columns represent the four linkers: EDA (1,2-ethylenediamine), HDA (1,6-hexanediamine), EDDA (2,2'-(ethylenedioxy)diethylamine) and BA (*p*-benzylamine); the rows represent: the ruthenium complexes (A, B and C), the zinc complexes (D, E) and the control electrodes 70a-c.

3.2 Preparation and synthesis of the 63 modified electrode library.

Preparation of the 63 member library started with individual polishing of the electrodes followed by electrochemical covalent attachment of four linkers at electrode surface carried out one by one using conventional cyclic voltammetry.
As was observed for individually modified electrodes (Section 2), attachment of the linker at the electrode surface generates currents in range of 200-300 μA, whereas the HTP multichannel potentiostat has a current limit of 50 μA. Therefore, attachment of the linkers for the 63 member library was not possible to perform in a parallel way using the multichannel potentiostat. However, subsequent steps of electrode modification involving solid-phase synthesis were carried out in a combinatorial and parallel way.

Firstly, the electrodes were polished with silicon carbide paper grade P1200 prior to covalent modification. High roughness or defect levels obtained during the polishing process might cause changes in the effective surface areas of the electrodes and be a source of variations between electrodes with the same modification. Polished blank electrodes were therefore screened one by one using cyclic voltammetry in phosphate buffer solution at pH 7. The resulting voltammograms gave consistent capacitance nonfaradaic currents (Figure 3.1). Comparison of the background currents for the blank electrodes gives an approximate view of the differences in their active areas after the polishing process. Voltammograms of all polished electrodes are presented in Appendix 1 and they clearly show that the capacitance currents measured at potential of 0 V *vs.* SCE is consistent for all of the polished blank electrodes.

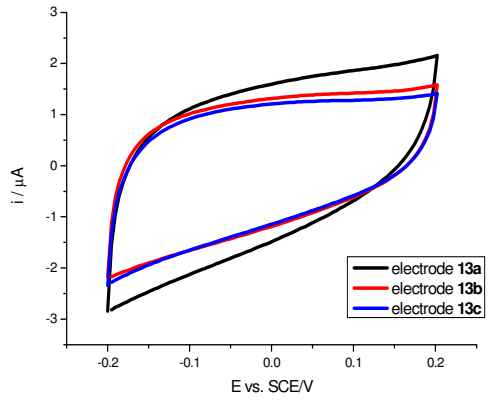

Figure 3.1 Typical cyclic voltammograms of background currents recorded for blank glassy carbon electrodes **13a-c** with geometrical area of 0.71 cm^2 in 0.1M phosphate buffer solution pH 7 at scan rate of 50 mV s^{-1}.

The first step of covalent modification was attachment of the *mono*-Boc protected linker as previously reported for the modification of individual electrodes (Section 2).[55] For attachment of the diamine linkers EDA, HDA and EDDA, the oxidation peak on the first cycle was observed at a potential of 1.96 V (Figure 3.2a), which is in good agreement with the results previously obtained for individual electrodes. The following cycles led to the disappearance of the faradaic curve, which indicates blocking of the surface by the Boc-protected amine functional groups and creates monolayer of the diamine linker at the GC surface. Similarly, during the attachment of the diazonium salt linker (BA), the reduction wave at −0.36 V was observed on the first cycle and decreased in the following cycles, which indicates blocking of the surface with the BA linker (Figure 3.2b). The electrode was covered with an expected monolayer of the BA linker after two cycles.

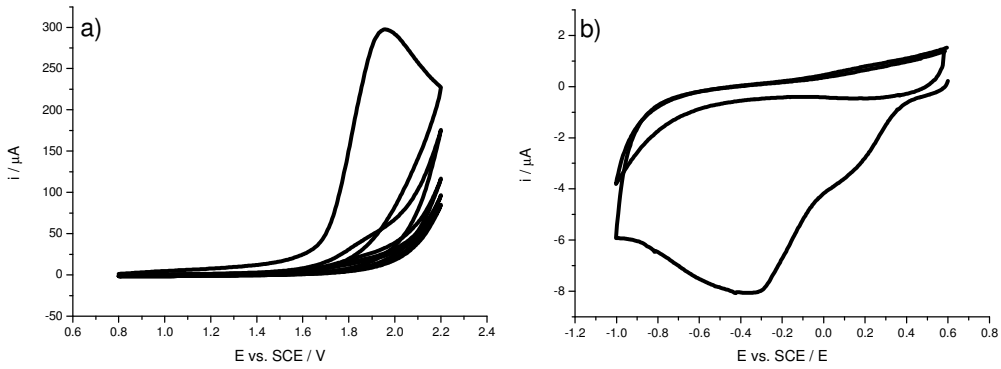

Figure 3.2 Typical cyclic voltammograms for linkers immobilisation at GC polished electrodes in 15 mM solution of linker in MeCN with 0.1 M TABTFB at a scan rate of 50 mV s^{-1}; a) attachment of the EDA linker for electrode **13c**; b) attchment of the BA linker for electrode **39a**.

The further steps of modification involved parallel solid-phase synthesis. Firstly, the *Boc* amine protecting group was removed by dipping all the electrodes in a bulk solution of 0.1 M hydrochloric acid in dioxane for 1 h. This time was enough to complete the deprotection reaction as shown in the previous results obtained for modifications of the individual electrodes (Section 2) and based on results reported Kilburn and Bartlett for electrodes modified with anthraquinone-2-carboxylic acid.[55,57]

The resulting free amine groups allowed for the attachment of 2,2'-bipyridine-5-carboxylic acid bidentate ligand **9** using peptide coupling conditions previously reported in the literature (Scheme 3.2).[55,136] The coupling reaction of ligand **1** was assumed to be completed within the same time (16 h) as previously shown in modifications of the individual electrodes with the ligand **9** (Section 2.3). In order to obtain identical coupling conditions during library preparation and decrease the experimental errors associated with the coupling reaction, the following electrodes **13a-c**, **41a-c**, **47a-c**, **56a-c**, **36a-c**, **43a-c**, **49a-c**, **58a-c**, **37a-c**, **44a-c**, **50a-c**, **59a-c**, **39a-c**, **46a-c**, **52a-c**, **61a-c** were dipped in one bulk solution of reaction mixture for exactly the same amount of time.

The preliminary experiments for attachment of the 2-(1-(carboxymethyl)-1H-imidazol-3-ium-2-yl)pyridin-1-ium trifluoroacetate salt **64** clearly showed that successful attachment of this linker was obtained in similar conditions as for linker **9** but with 10 equiv. excess of the DIEA base in order to neutralise the TFA salt. As

shown for ligand **9**, the coupling of ligand **64** was carried out in a parallel way, where the following electrodes **66a-c**, **67a-c**, **68a-c** and **69a-c** were all dipped in the one bulk solution of the reaction mixture for exactly the same amount of time.

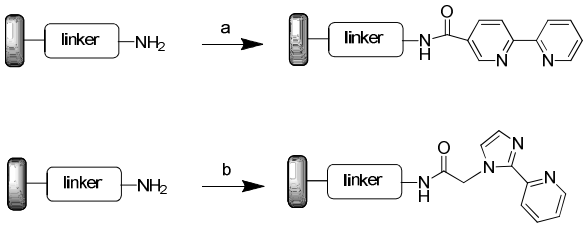

Scheme 3.2 Attachment of linkers **9** and **64** at the functionalised GC surface; a) ligand **9**, HBTU, DIPEA, DMF, R.T., 16 h; b) ligand **64**, HBTU, 10 equiv. DIEA, DMF, R.T., 16 h.

The presence of the bidentate ligand allowed for attachment of the ruthenium (II) metal complexes A, B and C or the zinc (II) metal complexes D and E by applying the conditions of solid-phase synthesis optimised in Section 2 (Scheme 3.3).

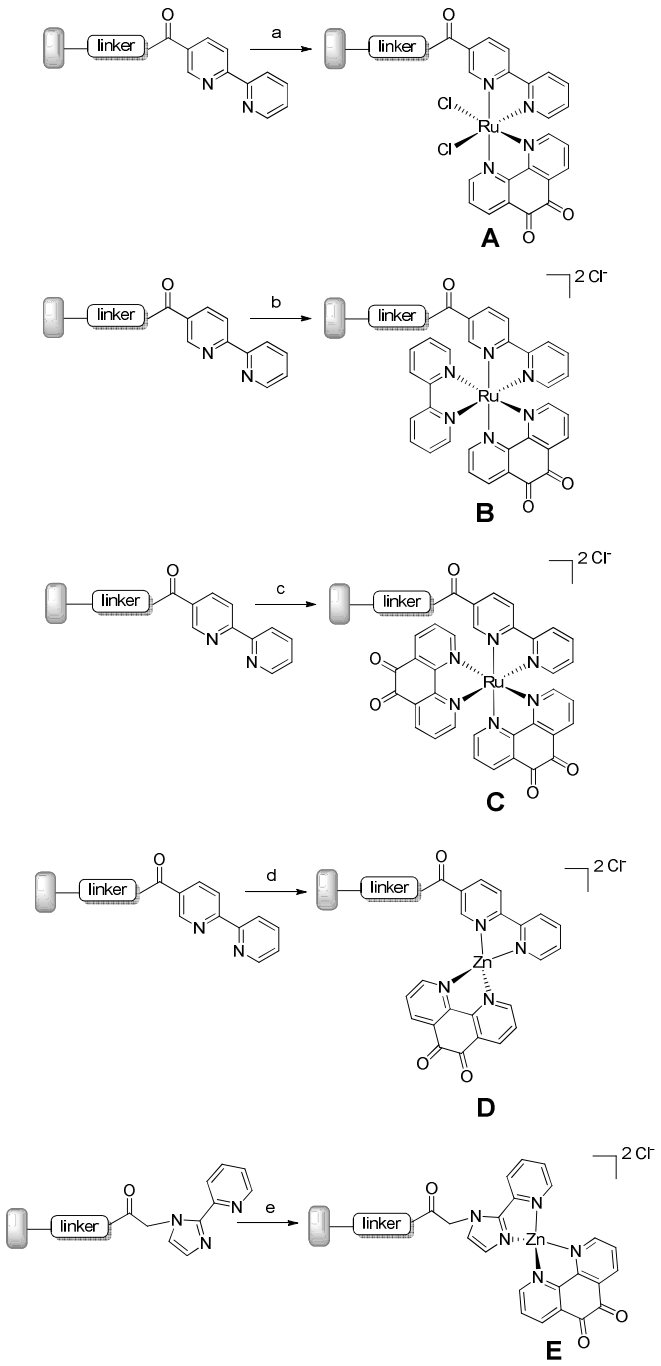

Scheme 3.3 Solid-phase synthesis of metal complexes at the functionalised GC electrodes; a) Ru(phendione)Cl_2(DMSO)$_2$, DMF, 100 °C, 16 h. b) Ru(phendione)(bipy)Cl_2, DMF, 100 °C, 16 h, c) Ru(phendione)$_2Cl_2$, DMF, 100 °C, 16 h, d) and e) Zn(phendione)Cl_2, DMF, 50 °C.

The solid-phase synthesis was carried out in parallel, using four-neck vessels, where each vessel contains four electrodes dipped in the solution of the appropriate metal complex (Figure 3.3).

Figure 3.3 Example of the parallel set up of reaction vessels used during solid-phase synthesis of metal complexes at GC electrodes; the inset shows the reaction vessel containing a solution of Zn(phendione)Cl_2 and electrodes **56c**, **58c**, **59c** and **61c**.

Table 3.2 shows the arrangement of the electrodes in vessels I to XVI. The electrodes modified with the same linker and bidentate ligand were placed in three different vessels, containing the same solutions of metal complex. The parallel preparation of the electrodes with the same modification but using different vessels allows us to evaluate the reproducibility and variation in each modification. Parallel and combinatorial preparation of all members of the library allowed us to avoid possible problems associated with low stability of the modified electrodes.

Metal complex	Number of reaction vessel	Linker/Electrode number			
		EDA	HDA	EDDA	BA
A 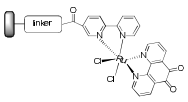	I	13a	36a	37a	39a
	II	13b	36b	37b	39b
	III	13c	36c	37c	39c
B 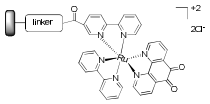	IV	41a	43a	44a	52
	V	41b	43b	44b	53
	VI	41c	43c	44c	54
C 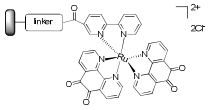	VII	47a	49a	50a	52a
	VIII	47b	49b	50b	52b
	IX	47c	49c	50c	52c
D 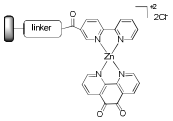	X	56a	58a	59a	61a
	XI	56b	58b	59b	61b
	XII	56c	58c	59c	62c
E 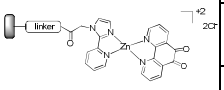	XIII	66a	67a	68a	69a
	XIV	66b	67b	68b	69b
	XV	66c	67c	68c	69c
Control electrodes 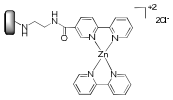	XVI	70a-c			

Table 3.2 Arrangment of electrodes and reaction vessels during parralel attachment of the metal complexes.

3.3 HTP electrochemical screening of the library.

The library of 63 modified electrodes was electrochemically screened in HTP mode using a multichannel potentiostat. Firstly, the electrodes were cycled in 0.1 M phosphate buffer solution, over the range –0.3 to 0.2 V to observe the surface redox process for the phendione ligand coordinated to the ruthenium or zinc metal ions (Appendix 3). The effect of sweep rate was studied by screening the library at range of scan rates from 10 to 500 mV s^{-1}. The anodic and cathodic peak currents increase linearly with scan rate as shown in Figure 3.4. This is consistent with surface immobilisation of the metal complexes and was observed for all modified electrodes in the library.[55,57]

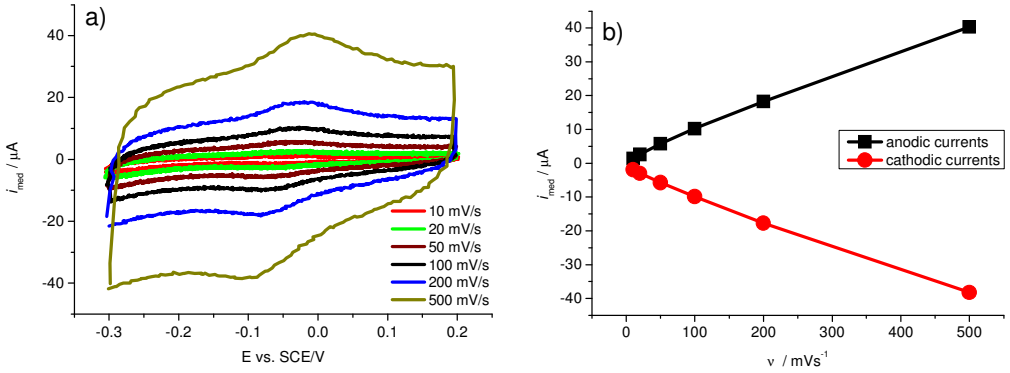

Figure 3.4 a) Effect of scan rate on modified GC electrode **13a** in 0.1 M phosphate buffer solution pH 7, electrode area of 0.71 cm^2; b) Plot of anodic (red) and cathodic (black) currents as a function of scan rate ν for modified electrode **13a**.

Table 3.3 reports the anodic (E_a) and cathodic (E_c) peak potentials, peak separation (ΔE_p) and midpoint potential (E_{mp}) (Figure 3.5). In general, the choice of the metal ion and geometry of the metal complex affect the kinetics of electron transfer as shown by the difference between anodic and cathodic potentials for the tetrahedral zinc and the octahedral ruthenium complexes.

Linker	Metal ion	Complex	E_a *vs.* SCE/mV	E_c *vs.* SCE/mV	ΔE_p *vs.* SCE/mV	E_{mp} *vs.* SCE/mV
EDA	Ru	A	−33	−78	−45	−56
	Ru	B	−33	−86	−53	−60
	Ru	C	−39	−84	−45	−61
	Zn	D	−44	−137	−93	−91
	Zn	E	−47	−135	−88	−91
HDA	Ru	A	−23	−81	−58	−52
	Ru	B	−17	−82	−65	−50
	Ru	C	−33	−82	−49	−58
	Zn	D	−35	−143	−108	−89
	Zn	E	−30	−151	−121	−90
EDDA	Ru	A	−24	−75	−51	−50
	Ru	B	−20	−87	−67	−54
	Ru	C	−34	−84	−50	−59
	Zn	D	−34	−147	−113	−91
	Zn	E	−12	−144	−132	−77
BA	Ru	A	−15	−98	−83	−56
	Ru	B	−10	−93	−84	−52
	Ru	C	−20	−92	−72	−56
	Zn	D	−5	−144	−139	−75
	Zn	E	−35	−147	−112	−91

Table 3.3 Summary of anodic and cathodic potentials peaks E_a and E_c, separation peak ΔE_p, midpoint potential $E_{mp} = (E_a + E_c) / 2$ obtained from cyclic voltammograms recorded in 0.1 M phosphate buffer solution pH 7 at a scan rate of 50 mV s^{-1}.

Slower electron transfer was observed for electrodes modified with zinc complexes where the average ΔE_p of 113±6 mV is significantly greater than for a ruthenium modified electrodes where ΔE_p of 60±4 mV. The choice of the metal ion also affects

the thermodynamics of the phendione ligand redox process as shown by the variation in the midpotential E_{mp} values with average E_{mp} of −55±1 mV *vs.* SCE for the ruthenium complexes and E_{mp} of −86±2 mV *vs.* SCE for the zinc complexes.

Similar values of ΔE_p and E_{mp} were observed between the metal complexes A, B and C, which might suggest that the presence of various ligands such as chloride ions, 2,2'-bipyridine ligand or increased number of the phendione ligands (complex C), have negligible effect on the kinetics and thermodynamics of the modified electrodes (Figure 3.5). A similar situation was observed for the electrodes modified with tetrahedral zinc complexes D and E, where the presence of different chelating ligands did not affect the values of ΔE_p and E_{mp}. Previously reported modification of the GC electrode by various linkers and anthraquinone as the redox probes showed that the nature of the linker has an effect on the electron transfer kinetics. The values of ΔE_p were found to increase with increasing chain length of the aliphatic linkers. Relatively high values of ΔE_p were observed for electrodes functionalised with the benzylamine linker BA.[55,57] A similar effect of the linker on the electron transfer kinetics was observed between different linkers in the library.

Based on the peak separation data ΔE_p, the electron transfer kinetics are faster for electrodes modified with the aliphatic linkers EDA, HDA and EDDA rather than the benzylamine linker BA. In the case of the ruthenium modified electrodes average values of ΔE_p of 54±3 and ΔE_p of 80±4 mV were obtained for aliphatic and BA linkers, respectively. The values of the peak separation ΔE_p for the modified electrodes with the zinc complexes were relatively smaller with ΔE_p of 109±7 mV for the aliphatic linkers and ΔE_p of 125±14 mV for the BA linker. However, the type of linkage does not influence the redox potential (E_{mp}) of the modified electrodes.

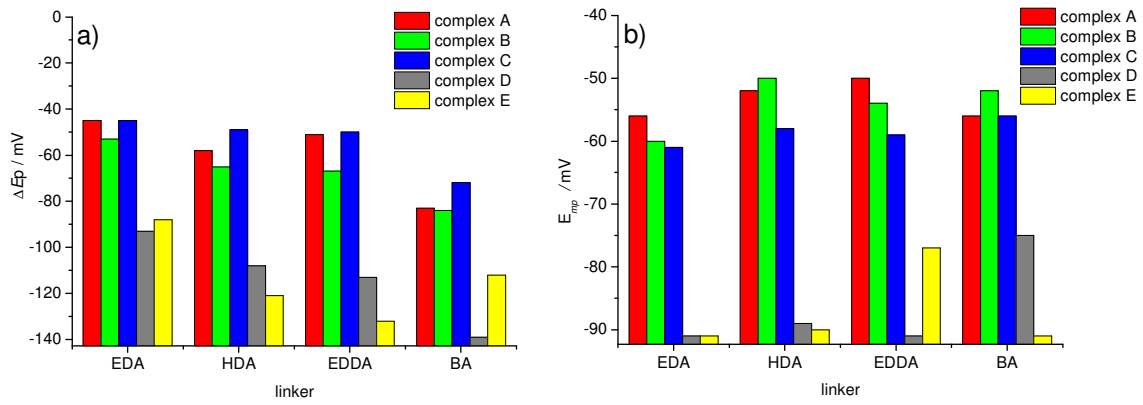

Figure 3.5 Average values of the separation pontential E_p (plot a) and the midpoint potential E_{mp} (plot b) observed for twenty different modifications in the library based on the experimental data recorded in 0.1 M phosphate buffer solution pH 7 at scan rate 50 mV s^{-1}.

The efficiency of the different modifications for the 63 member library was determined by calculating the amount of immobilised metal complex with redox active phendione ligands. The surface coverage, Γ_{med}, of the modified electrodes was calculated according to Equation 2.1. Figure 3.6a shows the summary of the mean values of the surface coverage Γ_{med} (mol cm^{-2}) calculated for twenty different modifications in the library and the standard errors of the mean value associated with each modification. The average value of Γ_{med} for each modification was calculated from three replicate electrodes. The reproducibility of each modification was justified by calculations of the standard errors of the mean using Origin 8.1 software. Electrodes modified with different linkers and metal complexes show variations in the calculated values of the coverages Γ_{med}. The coverage is related to the size of the immobilised metal complex at the surface. Electrodes modified with the relatively smaller zinc (II) complexes D and E show significantly higher coverage than electrodes modified with the bulkier ruthenium (II) complexes. The coordination environment also affects the surface coverage as observed for the electrodes modified by the three different ruthenium complexes A, B and C. Higher coverages were observed for complex A, which contains two relatively small chloride ligands. Substitution of the chloride by the more bulky 2,2'-bipyridine or phendione bidentate ligands decreases the coverage for the electrodes modified with complexes B and C. The presence of different bidentate ligands at the surface does not affect the coverage as shown by comparison between the modifications with the complexes D and E.

The attachment of linkers with different functionalities and chain lengths also influences the values of the surface coverage of the metal complexes. Electrodes functionalised with the EDA linker show higher values of Γ_{med} in comparison with electrodes modified with the longer aliphatic linkers HDA and EDDA. These results are in good agreement with modifications of the individual electrodes (Section 2). This might be rationalised by the fact that the coverage obtained after initial electrochemical attachment of the *mono*-Boc protected diamine linkers decreases for the amines with longer aliphatic chains. Approximate values of the surface coverages of the diamine linkers with different chain lengths were calculated based on XPS experimental data and clearly show that the coverages of the diamine linkers decrease with the length of the aliphatic chain.[57] The presence of the longer aliphatic chain in the diamine might cause a conformational disorder within the alkyl chains and hinder the access of the free amine group to the carbon surface thus preventing the amine from covalent attachment to the GC surface.[149] As a result, the surface coverages calculated from XPS data for the longer linkers are relatively smaller than for electrodes modified with shorter linkers such as EDA. Thus, lower number of the linker at the GC decreases yields of the subsequent steps of the electrode modification (Scheme 3.3), resulting in lower final coverage of the redox active metal complex attached at the surface.

Relatively low values of Γ_{med} were also obtained for electrodes modified by the BA linker. In this case, it might be explained by the limited flexibility of the bond between the aromatic ring of the linker and the GC surface. The rigid structure of the linker at the surface might prevent the 2,2'-bipyridine ligand from coordinating to the metal ion in the relatively large metal complex.

These results show that the length and flexibility of the linkers and the geometric arrangement of the metal complex at the surface all affect the surface coverage for the different modifications.

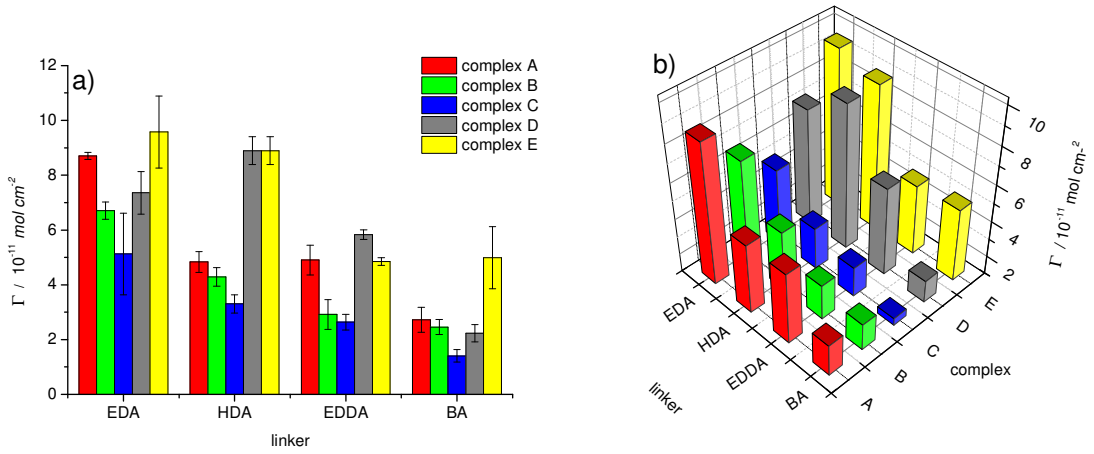

Figure 3.6 Average values of the surface coverage Γ_{med} of the metal complex calculated for 20 different modifications in the library using Equation 2.1 based on experimental data recorded in 0.1 M phosphate buffer solution pH 7 at scan rate of 50 mV s^{-1}; geometrical electrode area of 0.071 cm^2; Complexes A, B, D and E contain one phendione ligand whereas complex C has two phendione ligands; a) Each bar represents mean values of Γ_{med} with the and standard error of the mean for three replicate electrodes; b) three dimensional representation of the means.

3.4 Catalytic oxidation of NADH

The electrochemical HTP screening of the library was applied for rapid evaluation of the catalytic activity of the library towards NADH catalytic oxidation in a single set of parallel measurements.

The initial experiment was performed in a freshly prepared 1 mM aqueous solution of NADH at 50 mV s^{-1}. Figure 3.7 compares cyclic voltammograms in the absence (red line) and presence (black line) of NADH for modified electrode **13a**. The results are typical for all the modified electrodes in the array. A decrease in the potential of NADH oxidation E_{NADH} to 13±1 mV *vs.* SCE was observed relative to oxidation of NADH at bare GC, clearly indicating an electrocatalytic effect for all of the modifications.[158] A full set of cyclic voltammograms in the presence and absence of NADH for all members of the library are given in Appendix 2.

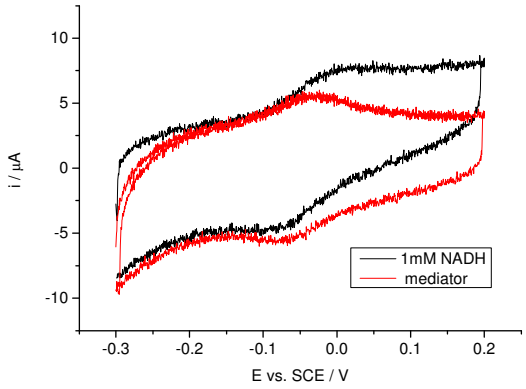

Figure 3.7 An example of a cyclic voltammograms recorded in the presence (black) and absence (red) of 1 mM NADH in 0.1 M phosphate buffer solution pH 7 at a scan rate of 50 mV s^{-1}, geometrical electrode area of 0.071 cm^2. Data shown in Figure 3.7 corresponds to a modified electrode **13a**.

The catalytic currents, i_{cat}, were defined as the difference between the anodic currents in the presence and absence of NADH at a potential of 0.15 V. Figure 3.8 shows a summary of average values of i_{cat} obtained for twenty different modifications in the library; the associated standard errors of the means for all of the modifications does not exceed twenty percent. This error might be related to the differences in roughness between individual electrodes. Each mean value of i_{cat} represents currents in the presence of NADH recorded for three replicate electrodes.

In general, the trends in the values of i_{cat} reflect the surface coverage of the metal complexes for electrodes modified with the ruthenium complexes A, B and C, where the values of i_{cat} increases with higher coverage of the metal complex (Figure 3.6). In this case, increase of the values of i_{cat} with the surface coverage would suggest all the phendione ligands present at the surface participate in the catalytic reaction.

The values of i_{cat} obtained for the modifications with the zinc complexes D and E are lower than would be expected for relatively high coverages calculated for the modifications with these complexes. This might suggest that not all of the phendione ligands coordinated to the zinc metal ion participate in the oxidation of the NADH. This explanation could be confirmed by designing modified GC electrodes, where zinc complexes D and E would create less than a full monolayer of the complex at the GC, which could be obtained by introduction of different blocking (capping) groups. The partial surface coverage of complexes D and E would be then studied for dependence of the coverage on the NADH catalytic currents.

The measured values of i_{cat} obtained for the various linkers are also affected by the surface coverage (Figure 3.8). The most pronounced catalytic activity was obtained for modifications with the EDA linker and decreases with longer aliphatic linkers as shown in modifications with HDA and EDDA linkers. Relatively low values of i_{cat} were found for electrodes modified with the BA linker, presumably due to its limited flexibility, which might prevent the orientation of the phendione ligand necessary for hydride transfer between the quinone groups at the surface and NADH molecules.

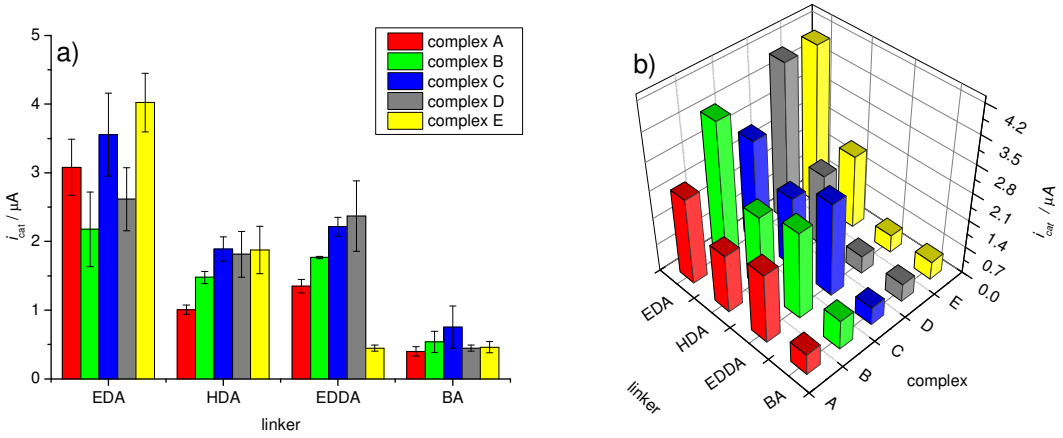

Figure 3.8 a) Means of the catalytic currents i_{cat} for 20 different modifications of the library measured in 1 mM NADH solution at a scan rate of 50 mV s^{-1}. Each bar represents an average value of i_{cat} and

the standard errors of the means calculated for 3 replicate electrodes; b) The means of i_{cat} values for 20 different modifications of the library presented in three dimensional bar plot.

In order to justify the differences in the catalytic efficiency between various modifications, the catalytic currents were normalised according to Equation 2.2. The values of catalytic currents obtained for 1 mM NADH and presented in Figure 3.8 were initially normalised by surface coverage of the phendione ligands (Figure 3.6).

In general, the structure and length of the linkers has a pronounced effect on the values of i_{norm} (units of A cm^5 mol^{-2}) (Figure 3.9). The values of i_{norm} calculated for electrodes modified with the aliphatic linkers show higher values of i_{norm} than for electrodes modified with the BA linker, which might be related to the limited flexibility of this linker as discussed previously. On the other hand, structure and geometry of the metal complex has a smaller effect on the values of i_{norm}. However, the general trend was observed for complexes B and C with phendione and 2,2'-bipyridine ligands showing slightly higher catalytic activity than complexes A, D or E. This might suggest that the presence of additional ligands with conjugated aromatic systems in the metal complex increases the catalytic activity towards NADH oxidation. The best catalytic effect was observed for modification with the complex B attached at the surface through the EDDA linker. This might be rationalised by long chain of the EDDA linker, which provides better accessibility of the mediator for the bulky NADH molecule and the presence of the 2,2'-bipyridine ligand in the structure of the complex C might also affect the catalytic activity towards NADH oxidation.

The values of i_{norm} presented in Figure 3.9 were calculated based on surface coverage of the phendione ligands, which is valid if we assume that all of the phendiones at the surface are involved in the catalytic oxidation of the NADH. For the octahedral complex C, the *cis* geometrical orientation of the two phendione ligands might limit access of both quinone groups simultaneously to the relatively large NADH molecule and prevent two molecules of the NADH being oxidised by the pair of phendione ligands in a single C complex at the same time.

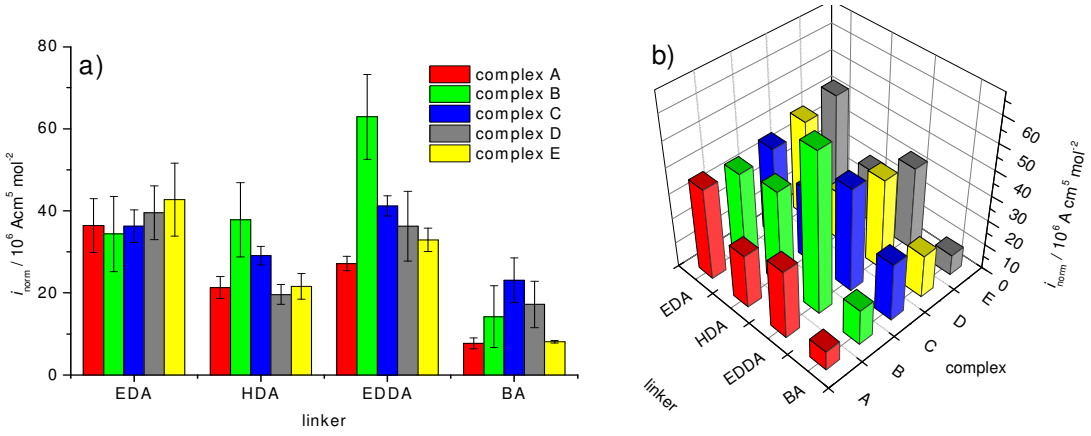

Figure 3.9 Average values of the normalised catalytic currents i_{norm} calcultated for 20 different modifications in the library based on the surface coverage of the phendione ligands using experimental data recorded for 1 mM NADH in phopshate buffer solution at scan rate of 50 mV s^{-1}; a) Each bar represents an average value of i_{norm} and the standard errors of the mean calculated for 3 replicate electrodes; b) The means of i_{norm} values presented in a three dimensional bar plot.

In order to present the experimental data in different way, the values of i_{norm} were recalculated based on the assumption that only one of the phendione ligands in the complex C participates in the oxidation of NADH. In this case, the catalytic currents were normalised by surface coverage of the metal complex as one molecule of the complex C can catalyse oxidation of one molecule of the NADH at a time.

As shown in Figure 3.10, the values of i_{norm} for the complex C are significantly higher than for others metal complexes in the library. According to this assumption the highest i_{norm} of 72.5 and 82.4 × 10^6 A cm^5 mol^{-2} were obtained for the complex C attached at the surface through the EDA and EDDA linker, respectively. These results clearly suggest that the presence of the additional phendione ligand coordinated to the metal centre might contribute to the catalysis of NADH oxidation at the GC surface.

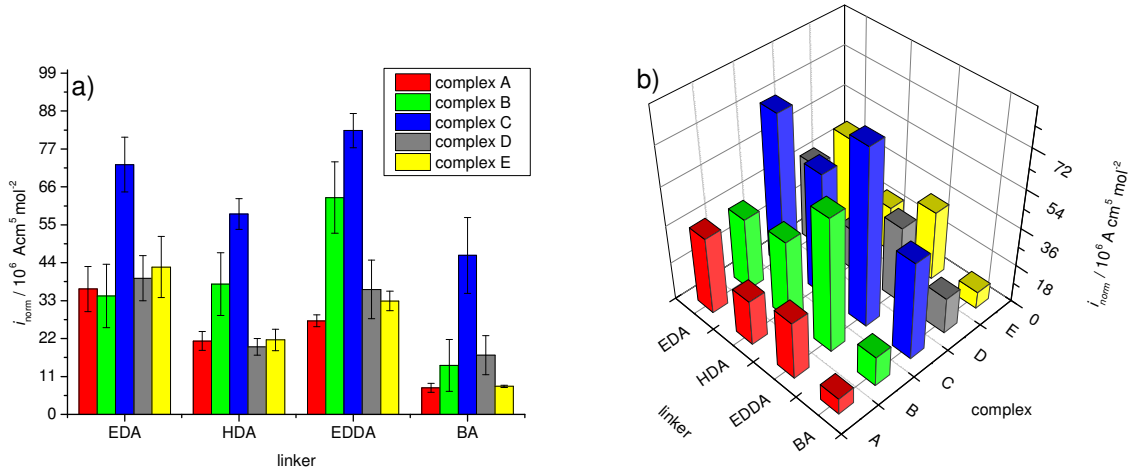

Figure 3.10 Average values of the normalised catalytic currents i_{norm} calcultated for 20 different modifications in the library based on the surface coverage of the metal complexes using experimental data recorded for 1 mM NADH in 0.1 M phopshate buffer solution at scan rate of 50 mV s^{-1}. Complexes A, B, D and E contain one phendione ligand whereas complex C has two phendione ligands; a) Each bar represents an average value of i_{norm} and the standard errors of the mean calculated for 3 replicate electrodes; b) The means of inorm values presented in a three dimensional bar plot.

3.5 Control electrodes.

Interesting results were observed for control electrodes 16-18 modified with electrochemically inactive (2,2'-bipyridine)zinc (II) chloride complex and EDA linker. Screening of these electrodes in 1 mM NADH solution gave faradaic current at potential of 0 V, which corresponds to the oxidation of NADH catalysed by quinone groups (Figure 3.11). In case of the control modifications, the only source of quinone groups are those present at the oxidised glassy carbon surface, which are known to catalyse the NADH oxidation at low overpotential.[99]

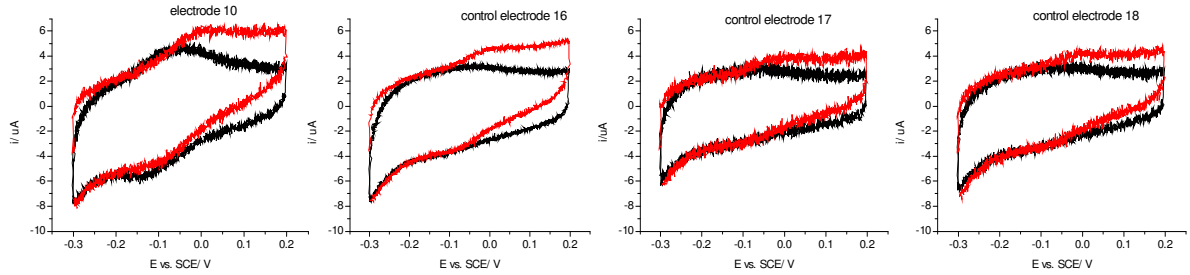

Figure 3.11 Cyclic voltammograms for the modified electrode **13a** and the control electrodes **70a-c** obtained duirng HTP screening in 0.1 M phosphate buffer solution pH 7, scan rate of 50 mV s^{-1} (black curve), in 1 mM NADH aqueous solution at scan rate of 50 mV s^{-1} (red curve).

An average value of i_{cat} measured for the control electrodes is about 1.5 μA and it is relatively low in comparison with the catalytic currents obtained for the modifications with the EDA linker and zinc complex D with an average value of i_{cat} about 3 μA. This indicates that the catalytic currents observed for all electrodes modified with complexes from A to E are result of the catalysis of NADH by the quinone groups of phendione ligand. As shown in Figure 3.11, the peaks for oxidation of NADH by quinone at the surface and quinone groups of the phendione occur at the same potential of 0 V. Therefore there is not possible to distinguish between the catalysis come from quinone of metal complexes and the oxidised carbon. In addition, the fraction of the NADH current catalysed by quinone directly bonded at the surface might also depend on size of the linker and the metal complex. As a result, values of i_{cat} and i_{norm} for modification of electrodes by complexes A, B, C, D and E discussed in Sections 2 and 3.4 also might include unknown amount of

the catalytic current obtained from oxidation of NADH by quinone functional groups directly bonded at the surface.

3.6 Kinetic analysis for 63 member library

3.6.1 General

HTP electrochemical screening of the library of 63 modified electrodes in NADH containing solution clearly showed that the complexes A-E bound at the electrode surface catalyse oxidation of NADH at low overpotential (Sections 2 and 3). The values of catalytic currents in the presence of NADH vary between different modifications and clearly indicate effect of the linker and metal complex on the catalytic activity towards NADH oxidation. In order to understand in more detail the mechanism of the catalytic reaction between modified electrode surface and NADH as well as justify the catalytic efficiency of individual modifications, the kinetics of the NADH oxidation were studied for modified electrodes A-E.

In general, catalytic oxidation of NADH by mediator M_{ox} can be described by a reaction sequence obeying the well-known Michaelis-Menten kinetic model (Section 1.5). Reversible formation of an intermediate charge complex {NADH-M_{ox}} allows for a hydride transfer reaction within the complex followed by its decomposition to yield reduced mediator M_{red} and NAD^+ with a heterogeneous rate constant k_{cat}.[43]

$$\text{NADH} + \text{Med}_{ox} \underset{}{\overset{K_M}{\rightleftarrows}} \{\text{NADH-Mediator}\} \xrightarrow{k_{cat}} \text{NAD}^+ + \text{Med}_{red}$$

Figure 3.12 Mechanism of NADH catalytic oxidation according to the Michaelis-Menten model.

This type of mechanism has been suggested for NADH oxidation at a number of chemically modified electrodes. The presence of the intermediate complex between mediators at the surface and NADH in solution was indicated for electrodes modified by conducting organic salts,[120] phenoxazine dyes,[108,159,160] such as Meldola blue or 1,2-benzophenoxazine7-one (BPO) adsorbed at the electrode surface. The theoretical kinetic model of the heterogeneous catalytic reaction was initially studied by Albery and co-workers suggesting the analogy between the enzyme electrode kinetics and heterogeneous redox catalysis.[120,161-167] As a result, they developed a mathematical model of the kinetics for heterogeneous catalysis where the amperometric response is governed by number of the surface processes, such as:

- Mass transport of the substrate to the electrode surface including concentration polarisation effect

- Bonding of the substrate to the mediator at surface to create an intermediate reaction complex, if the catalytic reaction occurs according to Michaelis-Menten model
- Electron and proton transfer within the intermediate complex followed by its decomposition to yield products of the catalytic reaction
- Electrochemical regeneration of the mediator at the electrode surface
- Diffusion of the product from the surface considering the effect of product inhibition.

Analytical treatment of the kinetics for heterogeneous catalysis proposed by Albery was also applied for investigation of the kinetics of NADH and ascorbate oxidised at polymer coated electrodes.[7,9,10] In this case, the substrate is assumed to diffuse into vacant sites within the polymer film, where the Michaelis-Menten type of reaction occurs and the kinetics of the catalytic reaction were also determined by the thickness of the film and the diffusion process of the substrate into the polymer.

Aspects of the kinetic studies of Albery were also applied by Lyons[168] and Bartlett[169] in a proposed theoretical model for oxidation of formate and glucose at hydrated oxide electrodes in alkaline solution.[168,170] The same theoretical model was applied for kinetic analysis of the library of 63 modified electrodes presented in this thesis. The following Section gives a brief explanation of the mathematical approach and discussion of its application to twenty different modifications in the library.

3.6.2 Theoretical kinetic model for NADH oxidation at modified electrodes.[168]

The Michaelis-Menten kinetic approximation was used by Lyons[168] and Bartlett[169] in order to design a kinetic model for heterogeneous redox catalysis for NADH oxidation at stationary electrodes. According to their approach, the Michealis-Menten catalytic reaction occurs at the solution/electrode interface, where NADH diffuses to the electrode surface then forms the intermediate complex with the immobilised mediator. This is followed by dissociation of the NAD^+ and subsequent electrochemical oxidation of the mediator to complete the catalytic cycle. The overall scheme for the catalytic reaction is analogous to that discussed by Bartlett (Figure 3.13).[169]

$$NADH_\infty \xrightarrow{k_D} NADH_o$$
$$NADH_o + [Q] \underset{}{\overset{K_M}{\rightleftharpoons}} [NADH\text{-}Q]$$
$$[NADH\text{-}Q] \xrightarrow{k_{cat}} NAD^+_o + [QH]$$
$$NAD^+_o \xrightarrow{k_D} NAD^+_\infty$$
$$[QH] \xrightarrow{k_E} [Q] + 2\bar{e} + H^+$$

Figure 3.13 Proposed reaction scheme for the oxidation of NADH at the mediator modified electrodes, according to Bartlett and Wallace.[169] Subscripts ∞ and $_O$ indicate NAD in the bulk solution and at the surface/solution interface. Q represents the oxidised form of the mediator; QH represents the reduced form of the mediator; [NADH-Q] represents the intermediate complex; k_D is the diffusion rate constant and is considered to have the same values for NADH and NAD^+; K_M is the Michaelis-Menten equlibrium constant for the complex [NADH-Q]; k_{cat} is heterogenous rate constant for the chemical reaction within [NADH-Q] complex; k_E is the rate constant for the electrochemical oxidation of the reduced mediator QH.

As shown in Figure 3.13 $NADH_\infty$ diffuses from bulk solution to the surface/solution interface $NADH_o$ with a diffusion rate constant k_D. [Q] represents the oxidised quinone groups of the phendione ligands, which binds the $NADH_o$ to give the [NADH-Q] complex. The strength of the interactions between Q and NADH is described by the equilibrium constant K_M (units of mol cm^{-3}). The bounded NADH is oxidised by the quinone groups, giving the reaction products NAD^+ and the reduced form of mediator [QH]. Chemical reaction within the [NADH-Q] complex

occurs with a rate constant k_{cat} (units of s^{-1}). The reduced form of the mediator [QH] is recycled electrochemically driven by the applied anodic potential at the electrode. Electron transfer between the electrode and the immobilised mediator is assumed to be rapid and its kinetics are described by the rate constant k_E (units of s^{-1}). Finally, the NAD^+ diffuses away from the surface with rate constant k_D and product inhibition by NAD^+ in this case is ignored. The mass transport rate constants k_D of the substrate and product are assumed to be the same.

Mathematical analysis reported by Lyons leads to an expression for the steady-state reaction rate or flux j, where the different possible rate-limiting steps can be distinguished

$$\frac{1}{j}=\left(1-\frac{j}{k_D[\mathrm{NADH}]}\right)\left\{\frac{1}{k_E\Gamma_{med}}+\frac{1}{k_{cat}\Gamma_{med}}\right\}+\frac{K_M}{k_{cat}\Gamma_{med}[\mathrm{NADH}]}+\frac{1}{k_D[\mathrm{NADH}]} \qquad 3.1$$

where term [NADH] represents the concentration of NADH in a bulk solution and Γ_{med} is a surface coverage of the mediator. The overall flux j is determined by the rate-limiting step in the catalytic reaction scheme, Equation 3.1 can be simplified for each case. When mass transport of NADH is slow, the term in k_D will be dominant. The overall flux can also be limited by the kinetics of the chemical reaction between mediator and NADH. For lower concentrations of NADH, the flux is limited by the binding constant between product and mediator and the catalytic rate constant given by K_M and k_{cat}, respectively. Equations can be then reduced to

$$\frac{1}{j}=\frac{K_M}{k_{cat}\Gamma_{med}[\mathrm{NADH}]} \qquad 3.2$$

In the case of saturated kinetics at high NADH concentrations, all quinone groups at the surface can take part in the catalytic reaction and the expression for j will be reduced to

$$\frac{1}{j}=\frac{1}{k_{cat}\Gamma_{med}} \qquad 3.3$$

When the overall reaction rate is governed by the rate of the electron transfer between the electrode and mediator k_E, then the Equation 3.1 reduces to

$$\frac{1}{j}=\frac{1}{k_E\Gamma_{med}} \qquad 3.4$$

In the case of the slow NADH transport through the diffusion layer, concentration polarisation will cause the surface concentration of NADH to be less than the concentration of NADH in the bulk solution and results in less saturated catalysis than would be expected. This effect is described in Equation 3.1 as

$$\frac{1}{j} = 1 - \frac{j}{k_D[\mathrm{NADH}]} \qquad 3.5$$

Next, using the relationship between current and flux,[171]

$$i = \mathrm{nFA}j \qquad 3.6$$

Equation 3.1 was rearranged by Lyons and Bartlett[168] to give an expression for the overall catalytic current i_{cat}

$$i_{cat} = nFA\left[\frac{k_D}{2}\left\{\left(K_{ME} + [\mathrm{NADH}_\infty]\right) - \sqrt{\left(K_{ME} + [\mathrm{NADH}_\infty]\right)^2 - \left(\frac{4K_{ME}k_{ME}[\mathrm{NADH}_\infty]}{k_D}\right)}\right\}\right] \qquad 3.7$$

where K_{ME} is the Michaelis-Menten constant for the modified electrode defined by

$$K_{ME} = \left(\frac{K_M}{k_{cat}} + \frac{\Gamma}{k_D}\right)\left(\frac{1}{k_E} + \frac{1}{k_{cat}}\right)^{-1} \qquad 3.8$$

and k_{ME} is the effective electrochemical rate constant for modified electrode at low substrate concentrations

$$k_{ME} = \left(\frac{K_M}{k_{cat}\Gamma} + \frac{1}{k_D}\right)^{-1} \qquad 3.9$$

The above expression for the catalytic current has four limiting cases depending on the relative values of NADH concentration and the different kinetic parameters.

I. Mass transport kinetics

When the mass transport of NADH to the electrode is the limiting factor, the rate constant k_D will be dominant in the expression for the overall current. This is valid only for unsaturated catalysis ([NADH]<K_{ME}) when the catalytic reaction and the electrochemical regeneration of the mediator are fast enough not to be considered as rate limiting (k_D<$k_{cat}\Gamma/K_M$). In this case the current can be described

$$i_I = \mathrm{nFA}k_D[\mathrm{NADH}]_{bulk} \qquad 3.10$$

In this work, the diffusion rate constant k_D was calculated using the Randles-Sevčik equation for the mass transport limited current at a stationary electrodes[172]

$$k_D = 0.46\sqrt{\frac{F}{RT}\ v\ \mathrm{n}\ D} \qquad 3.11$$

F, R and T have their usual meanings, v is the scan rate (V s^{-1}), n is the number of electrons taking part in the electrochemical reaction and D represents diffusion coefficient, which in this case equals 2.4×10^{-6} cm^2 s^{-1} for NADH in aqueous solution.[173]

II. Unsaturated reaction kinetics k_{cat}/K_M

In this case, the overall current is determined by the term in k_{cat}/K_M

$$i_{II} = \frac{\mathrm{nFA}k_{cat}\Gamma[\mathrm{NADH}]_{bulk}}{K_M} \qquad 3.12$$

In this situation, the kinetics of the chemical reaction are slower than the mass transport of the NADH ($k_D>k_{cat}/K_M$) and electrochemical reaction ($k_E>k_{cat}/K_M$).

III. Saturated catalysis and slow electrochemical reaction kinetics

For higher concentrations of NADH, where all the active sites of the mediators take part in catalysis ([NADH]>K_{ME}), if the rate of mass transport and the catalytic rate constant are assumed to be greater than the rate of electron transfer between mediator and surface ($k_E<k_{cat}$ and $k_E<k_D$). The overall current will be described by

$$i_{III} = nFAk_E\Gamma \qquad 3.13$$

IV. Saturated catalysis and slow chemical reaction kinetics

In the case of saturated catalysis at high NADH concentrations, the kinetics of the chemical reaction can also become the limiting step if the electrochemical and mass transport kinetics are fast ($k_E>k_{cat}$ and $k_E>k_D$). In this case, the chemical reaction within the intermediate complex between NADH and quinone groups is rate limiting. The current in this situation is given by

$$i_{IV} = \mathrm{nFA}k_{cat}\Gamma \qquad 3.14$$

3.6.3 Analysis of the heterogeneous rate constant k_{cat} and the equilibrium constant K_M for the library of 63 modified electrodes.

The mathematical model presented in Section 3.6.2 was applied to analyse the experimental data obtained from the HTP screening of the library, carried out at four different scan rates 10, 20 50 and 100 mV s^{-1} and a range of NADH concentrations from 1 to 4 mM. Plots of the catalytic currents as function of NADH concentration were fitted to the Equation 3.7, using commercial software (Origin 8.1). Figure 3.14 shows a typical example of the fitting curves for electrodes **13a-c**.

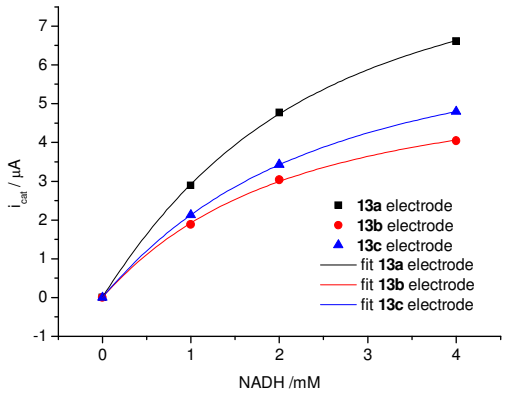

Figure 3.14 Plot of catalytic current i_{cat} as a function of NADH concentration at a scan rate 10 mV s^{-1} obtained for modifed electrodes **13a-c**; the points represent the experimental data and the lines are the best fits calculated from the theoretical model using Equation3.7.

Fitting of the theoretical model was also successfully obtained for experimental data at different scan rates, see Figure 3.15a for an example. However, the catalytic current at 100 mV s^{-1} in 2 mM NADH solution gives unexpected the lower values and leads to poor quality of the fitting curve. A similar problem was observed for most of the library members, which might be related to some unknown instrumental error during measurement. Fitting of the 100 mV s^{-1} curve was improved after excluding the data for 2 mM NADH solution for all members of the library (Figure 3.15b).

A similar problem occurred for some of the other experimental data, mostly for the electrodes modified with the BA linker at slow scan rates. The source of these errors is unknown. To obtain the best fits, these problematic data were excluded from our

calculations. Values of k_{ME} and K_{ME} for the best fits calculated for all members of the library are given in Appendixes 4-7.

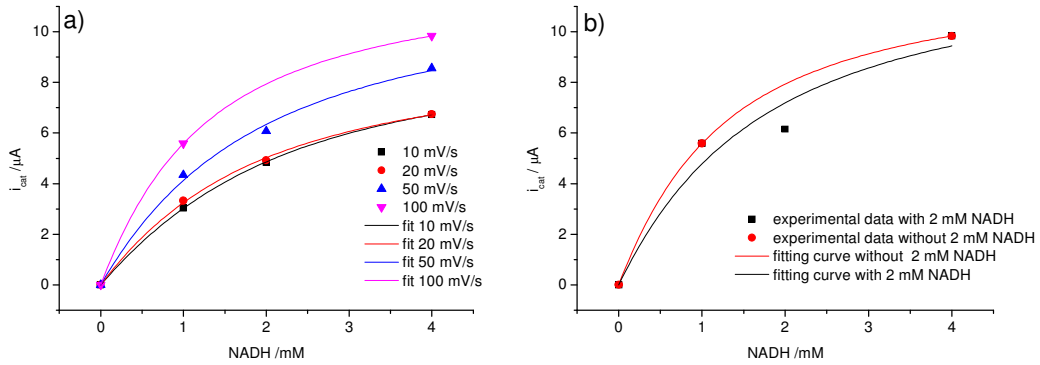

Figure 3.15 a) Plot of catalytic current as a function of NADH concentration at scan rates of 10, 20, 50 and 100 mV s^{-1}; the points are experimental data, the lines are fitting curves obtained calculated from Equation 3.7; b) Comparison of the fitting curves obtained for scan rate 100 mV s^{-1} with experimental data in 2 mM NADH (black line) and without 2 mM NADH (red line).

Rearrangement of Equation 3.8 and 3.9 leads to expressions for the catalytic rate constant k_{cat} and the Michaelis-Menten equilibrium constant K_M based on the assumption that the electrochemical regeneration of mediator at the electrode surface is not the rate-limiting step ($k_E > k_D$ and $k_E > k_{cat}$). The rate of electron transfer between electrode surface and mediator is relatively rapid as evidenced by constant peak potentials observed for all members of the library in range of applied scan rates. For values of $k_E \rightarrow \infty$, Equation 3.8

$$K_{ME} = \left(\frac{K_M}{k_{cat}} + \frac{\Gamma}{k_D}\right)\left(\frac{1}{k_{cat}}\right)^{-1} \qquad 3.15$$

which can be rewritten as

$$\frac{K_M}{k_{cat}} = \frac{K_{ME}}{k_{cat}} - \frac{\Gamma_{med}}{k_D} \qquad 3.16$$

Equation 3.16 was then substituted into Equation 3.9 to obtain an expression for the catalytic rate constant k_{cat}

$$k'_{ME} = \left(\left(\frac{K_{ME}}{k_{cat}} - \frac{\Gamma_{med}}{k_D}\right)\frac{1}{\Gamma_{med}} + \frac{1}{k_D}\right)^{-1} \qquad 3.17$$

$$k_{cat} = \frac{k'_{ME} K_{ME}}{\Gamma_{med}} \qquad 3.18$$

Rearrangement of Equations 3.15 and 3.18 gave the expression for the Michaelis-Menten constant

$$K_M = K_{ME}\left(1 - \frac{k_{ME}}{k_D}\right) \qquad 3.19$$

Values of the fitting parameters k_{ME}, K_{ME} and the calculated values of k_{cat} and K_M for all the electrodes in the library are presented in Appendix 8. Each value of k_{ME} and K_{ME} was calculated using experimental data obtained for three different NADH concentrations (1 mM, 2 mM and 4 mM) and screened at four different scan rates (10 mV s^{-1}, 20 mV s^{-1}, 50 mV s^{-1} and 100 mV s^{-1}). The values of k_{ME} and K_{ME} for each modified electrode in the library were then used to calculate k_{cat} and K_M. Average values of k_{cat} and K_M for twenty different modifications were calculated using three replicate electrodes and their summaries are presented in Figure 3.16-3.18. Overall, the mean value of k_{cat} or K_M for each modification represents experimental data obtained from 36 single sets of HTP measurments. The HTP electrochemical screening allowed for rapid evaluation and direct comparison of the kinetics between different modifications.

In case of the k_{cat}, structure of the metal complex has a pronounced effect on the heterogeneous rate constants k_{cat} (Figure 3.16). The highest values of k_{cat} were obtained for modifications with ruthenium complexes B and C with additional bidentate ligands such as 2,2'-bipyridine or phendione. In comparison, the values of k_{cat} obtained for electrodes modified with complex A containing two monodentate chloride ligands are relatively lower. This might indicate that the presence of the bidentate ligand with the conjugated aromatic system increases the rate of the catalytic reaction in the bound complex.

As seen from Figure 3.16, choice of the linker also affects the rates of the catalytic reaction. The highest calculated value of k_{cat} was obtained for modifications with relatively long EDDA, containing ethoxy functional groups in its structure. Relatively low values of k_{cat} were observed for modifications with the EDA linker. These results would clearly suggest that the longer linker increases the rate of the catalytic reaction, which might be rationalised by better accessibility of the bulk

metal complex to the large molecule of NADH. However, the proposed rationalisation could not be applied for modifications with the longer aliphatic linker HDA, where the values of k_{cat} were lower in comparison to the modifications with shorter EDA linker. For a given metal complex, the lowest values of k_{cat} were observed for the modifications with BA linker as would be expected from very low values of i_{cat} recorded for these modifications.

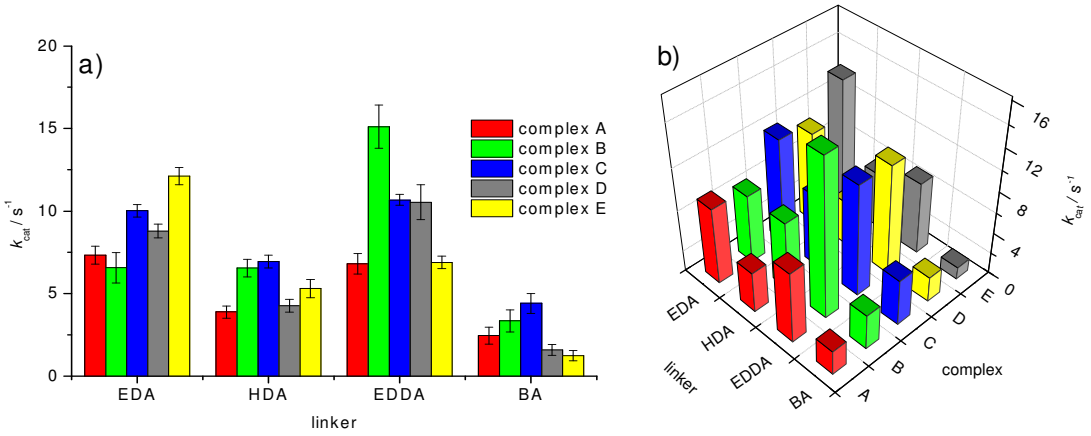

Figure 3.16 Average values of catalytic rate constants k_{cat} caclulated using surface coverage of the phendione ligands obtained for 20 different modifications in the library, where k_{cat} for each individual electrode was calculated using experimental data of 12 single sets of HTP measurments performed in 0.1 M phosphate buffer solution pH 7; complexes A, B, D and E contain one phendione ligand whereas complex C has two phendione ligands; a) means values of k_{cat} with the standard error of the mean of three replicate electro`des; b) 3D bar plot of average values of k_{cat} for 20 different modifications in the library.

According to Equation 3.18, the catalytic rate constants were normalised by surface coverage of the phendione ligands. For complex C, these results are based on the assumption that both of the phendione ligands participate in the catalytic oxidation of two molecules of NADH. However, oxidation of two molecules of NADH by both of the phendione ligands might be limited due to the *cis*-geometry of this complex, which might result in lower accessibility of the bulky NADH molecules to the quinone functional groups. Therefore, a second assumption was suggested in the analysis of k_{cat}, where only one phendione ligand in the metal complex participates in the catalytic oxidation of NADH. In this case, the catalytic

rate constants are normalised by surface coverage of the metal center as the whole molecule of the complex C participates in oxidation of molecule of the NADH. As a result, the calculated values of k_{cat} for the complex C increase their values by a factor of two making it by far the most efficient mediator towards NADH oxidation (Figure 3.17).

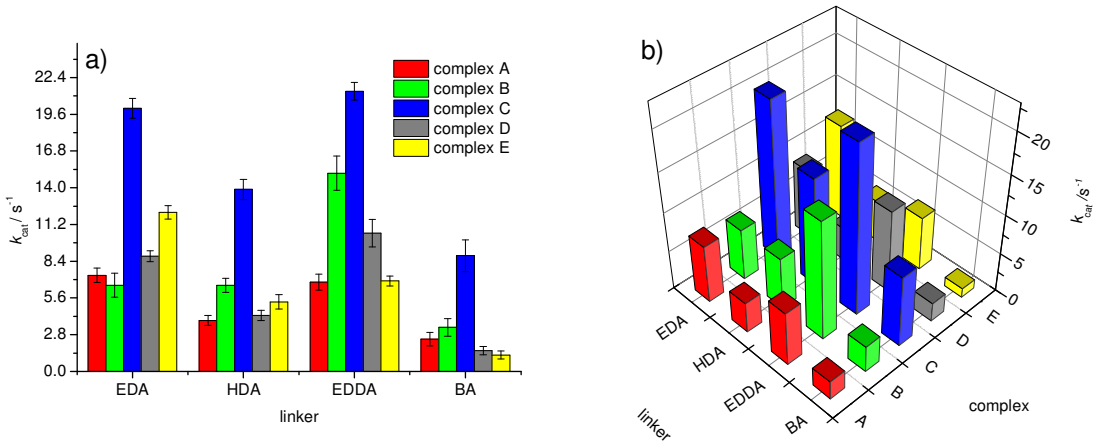

Figure 3.17 Average values of catalytic rate constants k_{cat} caclulated using surface coverage of the metal complex obtained for 20 different modifications in the library. The value of k_{cat} for each individual electrode was calculated using experimental data for 12 single sets of HTP measurments performed in 0.1 M phosphate buffer solution pH 7; a) mean values of k_{cat} with the standard error of the mean for the three replicate electrodes; b) 3D bar plot of average values of k_{cat} for 20 different modifications in the library.

The equilibrium constants K_M represent the strength of the intermediate complex formed between the NADH and the quinone groups. In general, values of the equilibrium constant K_M calculated for all modifications in the library are consistent for the electrodes modified by the aliphatic linkers EDA, HDA and EDDA at approximate K_M of 1.8 mM (Figure 3.18). A significant decrease in K_M was observed for modifications with the BA linker, which indicates that the charge transfer complex is more stable for the BA linker than for the aliphatic linkers. In this case, the relatively small amount of metal complex attached through this linker at the electrode surface might increase the number of uncoordinated 2,2'-bipyridine ligands present at the surface. This might additionally stabilises the intermediate complex by

interactions between free 2,2'-bipyridine ligands and the phosphate groups of the NADH.

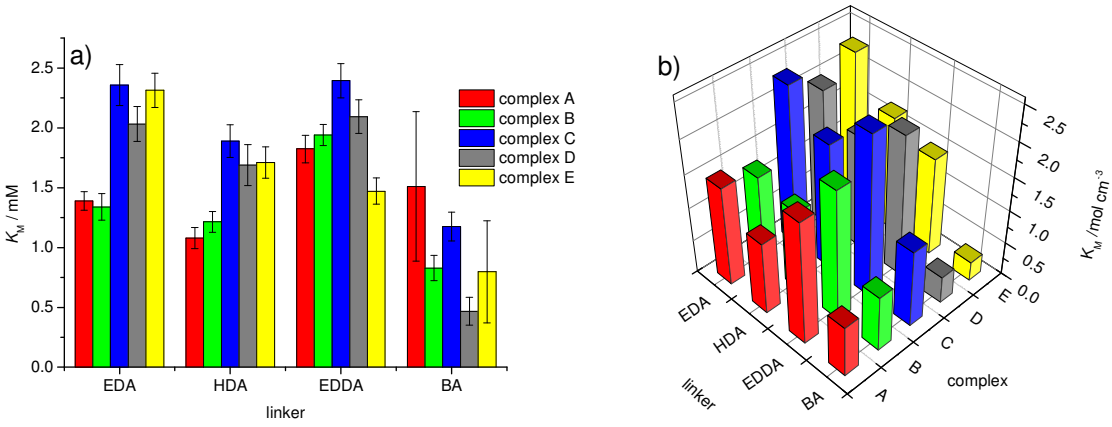

Figure 3.18 Average values of Michaelis-Menten constnat K_M and their three dimensional representation obtained for 20 different modifications in the library. Each bar represents mean value of K_M and standard error of the mean of three replicate electrodes, where K_M for each individual electrode was calculated using experimental data of 12 single sets of HTP measurments performed in 0.1 M phosphate buffer solution pH 7.

To the best of our knowledge, the discussed values of k_{cat} and K_M are the first report of quantitative analysis of the NADH catalysis by the phendione containing metal complexes based on the theoretical kinetic model proposed by Bartlett and Lyons. This theoretical kinetic model allowed us to evaluate the Michaelis-Menten constants and the first order rate constants k_{cat} corresponding to the saturated catalysis where the kinetics are independent on the NADH concentration. A similar kinetic model was also developed for oxidation of NADH at polymer coated electrodes, where the catalytic reaction occurs within the whole polymer film rather than at the polymer surface and the reaction is reversibly inhibited by the oxidation product NAD^+.[169,174] For the reported examples of polymer mediators, the values of rate constants were determined as a function of film thickness, electrode potential and NAD^+ concentration. Therefore, the literature examples could not be directly compared with the kinetic parameters obtained for the phendione complexes presented in the library, where the values of k_{cat} were determined based on assumptions that the reaction occurs at the electrode/solution interface and the NAD^+ inhibition was neglected.

However, a number of the phendione containing metal complexes physically adsorbed at the electrode surface were reported in the literature and showed significant amperometric response for NADH oxidation.[116,126,127,131,132,134,175] Kinetic studies for these complexes were based on a simplified kinetic model, where mass transport of the NADH is fast and concentration polarisation is negligible. The kinetic analysis reported for these complexes describes second order catalytic rate constants valid for low concentrations of NADH ([NADH] < K_M), where the chemical reaction between NADH and mediator is considered as bimolecular.

In order to compare the catalytic efficiency with the literature examples, the values of k_{cat} normalised by surface coverage of the metal complexes and the values of K_M were used to calculate a rate constant k_{cat}/K_M corresponding to unsaturated catalysis at low NADH concentrations ([NADH] < K_M). In this case, the reaction between quinone groups and the NADH is considered as bimolecular and the calculated rate constant k_{cat}/K_M is assumed to be second order (units of M^{-1} s^{-1}).

Figure 3.19a clearly shows that the values of k_{cat}/K_M depend on the metal complex for electrodes modified with the aliphatic linkers. Length and structure of the aliphatic linker has a minor effect on the values of k_{cat}/K_M. The best catalytic efficiency was obtained for electrodes modified with the complex C and EDDA linker with the highest k_{cat}/K_M of 7.44×10^3 M^{-1} s^{-1}. In general, high values of k_{cat}/K_M were obtained for complexes B and C in comparison with the other metal complexes. The effect of the linker for reaction rate at low NADH concentrations is negligible. In addition, relatively high average values of k_{cat}/K_M were observed for modifications with the BA linker, however high errors obtained for this linker unable compare them with other modifications in the library. For complex C, the catalytic rate constants k_{cat} were also calculated based on the assumption that only one phendione ligand participates in the catalytic reaction giving values of k_{cat} increased by a factor of two (Figure 3.16).

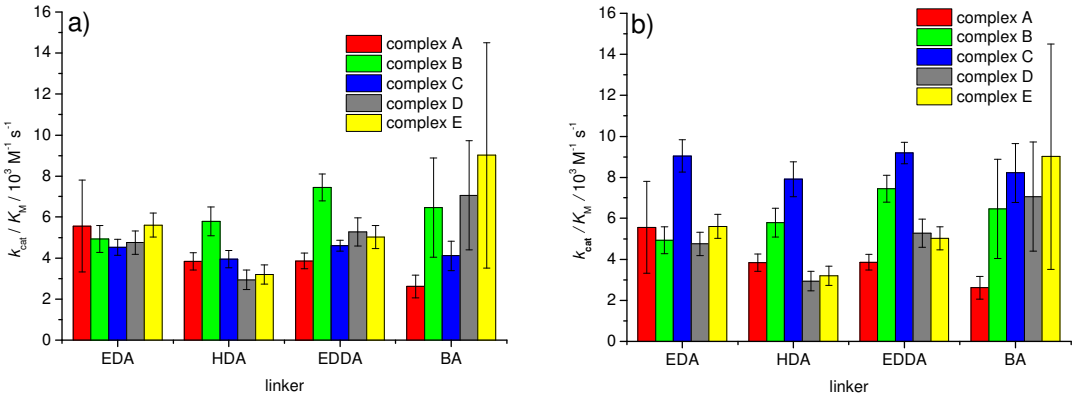

Figure 3.19 Average values of rate constants k_{cat}/K_M at low NADH concentrations ([NADH] < K_M) obtained for 20 different modifications in the library; Each bar represents mean values of k_{cat}/K_M with a standard error of the mean for three replicate electrodes; a) Means for k_{cat}/K_M calculated using values of k_{cat} presented in Figure 3.16 for the surface coverage of phendione ligands and K_M in Figure 3.18; b) Means for k_{cat}/K_M calculated using values of kcat presented in Figure 3.17 for the surface coverage of metal complexes and K_M in Figure 3.18.

The values of k_{cat}/K_M for the library members were compared with a number of literature examples for modified electrodes with adsorbed monolayers of phendione containing metal complexes. The reported rate constants for unsaturated catalysis suggest that metal complexes with a higher number of phendione ligands increase catalytic efficiency and vary from 0.9×10^3 (M^{-1} s^{-1}) for [Os(4,4'-dimethyl-2,2'-bipyridine)$_2$(phendione)]$^{2+}$ and 1.2×10^3 (M^{-1} s^{-1}) for [Ru(phendione)$_2$(5-amino-1,10-phenanthroline)]$^{2+}$ to 6.8×10^3 (M^{-1} s^{-1}) for a monolayer of [Fe(phendione)$_3$]$^{2+}$ complex.[134] The same effect was observed between modifications in the library, where complexes A, B, D and E with one phendione ligand gave lower values of k_{cat}/K_M than electrodes modified with complex C containing two phendione ligands (Figure 3.19). In comparison to the literature examples, the values of k_{cat}/K_M obtained for the complexes A, B, D and E attached at the surface through different linkers are relatively high. Similarly, second order rate constants for the modifications with complex C are significantly higher than k_{cat}/K_M reported for the literature examples. The pronounced catalytic efficiency observed for complex C in the case of only one phendione participating in the catalytic reaction (Figure 3.19b) is about two times higher than the catalytic efficiency reported for the [Fe(phendione)$_3$]$^{2+}$ complex.

These results would clearly suggest that the molecular architecture of the surface by combination of the metal complex and linker have a pronounced effect on the catalytic efficiency k_{cat}/K_M towards catalytic oxidation of NADH.

3.7 Conclusion

The library of 63 modified electrodes was designed based on previous results obtained for the individual electrodes and successfully prepared using combinatorial and solid-phase synthesis methods. To the best of our knowledge, the presented library of covalently modified electrodes is the first report on molecular design of the phendione type of mediators covalently bound at the electrode surface in a combinatorial way. HTP electrochemical screening allowed for evaluation and direct comparison of electrochemical properties and catalytic activity for all modified electrodes in the library in a single set of measurements.

Firstly, the library was screened in aqueous solution to evaluate the amount of the metal complex bound at the surface. Comparison of the calculated surface coverage between different modifications clearly suggested that the structure of the metal complex and type of the linker have an impact on the amount of the bound complex at the surface. The coverage decreased with the size and geometry of the metal complex with relatively high values of surface coverage obtained for tetrahedral zinc complexes D and E and low coverages were found for modifications with bulky octahedral ruthenium *tris*-complexes B and C. For modifications with aliphatic linkers, the coverage of metal complexes tends to decrease with longer aliphatic chain. Relatively small amounts of the bound complex were obtained for the rigid benzylamine linker BA, where limited flexibility of this linker decreases the amount of the complex bound at the surface.

HTP screening of the library in the presence of NADH allowed for direct comparison of the catalytic activity between different modifications. In general, the values of directly measured catalytic currents i_{cat} are proportional to the surface coverage, where high catalytic currents were recorded for modification with relatively small tetrahedral zinc complexes D and E and lower values of catalytic currents were observed for octahedral ruthenium complexes A, B and C.

Catalytic currents normalised by surface coverage of the metal complex or phendione ligands clearly showed that the presence of *tris*-ruthenium complex containing ligands with conjugated aromatic systems gave pronounced catalytic activity toward NADH oxidation. For coverage of phendione ligands, the highest catalytic activity was observed for modification with complex B and EDDA. For the coverage of

metal complex, the highest catalytic activity was observed for complex C attached at the surface through EDDA linker.

Similar results were obtained from studies of the kinetics for catalytic reaction in the presence of NADH based on a theoretical model for heterogeneous catalysis. The HTP electrochemical screening allowed for rapid evaluations of the heterogeneous rate constants using experimental data obtained for three different NADH concentrations at several scan rates. For rate constants in the case of saturated catalysis, comparison between different modifications in the library clearly suggested that the reaction rates depend on the geometry and structure of the metal complex. Any effect of the linker on the reaction rate is negligible. Relatively high rate constants were calculated for octahedral ruthenium complexes B and C with an additional bidentate ligand coordinated to the metal ion. Equally high values of the rate constants were obtained for modifications with the ruthenium complex C attached at the surface through EDA and EDDA linker.

In addition, catalytic rate constants obtained for twenty different modifications in the library in the case of unsaturated catalysis were significantly higher than reported literature examples of electrocatalysis of NADH oxidation by the metal complexes physically adsorbed at electrode surface.

In conclusion, the presented catalytic analysis for different modifications in the library suggests that molecular design of the surface electrode allows for control over the catalytic activity and kinetics of the catalytic reaction between mediator at the surface and NADH. The array of mediator systems analysed in the library, clearly suggests that the modifications with the highest catalytic activity are attractive mediators in biosensor applications. All of the modified electrodes regenerate the NADH to enzymatically active NAD^+ at low overpotentials, however they exhibit differences in the catalytic response. The electrode modified with complex E attached at the surface through the EDA linker generates the highest catalytic current corresponding to the number of NADH molecules being regenerated to NAD^+ during the catalytic cycle. Therefore this mediator would be the best choice to apply for activity-based biosensors.

However, the most effective mediator was found to be modifications with complex B or C and the EDDA linker, since these modifications gave the highest catalytic

activity independent on the coverage of mediator (i_{norm}) and fastest kinetics during regeneration of the NADH to enzymatically active NAD^+.

To the best of our knowledge, the presented analytical approach is the first report on the evaluation of library of mediators for NADH catalytic oxidation using HTP electrochemical screening. The HTP screening allowed for rapid evaluation of the electrochemical and catalytic properties of all modified electrodes and selection of modified electrodes with the best catalytic properties towards NADH oxidation, which could be used in the biosensor applications.

4 Experimental Section

4.1 Synthesis

4.1.1 General

Synthetic experiments were carried out under air unless otherwise specified. Experiments requiring dry conditions were performed under nitrogen atmosphere in dried glassware. Solvents and reagents were commercial grade and they were used without further purification or where necessary were distilled prior to use. DMF was distilled under reduced pressure and stored in a Schlenk bottle over M/S 4Å. Ethanol and DCM were distilled above calcium hydride directly before use. Dry THF was obtained by distillation of THF and benzophenone mixture above sodium wire under the argon atmosphere.

Flash chromatography columns were performed on Silica 60A, particle size 35-70 micron (Fisher Scientific). Thin layer chromatography was performed on silica pre-coated aluminium plates (Merck Silica gel F_{254}) and the spots were visualised with UV light or $KMnO_4$ stain.

The following compounds were synthesised according to the literature procedures: linkers 4-(*N*-Boc-aminomethyl)benzene diazonium tetrabluoroborate salt[147,148] and *tert*-butyl *N*-(aminomethyl)phenylmethyl)carbamate,[176] ligands 1,10-phenanthroline-5,6-dione[177] and 2,2'-bipyridine-5-carboxylic acid,[143] complexes dichloro*tetrakis*(dimethyl sulphoxide) ruthenium (II)[178] and (1,10-phenanthroline-5,6-dione)zinc (II) chloride.[150]

4.1.2 Instrumentation

Proton NMR were obtained at 300 MHz on a Bruker AC 300 and 400 MHz on a Bruker DPX 400 spectrometer. Carbon NMR spectra were recorded at 75.5 MHz on Bruker AC 300 and 100 MHz on Bruker DPX 400. Chemical shifts (δ) are reported in ppm and coupling constants (J) are given in Hz. Spectra were referenced with respect to the residual peak for the deuterated solvent. The following abbreviations are used for spin multiplicity: s = singlet, d = doublet, t = triplet, q = quadruplet, m =

multiplet and br = broad signal. For metal complexes, assignment abbreviations are: pd for 1,10-phenanthroline-5,6-dione ligand and bpy for 2,2'-bipyridine ligand. Carbon spectra were proton decoupled and the multiplicities of the signals quoted within the brackets using the following notation: primary carbon (3), secondary (2), tertiary (1) and quaternary (0).

Infra-red spectra were recorded on BIORAD Golden Gate FTS 135. Melting points were determined in open capillary tubes using a Gallenkamp Electrothermal melting point apparatus. Mass spectra were obtained on VG analytical 70-250 SE normal geometry double focusing mass spectrometer. All electrospray (ES) spectra were recorded on a Micromass Platform quadruple mass analyser with an electrospray ion source using acetonitrile as a solvent. High resolution accurate mass measurements were carried out at 10,000 resolution on a Bruker Apex III FT-ICR mass spectrometer. MALDI mass spectra were recorded at Micromass TofSpec2E spectrometer.

4.1.3 Synthesis of 2-(2-(pyridin-2-yl)-1*H*-imidazol-1-yl)acetic acid ligand.

4.1.3.1 *tert*-Butyl 2-(2-(pyridin-2-yl)-1H-imidazol-1-yl)acetate.[154]

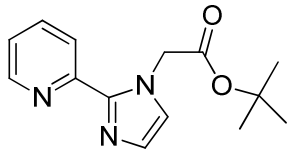

2-(1H-Imidazol-2-yl)pyridine (1.45 g, 10 mmol) was prepared according to literature procedure[157] and dissolved in dry THF (20 mL) under nitrogen. The solution was cooled to −78 °C and *n*-butyl lithium (2.5 M in hexane) (4.5 mL, 11 mmol) was added dropwise. The stirred reaction mixture was kept at −78 °C for 3 h and a solution of *tert*-butylbromoacetate (1.6 mL, 11 mmol) in dry THF (20 mL) was then added dropwise. The reaction mixture was allowed to warm to room temperature followed by stirring overnight under nitrogen. The reaction mixture was quenched with 10 mL of water and three times extracted with DCM (3 × 25 mL) The organic layers were dried over magnesium sulphate and solvent was evaporated in vacuo The residue was purified by flash chromatography (eluent MeOH : DCM, 1 : 9) to give *tert*-butyl 2-(2-(pyridin-2-yl)-1H-imidazol-1-yl)acetate as a brown oil in 76 % yield (2 g). *Rf* = 0.8 (eluent MeOH : DCM, 1 : 9), **^{1}H NMR (300 MHz, $CDCl_3$)**: δ= 8.49 (1 H, d, *J* = 4.8, Py*H*), 8.25 (1 H, d, *J* = 8.1, Py*H*), 7.74 (1 H, td, *J* = 7.7, 1.8, Py*H*), 7.18-7.22 (1 H, m, Py*H*), 7.17 (1 H, s, Im*H*), 6.97 (1 H, s, Im*H*), 5.20 (2 H, s, CH_2), 1.39 (9 H, s, C(CH_3)$_3$), **^{13}C NMR (75 MHz, $CDCl_3$)**: δ = 167.4 (0), 150.2 (0), 147.9 (1), 144.5 (0), 136.6 (1), 128.1 (1), 124.3 (1), 122.4 (1), 122.1 (1), 82.0 (0), 51.3 (2), 27.9 (3), **IR (cm^{-1}):** 2978 (v), 1743 (s), 1589 (m), 1152 (s), 1093 (m), 740 (m), 705 (m), **LR-MS ES+** (*m/z):* 282.2 $[M + Na]^+$ (100%), 260.2 $[M + H]^+$ (47%), **HR-MS ES+** (*m/z):* found 260.1395 $[M + H]^+$, calculated 260.1394.

4.1.3.2 2-(1-(carboxymethyl)-1H-imidazol-3-ium-2-yl)pyridin-1-ium trifluoroacetate salt.

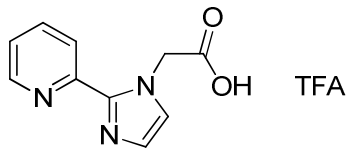

tert-Butyl 2-(2-(pyridin-2-yl)-1H-imidazol-1-yl)acetate (0.26 g, 1 mmol) was dissolved in 20 % solution of TFA in DCM (15 mL) and stirred overnight at room temperature under nitrogen atmosphere. The solvent was evaporated to give an oily residue and azeotropic distillation in toluene and subsequent washing with DCM and ethyl acetate gave 2-(1-(carboxymethyl)-1H-imidazol-3-ium-2-yl)pyridin-1-ium trifluoroacetate salt as a bright yellow solid in 97 % yield (0.42 g). M.p. (crystallised from MeOH) 158-162 °C.

^{1}H NMR (300 MHz, DMSO-d_6): δ = 12.2 (1 H, br. s, CO_2H), 8.63-8.75 (1 H, m, Py*H*), 8.13-8.21 (1 H, m, Py*H*), 8.17 (1 H, d, *J* = 8.1, Py*H*) 8.07 (1 H, td, *J* = 7.7, 1.8, Py*H*), 7.76 (1 H, d, J = 1.5, Im*H*), 7.66 (1 H, d, J = 1.5, Im*H*), 7.56 (1 H, dd, *J* = 7.7, 4.8, Py*H*), 5.45 (2 H, s, CH_2), **^{13}C NMR (75 MHz, DMSO-d_6)**: δ = 168.8 (0), 149.4 (1), 144.9 (0), 141.8 (0), 138.0 (1), 126.2 (1), 125.2 (1), 123.2 (1), 121.9 (1), 50.8 (2), **IR (cm^{-1}):** 3131 (v), 3165 (v), 1688 (m), 1582 (v), 1141 (s), 777 (s), 714 (s), **LR-MS ES+** (*m/z):* 204.2 $[M - H]^+$ (100%), **HR-MS ES+** (*m/z):* found 204.0770 $[M– H]^+$, calculated 204.0768.

4.1.4 Synthesis of ruthenium (II) complexes.

4.1.4.1 Synthesis of *bis*-(dimethyl sulphoxide)(1,10-phenanthroline-5,6-dione) ruthenium (II) chloride.[179]

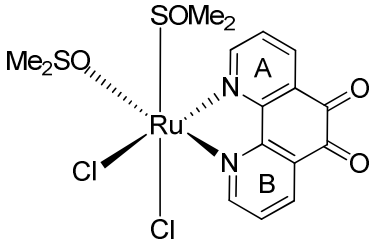

Complex dichloro*tetrakis*(dimethyl sulphoxide) ruthenium (II) (0.1 g, 0.2 mmol) and 1,10-phenanthroline-5,6-dione (42 mg, 0.2 mmol) were dissolved in distilled ethanol

(3 mL) and refluxed overnight under nitrogen. The brown reaction mixture was cooled to room temperature and precipitated brown solid was washed with diethyl ether and dried under vacuum to give *bis*-(dimethyl sulphoxide)(1,10-phenanthroline-5,6-dione) ruthenium (II) chloride in 55 % yield (0.06 g). M.p. above 300 °C.

^{1}H NMR (400 MHz, DMSO-*d*$_6$): δ = 9.84 (1 H, d, *J* = 5.5, C_qCH-ring B), 9.72 (1 H, d, *J* = 5.0, C_qCH-ring A), 8.63 (1 H, d, *J* = 8.0, NC*H*-ring B), 8.49 (1 H, d, *J* = 8.0, NC*H*-ring A), 7.98 (1 H, dd, *J* = 8.0, 5.5, $(CH)_2CH$-ring B), 7.83 (1 H, dd, *J* = 8.0, 5.0, $(CH)_2CH$-ring A), 3.43 (6 H, s, $SO(CH_3)_2$), 2.89 (3 H, s, $SO(CH_3)_2$), 2.33 (3 H, s, $SO(CH_3)_2$), **^{13}C NMR (100 MHz, DMSO-*d*$_6$)**: δ = 181.2 (0), 174.5 (0), 159.0 (1), 157.5 (0), 155.5 (1), 155.4 (1), 136.3 (1), 135.3 (1), 131.6 (0), 130.9 (0), 127.4 (1), 127.2 (1), 46.2 (3), 45.6 (3), 44.6 (3), 44.1 (3), **IR (cm^{-1}):**3085 (w), 3006 (w), 2920 (w), 1705 (m), 1431 (m), 1078 (s), 727 (m), 440 (w), **MS-MALDI TOF (LD+)** *(m/z)*: found 539.9 for $[M]^+$, calculated 539.9.

4.1.5 Synthesis of (2,2'-bipyridine)(1,10-phenanthroline-5,6-dione) ruthenium (II) chloride.[142]

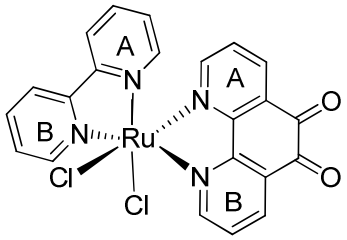

Complex *bis*-(dimethyl sulphoxide)(1,10-phenanthroline-5,6-dione) ruthenium (II) chloride (0.1 g, 0.2 mmol) and 2, 2'-bipyridine (31 mg, 0.2 mmol) were dissolved in DMF (16 mL) and dark solution was heated under reflux for 4 h under nitrogen atmosphere and reduced light. The dark purple solution was then evaporated to dryness in vacuo and the residue dissolved in 4 mL of methanol. The purple solution was left overnight at low temperature to give black-purple microcrystalline solid, which was collected by filtration, washed ten times with 50 mL of diethyl ether and dried *in vacuo* to give (2,2'-bipyridine)(1,10-phenanthroline-5,6-dione) ruthenium (II) chloride as a microcrystalline solid in 60 % yield (60 mg). M.p. decomposed above 300 °C. **^{1}H NMR (400 MHz, DMSO-*d*$_6$):** δ = 10.08 (1H, d, *J* = 5.0, C_qCH-

ring B *pd*), 10.01 (1 H, d, *J* = 5.5, C_qC*H*-ring A *pd*), 8.66 (1 H, d, *J* = 8.5, C_qC*H*-ring B *bpy*), 8.51 (1 H, d, *J* = 8.0, C_qC*H*-ring A *bpy*), 8.44 (1 H, *J* = 7.5, NC*H*-ring B *pd*), 8.11 (1 H, t, *J* = 8.3, $(CH)_2$C*H*-ring B *bpy*),8.06 (1 H, d, J = 8.0, NC*H*-ring B *bpy*) 7.97 (1 H, dd, *J* = 7.8, 5.5, $(CH)_2$C*H*-ring B *pd*), 7.79–7.85 (2 H, m, $(CH)_2$C*H* and NC*H*-ring A *bpy*), 7.73 (1 H, t, *J* = 7.5 $(CH)_2$C*H*-ring B *bpy*), 7.51 (1 H, d, *J* = 5.5 Hz, NC*H*-ring A *pd*), 7.30 (1 H, dd, *J* = 7.5, 6.0, $(CH)_2$C*H*-ring A *pd*), 7.14 (1 H, t, *J* = 6.5, $(CH)_2$C*H*-ring A *bpy*), **^{13}C NMR (100 MHz, DMSO-*d*$_6$)**: δ = 180.9 (0), 175.0 (0), 174.8 (0), 159.8 (0), 159.4 (0), 158.1 (0), 157.5 (0), 156.7 (1), 155.6 (1), 153.2 (1), 152.4 (1), 135.1 (1), 134.0 (1), 132.0 (1), 2 × 130.73 (1), 130.70 (1), 130.4 (0), 126.2 (1), 125.5 (1), 125.2 (1), 122.8 (1), 122.6 (1), **IR (cm^{-1}):** 2990 (v), 1688 (s), 1459 (v), 761 (s), 722 (s), **MS-MALDI TOF (LD+)** *(m/z)*: found 503.3 $[M - Cl]^+$, calculated 503.0.

4.1.6 Synthesis of *bis*-(1,10-phenanthroline-5,6-dione)ruthenium (II) chloride.[142]

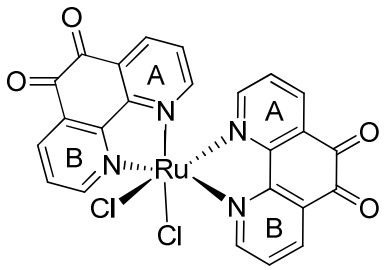

Complex *di*chloro*tetrakis*(dimethyl sulphoxide) ruthenium (II) (0.1 g, 0.2 mmol) and 1,10-phenanthroline-5,6-dione (0.087 g, 0.4 mmol) were dissolved in dry DMF (25 mL) under nitrogen and heated under reflux for 4 hours. The black reaction mixture was evaporated to dryness in vacuo and the black residue was dissolved in 4 mL of methanol. The solution was left overnight at 5 °C to precipitate the black microcrystalline solid, which was collected by filtration and washed with 50 mL of diethyl ether followed by drying *in vacuo* to give *bis*-(1,10-phenanthroline-5,6-dione)ruthenium (II) chloride in 33 % yield (0.04 g). M.p. above 300 °C. **^{1}H NMR (400 MHz, DMSO-*d*$_6$):** δ = 10.12 (2 H, d, *J* = 5.5, C_qC*H*-ring B), 8.49 (2 H, d, *J* = 8.0, C_qC*H*-ring A), 8.10 (2 H, d, *J* = 8.0, NC*H*-ring B), 8.02 (2 H, dd, *J* = 8.0, 5.5, $(CH)_2$C*H*-ring B) 7.77 (2 H, d, *J* = 5.5, NC*H*-ring A), 7.35 (2 H, dd, *J* = 8.0, 5.5, $(CH)_2$C*H*-ring A), **^{13}C NMR (100 MHz, DMSO-*d*$_6$)**: δ = 175.3 (0), 175.2 (0), 159.6

(0), 157.9 (0), 157.2 (1), 156.5 (1), 133.0 (1), 131.9 (1), 131.1 (0), 131.0 (0), 126.9 (1), 126.6 (1), **IR (cm^{-1}):** 1689 (s), 1557 (v), 1297 (m), 1103 (m), 833 (m), 824 (m), **MS-MALDI TOF (LD+)** *(m/z)*: found 557.3 $[M - Cl^-]^+$, calculated 557.0 $[M - Cl^- + MeCN]^+$.

4.2 Electrochemical and solid-phase covalent modification of GC electrodes.

4.2.1 Instrumentation

Electrochemical experiments for single electrodes were recorded on an Autolab PGSTAT30 Potentiostat/Galvanostat (Eco Chemie, Netherlands) and done in 10 mL glassy 3-neck electrochemical cells. All glassware was soaked in 5% aq. solution of Decon 90 for 48 h followed by extensive washing with water and drying overnight in an oven at 50 °C. All electrochemical experiments presented in this thesis were carried out with the use of Faraday's cage. A homemade Ag/AgCl electrode and homemade standard calomel electrode (SCE) were used as the reference electrodes prepared according to literature procedure.[180] Platinum gauze (1 cm^2) was used as the counter electrode for the single electrode electrochemical experiments. The working electrode was 3 mm diameter (0.071 cm^2) glassy carbon rod (HTW Hochtemperatur-Werkstoffe GmbH, Germany) sealed in glass (by Southampton University glassblowers) and wired up with a copper wire using melted indium (Sigma-Aldrich). Directly before electrochemical modification, blank GC electrodes were polished with dry silicon-carbide polishing paper (grade 1200, 3M), rinsed with acetone and sonicated in MeCN (HPLC grade) for 15 min.

4.2.2 Reagents

Linkers *mono*-Boc-1,2-ethylenediamine (EDA), *mono*-Boc-1,4-butanediamine, *mono*-Boc-1,6-hexanediamine and *mono*-Boc-(ethylenedioxy)diethylamine (EDDA) were purchased from Sigma-Aldrich and used without further purification. Linkers -(*N*-Boc-aminomethyl)benzene diazonium tetrabluoroborate salt[147,148] and *tert*-butyl *N*-(aminomethyl)phenylmethyl)carbamate[176] were prepared according to the literature procedures. *N*,*N*-Dimethylformamide (DMF, analytical grade) was obtained from Fisher Scienitfic and purified by distillation under reduced pressure. Coupling reagent *O*-benzotriazol-1-yl)-*N,N,N',N'*-tetramethylammonium hexafluorophosphate (HBTU) was obtained from Novabiochem. Disopropylethylamine (DIEA) (reagent grade) was purchased from Sigma-Aldrich.

Acetonitrile (HPLC grade) used for electrochemical experiments was obtained from Rathburn. Aqueous solutions for electrochemical experiments were prepared using water purified by Whatmann RO80 system coupled to a Whatmann „Still Plus". Homemade aqueous solution of 0.1 M phosphate buffer pH 7 was prepared using 0.1 M phosphoric acid (Fisher Scientific) and saturated solution of sodium hydroxide. All other solvents and reagents were purchased from Sigma-Aldrich and used as received without further purification.

4.2.3 Electrochemical modifications of GC electrodes.

3.2.1.1 General procedure for attachment of diamine linkers.[181]

Electrochemical attachment of mono-Boc diamine linkers (EDA, EDDA, BDA and HDA) was performed in a solution of 20 mM *mono*-Boc-protected diamine and 0.1 M TBATFB in acetonitrile by electrochemical cycling (5–10 cycles) the electrode potential in a potential range from 0 to 2.2 V *vs*. Ag/AgCl at a scan rate of 50 mV s^{-1}.

4.2.4 Attachment of (*N*-Boc-aminomethyl)benzene diazonium tetrabluoroborate salt.[181]

Covalent attachment of diazonium salt to the GC surface was performed by electrochemical reduction from a solution of 10 mM 4-(N-Boc-aminomethyl)benzene diazonium tetrafluoroborate salt and 0.1 mM TBATFB in acetonitrile. Modification of GC electrodes was carried out by cycling the electrode potential from 0.6 to −1 V *vs.* Ag/AgCl for three cycles at scan rate of 50 mV s^{-1}.

4.3 Solid-phase modification of the GC electrodes.

4.3.1 General procedure for Boc removal of modified GC electrodes.[181]

A Boc-protected modified GC electrode was suspended in a solution of HCl in dioxane (4.0 M) at room temperature for 1 hour. The electrode was then washed in DMF (0.5 mL), followed by subsequent washing with deionised water (0.5 mL) and absolute EtOH (0.5 mL) before further solid-phase modification.

4.3.2 General procedure for the coupling reaction of 2,2'-bipyridine-5-carboxylic acid at the GC surface.

2,2'-Bipyridine-5-carboxylic acid, HBTU, and DIEA were dissolved in DMF. The mixture was gently heated for 2 minutes with a heat gun to obtain a homogenous solution. An unprotected modified GC electrode was then suspended in this solution which was allowed to cool to room temperature and stirred for 16 h. The electrode was then washed with DMF, followed by absolute EtOH and allowed to dry in air for 5 minutes.

4.3.3 General procedure for coupling of the 2-(1-(carboxymethyl)-1*H*-imidazol-3-ium-2-yl)pyridin-1-ium trifluoroacetate salt at the GC electrodes.

2-(1-(Carboxymethyl)-1*H*-imidazol-3-ium-2-yl)pyridin-1-ium trifluoroacetate salt, HBTU (0.46 g, 1.2 mmol) and DIEA (1.74 mL, 10 mmol) were dissolved in DMF (1 mL). The mixture was gently warmed with a heat gun to obtain a homogenous solution. An unprotected modified GC electrode was then suspended in this solution which was allowed to cool to room temperature and stirred for 16 h. The electrode was subsequently washed with 1 mL of DMF followed by 1 mL of absolute EtOH and allowed to dry in air for 5 minutes.

4.3.4 General procedure for grafting of ruthenium (II) complexes at the modified GC electrodes.

The modified GC electrode with linker and binedate ligand was dipped in a solution of the ruthenium (II) complex (27 mg, 0.05 mmol) in DMF (5 mL). The reaction mixture was heated at 100 C° for 16 h under nitrogen. The electrode was then dipped in 5 mL of DMF for 10 minutes followed by washing with 5 mL of EtOH and dry in air for 5 minutes before electrochemical characterisation.

4.3.5 General procedure for grafting (1,10-phenanthroline-5,6-dione)zinc (II) chloride complex at the GC surface.

(1,10-Phenanthroline-5,6-dione)zinc (II) chloride complex (17 mg, 0.05 mmol) was placed in a dry multi-neck vessel and DMF (5 mL) was added under nitrogen. The GC electrodes were dipped in the solution and heated at 50 °C overnight under nitrogen. The electrode was dipped in 5 mL of DMF for 10 minutes followed by washing with 5 mL of EtOH and dry in air for 5 minutes before electrochemical characterisation.

4.4 General procedure for electrochemical characterisation of the individual modified GC electrodes.

The modified electrode, SCE reference electrode and Pt counter electrode were placed in 5 mL of 0.1 M phosphate buffer solution and degassed with argon for 5 minutes. The GC modified electrodes were characterised by cycling the potential between −0.2 and 0.2 V *vs.* SCE at a scan rate of 50 mV s^{-1}. After 10 cycles, stable and reproducible peaks were obtained, which correspond to the redox process of the mediator. The last cycle was saved and used for calculation of the surface coverage of the mediator at GC electrode. Afterwards, the modified GC electrode was dipped in 1 mM solution of NADH in aqueous solution of 0.1 M phosphate buffer solution pH 7, which was degassed with argon for 5 minutes. The modified GC electrode was then screened in a potential window from −0.2 to 0.2 V *vs.* SCE at a scan rate of 50 mV s^{-1}. The first cycle was saved and used for analysis of the electrocatalytic activity of the modified electrode for NADH oxidation.

The electrochemical data were reprocessed using Origin 7.0 and Origin 8.1 software.

4.5 Electrochemical screening of the library of 63 modified electrodes.

High-throughput electrochemical experiments were carried out using a high-throughput electrochemistry analyser HTEA Mark II Potentiostat (ILIKA). The HTP electrochemical experiments were performed in a 250 mL Petri dish in homemade 0.1 M phosphate buffer solution at pH 7 as supporting electrolyte. The Petri dish was soaked in a 5% aq. solution of Decon 90 for 48 h followed by drying overnight in an oven at 50 °C. A homemade standard calomel electrode was used as reference electrode and 3 cm^3 Pt gauze as the counter electrode. The 0.1 M phosphate buffer solution was degassed with argon for 5 minutes directly prior to each electrochemical measurement.

The 63 modified electrodes were placed in a Teflon stand and dipped in 200 mL aqueous solution of 0.1 M phosphate buffer pH 7. The solution was degassed with argon for 15 minutes prior to each electrochemical screening. Initially, the library was screened in a potential window from −0.3 to 0.2 V *vs.* SCE at a scan rate of 50 mV s^{-1} for 4 cycles in order to remove the residues of metal complexes physically adsorbed at the carbon surface. Stable and reversible redox peaks were observed after three cycles. The same procedure was repeated for screening of the library at the following scan rates: 10, 20, 100, 200, 500 and 100 mV s^{-1}. The solution was degassed for 5 minutes between each measurement. The last recorded cycle for all modified electrodes was used for evaluation of surface coverage of the mediator.

Afterwards, all electrodes in the library were dipped in a freshly prepared solution of 1 mM NADH in aqueous 0.1 M phosphate buffer pH 7 and degassed for 15 minutes. The library was screened from −0.3 to 0.2 V *vs.* SCE at a scan rate of 50 mV s^{-1}. The same procedure was repeated for the following scan rates: 10, 100 and 200 mV s^{-1}.

Similarly, 2 and 4 mM NADH solutions were prepared and in each case the same screening procedure was repeated for all scan rates. The electrochemical and kinetic analysis was performed by introducing electrochemical data in to Origin 8.1 software and using theoretical model as described in Section 3.6.

5 Conclusion

The work presented in this thesis has demonstrated a novel strategy for the molecular design of glassy carbon (GC) electrodes modified by various metal complexes bearing the redox active 1,10-phenanthroline-5,6-dione ligand based on sequential electrochemical and solid-phase synthesis methods. This strategy was successfully applied for the preparation of a library of modified GC electrodes, followed by HTP electrochemical screening and evaluation of the library as electrocatalysts towards NADH oxidation.

Initial studies involved covalent functionalisation of individual GC electrodes using sequential electrochemical attachment of different linkers followed by introduction of different ligands and metal complexes under solid-phase conditions. The individual modified electrodes were characterised using conventional cyclic voltammetry towards their electrochemical and electrocatalytic properties for oxidation of NADH. In general, the surface coverage of the covalently attached metal complex strongly depends on the size and geometry of the metal complex. Relatively high surface coverage was observed for tetrahedral zinc complexes at the GC surface in comparison with the more bulky octahedral *tris* ruthenium complexes bearing 2,2'-bipyridine or additional phendione chelating ligands. The metal complexes were also attached at the surface through six different linkers in order to study the effect of length and structure of the linker on electrochemical and electrocatalytic activity of the modified GC electrodes. In general, calculated values of surface coverage decreased with the length of the linker for aliphatic linkers. Relatively low values of coverage were obtained for metal complexes attached through the rigid benzylamine linker.

Preliminary studies on the individual modified electrodes towards electrocatalytic activity for NADH oxidation showed that different metal complexes and different types of linkage affect the electrocatalytic activity of the phendione redox active ligand(s). In general, a decrease in overvoltage was observed for the oxidation of NADH for all of the modified electrodes. An enhanced NADH electrocatalytic activity was observed for electrodes modified with octahedral ruthenium complexes bearing additional bidentate ligands with conjugated aromatic systems. In the case of

the aliphatic linkers, a decrease in the NADH catalytic activity of the modified electrodes was observed with increase in length of the linkers. Relatively low values of catalytic currents were recorded for the rigid benzylamine linker, which might limit the phendione ligand access to the bulky NADH molecule in solution.

Based on the initial results obtained for individual electrodes, a library of 63 GC electrodes modified by different linkers, ligands and metal complexes was designed and prepared in a combinatorial and parallel way. HTP electrochemical screening of the library using a multichannel potentiostat allowed instant comparison of different modification in the library during single set of measurements. An initial result of HTP screening showed that the highest NADH catalytic currents were recorded for modifications with the zinc complex attached at the surface through ethylenediamine linker and this mediator system would be the best choice to apply for activity-based biosensors. The experimental data extracted from HTP screening of the library were also applied for evaluation of heterogeneous rate constants of the NADH catalytic reaction according to the kinetic model reported for electrocatalysis at different modified electrodes. Based on the catalytic rate constants, k_{cat}, the most effective mediator system was modification with the *tris* ruthenium complex attached at the surface through the ethylenediethoxydiamine linker.

In conclusion, the results obtained for the modified GC electrodes confirmed that the proposed strategy of sequential functionalisation of the carbon surface allows control over the electrochemical and electrocatalytic properties of the modified surfaces. To the best of our knowledge, the presented work is the first report describing detailed high-throughput electrochemical and kinetic analysis towards development of novel modified electrodes for biosensor application.

The successful preparation of array of covalently modified GC electrodes using combinatorial methodology and the HTP screening can be applied for different redox systems towards electrocatalytic oxidation of NADH and other substrates.

The molecular design of the carbon surface proposed in this thesis allowed for control over the surface coverage and NADH electrocatalytic activity by introduction of different linkers and metal complexes containing redox active phendione ligands. In order to investigate in more detail the effect of environment on the catalytic activity of the redox centre, a number of redox centres at the GC surface would be decreased in a controlled manner. This can be achieved by formation of partial

coverage of different redox centres using blocking groups with different functionalities and applying the well-known solid-phase synthesis and electrochemical methodologies.

6 References

(1) Bunin, B. A. *The Combinatorial Chemistry*; Academic Press: San Francisco, 1998.

(2) Jandeleit, B.; Schaefer, D. J.; Powers, T. S.; Turner, H. W.; Weinberg, W. H. *Angew. Chem. Int. Ed.* **1999**, *38*, 2494.

(3) Nicolaou, K. C. H., R.; Hartwig, W. *Handbook of Combinatorial Chemistry*; Wiley-VCH: Weinheim, 2002; Vol. 2.

(4) Terrett, N. K. *Combinatorial Chemistry*; Oxford Chemistry Press Inc.: New York, 1998.

(5) Hanak, J. J. *J. Mater. Sci.* **1970**, *5*, 964.

(6) Furka, Á.; SebestyÉN, F.; Asgedom, M.; DibÓ, G. *Int. J. Pept. Protein Res.* **1991**, *37*, 487.

(7) Merrifield, R. B. *J. Am. Chem. Soc.* **1963**, *85*, 2149.

(8) Ronald, F. *Tetrahedron* **1992**, *48*, 9217.

(9) Jung, G. *Combinatorial Chemistry, Synthesis, Analysis, Screening*; Wiley-VCH: Weinheim, 1999.

(10) Pinilla, C.; Appel, J. R.; Blondelle, S. E.; Dooley, C. T.; Eichler, J.; Ostresh, J. M.; Houghten, R. A. *Drug Dev. Res.* **1994**, *33*, 133.

(11) Richard A, H. *Gene* **1993**, *137*, 7.

(12) Dooley, C. T.; Chung, N. N.; Schiller, P. W.; Houghten, R. A. *Proc. Natl. Acad. Sci.* **1993**, *90*, 10811.

(13) Houghten, R. A.; Pinilla, C.; Blondelle, S. E.; Appel, J. R.; Dooley, C. T.; Cuervo, J. H. *Nature* **1991**, *354*, 84.

(14) Konings, D. A. M.; Wyatt, J. R.; Ecker, D. J.; Freier, S. M. *J. Med. Chem.* **1997**, *40*, 4386.

(15) Campbell, D. A.; Bermak, J. C.; Burkoth, T. S.; Patel, D. V. *J. Am. Chem. Soc.* **1995**, *117*, 5381.

(16) Vetter, D.; Tate, E. M.; Gallop, M. A. *Bioconjugate Chem.* **1995**, *6*, 319.

(17) Yudin, A. K.; Siu, T. *Curr. Opinion Chem. Biol.* **2001**, *5*, 269.

(18) Akporiaye, D. E.; Dahl, I. M.; Karlsson, A.; Wendelbo, R. *Angew. Chem. Int. Ed.* **1998**, *37*, 609.

(19) Baker, B. E.; Kline, N. J.; Treado, P. J.; Natan, M. J. *J. Am. Chem. Soc.* **1996**, *118*, 8721.

(20) Danielson, E.; Devenney, M.; Giaquinta, D. M.; Golden, J. H.; Haushalter, R. C.; McFarland, E. W.; Poojary, D. M.; Reaves, C. M.; Weinberg, W. H.; Wu, X. D. *Science* **1998**, *279*, 837.

(21) Danielson, E.; Golden, J. H.; McFarland, E. W.; Reaves, C. M.; Weinberg, W. H.; Wu, X. D. *Nature* **1997**, *389*, 944.

(22) Izatt, R. M.; Pawlak, K.; Bradshaw, J. S.; Bruening, R. L. *Chem. Rev.* **1991**, *91*, 1721.

(23) Burgess, K.; Lim, H.-J.; Porte, A. M.; Sulikowski, G. A. *Angew. Chem. Int. Ed.* **1996**, *35*, 220.

(24) Cole, B. M.; Shimizu, K. D.; Krueger, C. A.; Harrity, J. P. A.; Snapper, M. L.; Hoveyda, A. H. *Angew. Chem. Int. Ed.* **1996**, *35*, 1668.

(25) Lam, K. S.; Salmon, S. E.; Hersh, E. M.; Hruby, V. J.; Kazmierski, W. M.; Knapp, R. J. *Nature* **1991**, *354*, 82.

(26) Shimizu, K. D.; Snapper, M. L.; Hoveyda, A. H. *Chem. Eur. J.* **1998**, *4*, 1885.

(27) Francis, M. B.; Jamison, T. F.; Jacobsen, E. N. *Curr. Opinion Chem. Biol.* **1998**, *2*, 422.

(28) Bein, T. *Angew. Chem. Int. Ed.* **1999**, *38*, 323.

(29) Ohlmeyer, M. H.; Swanson, R. N.; Dillard, L. W.; Reader, J. C.; Asouline, G.; Kobayashi, R.; Wigler, M.; Still, W. C. *Proc. Natl. Acad. Sci.* **1993**, *90*, 10922.

(30) Reddington, E. *Science* **1998**, *280*, 1735.

(31) Chen, G.; Delafuente, D. A.; Sarangapani, S.; Mallouk, T. E. *Catalysis Today* **2001**, *67*, 341.

(32) Morris, N. D.; Mallouk, T. E. *J. Am. Chem. Soc.* **2002**, *124*, 11114.

(33) Sun, Y.; Buck, H.; Mallouk, T. E. *Anal. Chem.* **2001**, *73*, 1599.

(34) Sullivan, M. G.; Utomo, H.; Fagan, P. J.; Ward, M. D. *Anal. Chem.* **1999**, *71*, 4369.

(35) Hintsche, R.; Albers, J.; Bernt, H.; Eder, A. *Electroanalysis* **2000**, *12*, 660.

(36) Spong, A. D.; Vitins, G.; Guerin, S.; Hayden, B. E.; Russell, A. E.; Owen, J. R. *J. Power Sources* **2003**, *119-121*, 778.

(37) Guerin, S.; Hayden, B. E.; Lee, C. E.; Mormiche, C.; Owen, J. R.; Russell, A. E.; Theobald, B.; Thompsett, D. *J. Comb. Chem.* **2003**, *6*, 149.

(38) Cooper, J. S.; McGinn, P. J. *J. Power Sources* **2006**, *163*, 330.

(39) Murray, R. M. *Chemically Modified Electrodes*; Marcel Dekker, Inc.: New York, 1984; Vol. 13.

(40) Tagliazucchi, M. C., E. *Chemically Modified Electrodes*; Wiley-VCH, 2009; Vol. 11.

(41) Scheller, F. W.; Wollenberger, U.; Lei, C.; Jin, W.; Ge, B.; Lehmann, C.; Lisdat, F.; Fridman, V. *Rev. Mol. Biotech.* **2002**, *82*, 411.

(42) Collman, J. P.; Denisevich, P.; Konai, Y.; Marrocco, M.; Koval, C.; Anson, F. C. *J. Am. Chem. Soc.* **1980**, *102*, 6027.

(43) Simon, E.; Bartlett, P. N. In *Biomolecular Films: Design, Function, and Applications*; Rusling, J. F., Ed.; Marcel Dekker: New York, 2003, p 499.

(44) Jiang, R.; Chu, D. *J. Electroanal. Chem.* **2002**, *527*, 137.

(45) Downard, A. J.; Roddick, A. D.; Bond, A. M. *Anal. Chim. Acta* **1995**, *317*, 303.

(46) Kishioka, S.-y.; Ohki, S.; Ohsaka, T.; Tokuda, K. *J. Electroanal. Chem.* **1998**, *452*, 179.

(47) Zoski, C. E. *Handbook of Electrochemistry*; Elsevier: Amsterdam, 2007.

(48) Pilloud, D. L.; Chen, X.; Dutton, P. L.; Moser, C. C. *J. Phys. Chem. B* **2000**, *104*, 2868.

(49) Hong, H.-G.; Park, W. *Langmuir* **2001**, *17*, 2485.

(50) Laforgue, A.; Addou, T.; Bélanger, D. *Langmuir* **2005**, *21*, 6855.

(51) Paulik, M. G.; Brooksby, P. A.; Abell, A. D.; Downard, A. J. *J. Phys. Chem. C* **2007**, *111*, 7808.

(52) McCreery, R. L. *Chem. Rev.* **2008**, *108*, 2646.

(53) Heller, A.; Feldman, B. *Chem. Rev.* **2008**, *108*, 2482.

(54) Murray, R. W. *Acc. Chem. Res.* **1980**, *13*, 135.

(55) Chrétien, J.-M.; Ghanem, M. A.; Bartlett, P. N.; Kilburn, J. D. *Chem. Eur. J.* **2008**, *14*, 2548.

(56) Ghanem, M. A.; Chrétien, J.-M.; Kilburn, J. D.; Bartlett, P. N. *Bioelectrochem.* **2009**, *76*, 115.

(57) Ghanem, M. A.; Chrétien, J.-M.; Pinczewska, A.; Kilburn, J. D.; Bartlett, P. N. *J. Mater. Chem.* **2008**, *18*, 4917.

(58) Evans, J. F.; Kuwana, T. *Anal. Chem.* **1977**, *49*, 1632.

(59) Strelko, V.; Malik, D. J. *J. Colloid Interface Sci.* **2002**, *250*, 213.

(60) Yacynych, A. M.; Kuwana, T. *Anal. Chem.* **1978**, *50*, 640.

(61) Barbier, B.; Pinson, J.; Desarmot, G.; Sanchez, M. *J. Electrochem. Soc.* **1990**, *137*, 1757.

(62) Deinhammer, R. S.; Ho, M.; Anderegg, J. W.; Porter, M. D. *Langmuir* **1994**, *10*, 1306.

(63) Andrieux, C. P.; Gonzalez, F.; Savéant, J.-M. *J. Am. Chem. Soc.* **1997**, *119*, 4292.

(64) Delamar, M.; Hitmi, R.; Pinson, J.; Saveant, J. M. *J. Am. Chem. Soc.* **1992**, *114*, 5883.

(65) Downard, A. J. *Electroanalysis* **2000**, *12*, 1085.

(66) Adenier, A.; Chehimi, M. M.; Gallardo, I.; Pinson, J.; Vilà, N. *Langmuir* **2004**, *20*, 8243.

(67) Maeda, H. Y., Y.; Hosoe, M.; Li, T.-X.; Yamaguchi, E.; Kasamatsu, M.; Ohmori, H.; *Chem. Pharm Bull.* **1994**, *42*, 1870.

(68) Gooding, J. J. *Electroanalysis* **2008**, *20*, 573.

(69) Saby, C.; Ortiz, B.; Champagne, G. Y.; Bélanger, D. *Langmuir* **1997**, *13*, 6805.

(70) Anariba, F.; Steach, J. K.; McCreery, R. L. *J. Phys. Chem. B* **2005**, *109*, 11163.

(71) Liu, G.; Liu, J.; Böcking, T.; Eggers, P. K.; Gooding, J. J. *Chemical Physics* **2005**, *319*, 136.

(72) Liu, G.; Liu, J.; Davis, T. P.; Gooding, J. J. *Biosensors and Bioelectronics* **2011**, *26*, 3660.

(73) Pinson, J.; Podvorica, F. *Chem. Soc. Rev.* **2005**, *34*, 429.

(74) Kariuki, J. K.; McDermott, M. T. *Langmuir* **2001**, *17*, 5947.

(75) Anariba, F.; DuVall, S. H.; McCreery, R. L. *Anal. Chem.* **2003**, *75*, 3837.

(76) Bugg, T. *Introduction to Enzyme and Coenzyme Chemistry*; Blackwell Publishing Ltd., 2004.

(77) Groton, L.; Bartlett, P. N. *Bioelectrochemistry; Fundamentals, Experimental Technqiues and Applications*; Wiley, 2008.

(78) Tanner, J. J. T., S.; Barbour, C. L. J.; Barnes, C. L.; Krause, K. L. *Protein Science* **1999**, *8*, 1725.

(79) Loewus, F. A.; Ofner, P.; Fisher, H. F.; Westheimer, F. H.; Vennesland, B. *J Biol Chem* **1953**, *202*, 699.

(80) Loewus, F. A.; Westheimer, F. H.; Vennesland, B. *J. Am. Chem. Soc.* **1953**, *75*, 5018.

(81) Miles, D. W. U., D. W. *J. Biol. Chem.* **1968**, *243*, 4181.

(82) Smith, P. E. *J. Am. Chem. Soc.* **1999**, *121*, 8637.

(83) Bell, C. E. Y., T. O.; Eisenberg, D. *Protein Science* **1997**, 2084.

(84) Rossman, M. G. L., Anders; Branden, Carl-Ivar; Banaszak, Leonard J. *Evolutionaly and Structurally Relationship among Dehydrogenases*; Academic Press: Los Angeles; Vol. 11.

(85) Branden, C. T., John *Introduction to protein structure*; Second ed.; Garland Publishing, Inc.: New York, 1999.

(86) Arthur M, L. *Curr. Opin. Struct. Biol.* **1995**, *5*, 775.

(87) Brändén, C.-I. *Q. Rev. Biophys.* **1980**, *13*, 317.

(88) Lobo, M. J.; Miranda, A. J.; Tuñón, P. *Electroanalysis* **1997**, *9*, 191.

(89) Devaux-Basseguy, R.; Bergel, A.; Comtat, M. *Enzyme Microb. Tech.* **1997**, *20*, 248.

(90) Rodkey, F. L. *J Biol Chem* **1955**, *213*, 777.

(91) Clark, W. M. *Oxidation-Reduction Potentials of Organic Systems*; Robert E. Krieger Publishing: Huntington, 1972.

(92) Burnett, J. N.; Underwood, A. L. *Biochemistry* **1965**, *4*, 2060.

(93) Samec, Z. E., Philip J. *J. Electroanal. Chem.* **1983**, *144*, 217.

(94) Blaedel, W. J.; Jenkins, R. A. *Anal. Chem.* **1975**, *47*, 1337.

(95) Braun, R. D.; Santhanam, K. S. V.; Elving, P. J. *J. Am. Chem. Soc.* **1975**, *97*, 2591.

(96) Blankespoor, R. L. M., Larry L. *J. Electroanal. Chem.* **1984**, *171*, 231.

(97) Gorton, L. *J. Chem. Soc., Faraday Trans.* **1986**, *82*, 1245.

(98) Moiroux, J.; Elving, P. J. *J. Am. Chem. Soc.* **1980**, *102*, 6533.

(99) Tse, D. C.-S.; Kuwana, T. *Anal. Chem.* **1978**, *50*, 1315.

(100) Jaegfeldt, H. *Bioelectrochem. Bioelectron.* **1981**, *8*, 355.

(101) Elving, P. J. B., William T.; Morioux, Jacques; Samec, Zdenek *Bioelectrochem. Bioelectron.* **1982**, *9*, 365.

(102) Bartlett, P. N.; Wallace, E. N. K. *J. Electroanal. Chem.* **2000**, *486*, 23.

(103) Jaegfeldt, H.; Kuwana, T.; Johansson, G. *J. Am. Chem. Soc.* **1983**, *105*, 1805.

(104) Bartlett, P. N. T., P.; Whitaker, R. G. *Prog. React. Kinet.* **1991**, *16*, 55.

(105) Gorton, L.; Dominguez, E. In *Encyclopedia of Electrochemistry*; Bard, A. J., Stratmann, M., Eds.; Wiley-VCH Verlag GmbH & Co.: Weinheim, 2002; Vol. 9, p 69.

(106) Bartlett, P. N.; Birkin, P. R.; Wallace, E. N. K. *J. Chem. Soc., Faraday Trans.* **1997**, *93*, 1951.

(107) Kitani, A.; So, Y. H.; Miller, L. L. *J. Am. Chem. Soc.* **1981**, *103*, 7636.

(108) Gorton, L.; Torstensson, A.; Jaegfeldt, H.; Johannson, G. *J. Electroanal. Chem.* **1984**, *161*, 103.

(109) Pariente, F.; Lorenzo, E.; Abruna, H. D. *Anal. Chem.* **1994**, *66*, 4337.

(110) Ni, F.; Feng, H.; Gorton, L.; Cotton, T. M. *Langmuir* **1990**, *6*, 66.

(111) Cosnier, S.; Le Lous, K. *J. Electroanal. Chem.* **1996**, *406*, 243.

(112) Chen, H.-Y.; Zhou, D.-M.; Xu, J.-J.; Fang, H.-Q. *J. Electroanal. Chem.* **1997**, *422*, 21.

(113) Ohtani, M.; Kuwabata, S.; Yoneyama, H. *J. Electroanal. Chem.* **1997**, *422*, 45.

(114) Bartlett, P. N.; Simon, E. *Phys. Chem. Chem. Phys.* **2000**, *2*, 2599.

(115) Schuhmann, W.; Lammert, R.; Hämmerle, M.; Schmidt, H.-L. *Biosensors and Bioelectronics* **1991**, *6*, 689.

(116) Wu, Q.; Maskus, M.; Pariente, F.; Tobalina, F.; Fernández, V. M.; Lorenzo, E.; Abruña, H. D. *Anal. Chem.* **1996**, *68*, 3688.

(117) Ju, H.; Leech, D. *Anal. Chim. Acta* **1997**, *345*, 51.

(118) Storrier, G. D.; Takada, K.; Abruña, H. D. *Inorg. Chem.* **1999**, *38*, 559.

(119) Gaspar, S.; Habermüller, K.; Csöregi, E.; Schuhmann, W. *Sensors and Actuators B: Chemical* **2001**, *72*, 63.

(120) Albery, W. J.; Bartlett, P. N. *J. Chem. Soc., Chem. Comm.* **1984**, 234.

(121) Cai, C. X.; Xue, K. H. *Microchem. J.* **1998**, *58*, 197.

(122) Mano, N.; Kuhn, A. *J. Electroanal. Chem.* **1999**, *477*, 79.

(123) Casero, E.; Darder, M.; Takada, K.; Abruña, H. D.; Pariente, F.; Lorenzo, E. *Langmuir* **1998**, *15*, 127.

(124) Eckert, T. S.; Bruice, T. C. *J. Am. Chem. Soc.* **1983**, *105*, 4431.

(125) Evans, D. H. G., D. A. *J. Electroanal. Chem.* **1982**, *134*, 301.

(126) Hilt, G.; Steckhan, E. *J. Chem. Soc., Chem. Comm.* **1993**, 1706.

(127) Goss, C. A.; Abruna, H. D. *Inorg. Chem.* **1985**, *24*, 4263.

(128) Inglett, G. E.; Smith, G. F. *J. Am. Chem. Soc.* **1950**, *72*, 842.

(129) Eckert, T. S.; Bruice, T. C.; Gainor, J. A.; Weinreb, S. M. *Proc. Natl. Acad. Sci.* **1982**, *79*, 2533.

(130) Rivera, N.; Colón, Y.; Guadalupe, A. R. *Bioelectrochem. Bioenerget.* **1994**, *34*, 169.

(131) Hedenmo, M.; Narvaez, A.; Dominguez, E.; Katakis, I. *Analyst* **1996**, *121*, 1891.

(132) Santiago, M. E. B.; Vélez, M. M.; Borrero, S.; Díaz, A.; Casillas, C. A.; Hofmann, C.; Guadalupe, A. R.; Colón, J. L. *Electroanalysis* **2006**, *18*, 559.

(133) Tobalina, F.; Pariente, F.; Hernández, L.; Abruña, H. D.; Lorenzo, E. *Anal. Chim. Acta* **1999**, *395*, 17.

(134) Catalin Popescu, I.; DomInguez, E.; Narváez, A.; Pavlov, V.; Katakis, I. *J. Electroanal. Chem.* **1999**, *464*, 208.

(135) Dixon, M.; Webb, E. C. *Enzymes*; Longman: London, 1979.

(136) Chrétien, J.-M.; Ghanem, M. A.; Bartlett, P. N.; Kilburn, J. D. *Chem. Eur. J.* **2009**, *15*, 11928.

(137) Evans, I. P.; Spencer, A.; Wilkinson, G. *J. Chem. Soc. Dalton Trans.* **1973**, 204.

(138) Yamada, M.; Tanaka, Y.; Yoshimoto, Y.; Kuroda, S.; Shimao, I. *Bull. Chem. Soc. Jpn.* **1992**, *65*, 1006.

(139) Hudali, H. A.; Kingston, J. V.; Tayim, H. A. *Inorg. Chem.* **1979**, *18*, 1391.

(140) Alessio, E. *Chem. Rev.* **2004**, *104*, 4203.

(141) Lever, A. B. P. *Inorg. Chem.* **1990**, *29*, 1271.

(142) Zakeeruddin, S. M.; Nazeeruddin, M. K.; Humphry-Baker, R.; Gratzel, M.; Shklover, V. *Inorg. Chem.* **1998**, *37*, 5251.

(143) Chung, C. W. Y.; Toy, P. H. *J. Comb. Chem.* **2007**

9, 115.

(144) Jiang, B.; Hao, W.-J.; Wang, X.; Shi, F.; Tu, S.-J. *J. Comb. Chem.* **2009**, *11*, 846.

(145) Boland, S.; Barrière, F.; Leech, D. *Langmuir* **2008**, *24*, 6351.

(146) Blaedel, W. J.; Haas, R. G. *Anal. Chem.* **1970**, *42*, 918.

(147) Lee, J.; Lee, J.; Kang, M.; Shin, M.; Kim, J.-M.; Kang, S.-U.; Lim, J.-O.; Choi, H.-K.; Suh, Y.-G.; Park, H.-G.; Oh, U.; Kim, H.-D.; Park, Y.-H.; Ha, H.-J.; Kim, Y.-H.; Toth, A.; Wang, Y.; Tran, R.; Pearce, L. V.; Lundberg, D. J.; Blumberg, P. M. *J. Med. Chem.* **2003**, *46*, 3116.

(148) McNab, H.; Monahan, L. C. *J. Chem. Soc., Perkin Trans. 1* **1989**, 419.

(149) Hoekstra, K. J.; Bein, T. *Chem Mater* **1996**, *8*, 1865.

(150) Boghaei, D. M.; Behzadian-Asl, F. *J. Coord. Chem.* **2007**, *60*, 347

(151) Moulder, J. F.; Stickle, W. F.; Sobol, P. E.; Bomben, K. D. *Handbook X-Ray Photoelectron Spectroscopy* Perkin-Elmer Corporation: Minnesota, US, 1992.

(152) Huang, L.; Wang, K.-Z.; Huang, C.-H.; Li, F.-Y.; Huang, Y.-Y. *J. Mater. Chem.* **2001**, *11*, 790.

(153) Leirer, M.; Knör, G.; Vogler, A. *Inorg. Chim. Acta* **1999**, *288*, 150.

(154) Yi, H.; Crayston, J. A.; Irvine, J. T. S. *Dalton Trans.* **2003**, 685.

(155) Ackermann, Y.; Guschin, D. A.; Eckhard, K.; Shleev, S.; Schuhmann, W. *Electrochem. Comm.* **2010**, *12*, 640.

(156) Wagner, H. J.; Loutfy, R. O.; Hsiao, C.-K. *J. Mater. Sci.* **1982**, *17*, 2781.

(157) Yue, S.-M.; Xu, H.-B.; Ma, J.-F.; Su, Z.-M.; Kan, Y.-H.; Zhang, H.-J. *Polyhedron* **2006**, *25*, 635.

(158) Huan, Z.; Persson, B.; Gorton, L.; Sahni, S.; Skotheim, T.; Bartlett, P. *Electroanalysis* **1996**, *8*, 575.

(159) Gorton, L. *J. Chem. Soc., Perkin Trans. 1* **1986**, *82*, 1245.

(160) Gorton, L.; Johansson, G.; Torstensson, A. *J. Electroanal. Chem.* **1985**, *196*, 81.

(161) Albery, W. J.; Bartlett, P. N.; Lithgow, A. M.; Riefkohl, J. L.; Rodriguez, L. A.; Romero, L.; Souto, F. A. *J. Org. Chem.* **1985**, *50*, 596.

(162) Albery, W. J.; Bartlett, P. N.; Wilde, C. P.; Darwent, J. R. *J. Am. Chem. Soc.* **1985**, *107*, 1854.

(163) Albery, W. J.; Knowles, J. R. *Biochem.* **1976**, *15*, 5627.

(164) Albery, W. J.; Knowles, J. R. *Biochem.* **1976**, *15*, 5588.

(165) Albery, W. J.; Knowles, J. R. *Biochem.* **1976**, *15*, 5631.

(166) Albery, W. J.; Bartlett, P. N. *J. Electroanal. Chem.* **1985**, *194*, 211.

(167) Albery, J. W.; Bartlett, P. N.; Craston, D. H. *J. Electroanal. Chem.* **1985**, *194*, 223.

(168) Lyons, M. E. G.; Lyons, C. H.; Michas, A.; Bartlett, P. N. *J. Electroanal. Chem.* **1993**, *351*, 245.

(169) Bartlett, P. N.; Wallace, E. N. K. *Phys. Chem. Chem. Phys.* **2001**, *3*, 1491.

(170) Lyons, M. E. G.; Fitzgerald, C. A.; Smyth, M. R. *Analyst* **1994**, *119*, 855.

(171) Albery, J. *Electrode kinetics*; Clarendon Press: Oxford, 1975.

(172) Zanello, P. *Inorganic Electrochemistry; Theory, Practice and Application*; Royal Society of Chemistry, 2003.

(173) Wallace, E. N. K. Ph.D. Thesis, University of Southampton, 1997.

(174) Bartlett, P. N.; Birkin, P. R.; Wallace, E. N. K. *J. Chem. Soc., Faraday Trans.* **1997**, *93*, 1951.

(175) Yokoyama, K.; Ueda, Y.; Nakamura, N.; Ohno, H. *Chem. Lett.* **2005**, *34*, 1282.

(176) Goodyer, C. L. M.; Chinje, E. C.; Jaffar, M.; Stratford, I. J.; Threadgill, M. D. *Biorg. Med. Chem.* **2003**, *11*, 4189.

(177) M. Yamada, Y. T., Y. Yoshimoto, S. Kuroda, J. Shimaro *Bull. Chem. Soc. Jpn.* **1992**, *65*, 1006.

(178) Evans, I. P.; Spencer, A.; Wilkinson, G. *J. Chem. Soc., Dalton Trans.* **1973**, 204.

(179) Akasheh, T. S.; Marji, D.; Al-Ahmed, Z. M. *Inorg. Chim. Acta* **1988**, *141*, 125.

(180) Bartlett, P. N. *Biosensors: A Practical Approach*; 1st ed.; Oxford University Press: Oxford, 1990.

(181) Chrétien, J.-M.; Ghanem, M. A.; Bartlett, P. N.; Kilburn, J. D. *Chem. Eur. J.* **2008**, *14*, 2548.